Unterschrift des Betreuers

TECHNISCHE UNIVERSITÄT WIEN

# D I P L O M A R B E I T

_____

Thema

Ausgeführt am Institut für

_____

der Technischen Universität Wien

unter der Anleitung von _____

durch

_____

Name

_____

Anschrift

_____ _____

Datum Unterschrift (Student)

**Master Thesis**

# „$NH_3$ Reformer for an SOFC System“

carried out for the purpose of obtaining the degree of Master of Science (MSc or Dipl.-Ing.), submitted at TU Wien, Faculty of Technical Chemistry, by

Jan Schmidt, BSc

Mat.Nr.: 0935304

Vienna, April 2018

| | |
|---|---|
| Studienkennzahl lt. Studienblatt: | 066 473 |
| Mastergebiet lt. Studienblatt: | Masterstudium Verfahrenstechnik |
| Supervisor: | Univ.Prof. Dipl.-Ing. Dr.techn. Hermann Hofbauer (TU Wien) |
| | Dipl.-Ing. Michael Seidl (AVL) |

# Affidavit

I declare in lieu of oath, that I wrote this thesis and performed the associated research myself, using only literature cited in this volume. If text passages from sources are used literally, they are marked as such.

I confirm that this work is original and has not been submitted elsewhere for any examination, nor is it currently under consideration for a thesis elsewhere.

Vienna, April, 2018 .....

Signature

# Acknowledgement

This master thesis was written based on a cooperation between the AVL List GmbH and the Technical University of Vienna. For the initial contact I would like to say thank you to Matthias Werl who was the first one to point out that there was the chance to cooperate with the company AVL.

Furthermore, I would like to acknowledge my professor Univ.Prof. Dipl.-Ing. Dr.techn. Hermann Hofbauer, who was willing to back up my desire to write my master thesis in cooperation with the company AVL. At this point it also needs to get mentioned that Professor Hofbauer supported me not just during my master thesis but during the whole time as a student. He was a worthy dean for my study mates and me, who always tried to solve our problems as good as possible.

A special thank you also needs to be said to my supervisor at AVL, Dipl.-Ing. Michael Seidl, who did everything to make my time as comfortable as possible and even grow to a friend of mine. His efforts especially during the correction period were essential to finish this thesis on time. A big thank you also goes to every member of the AVL fuel cell department, who included me into their group from the first day on.

Not directly involved, but definitely essential was the positive effect my family, my mum, my dad and especially my brother had on me. During hard times I was always able to rely on you and without your support I would not be sanding where I am.

Last but not least I want to say thank you to the person who enabled me to write this master thesis in English. I want to say thank you to Stephani Theodosiou for being the reason I never backed down in all the challenging moments I had to face during the last few years.

# Abstract

The $NH_3$ dissociation performance of four commercially available catalysts, consisting of different Ni and Ru compositions, was tested. Therefore, ammonia was taken from a gas bottle and was alternately mixed with steam or was taken as pure $NH_3$ gas, before it was sent through an electrically heated reformer. The reformer was developed and manufactured by the company AVL. Based on the residual $NH_3$ concentration after the reformer and the temperature at the end of the reformer the different catalysts were compared to each other. The tests showed that Ni based catalysts had a better performance than Ru based catalysts in terms of $NH_3$ dissociation under both moist and dry conditions. The desorption of the nitrogen atom from the catalyst surface was determined to be the reaction rate-limiting step. Furthermore, it was found that during moist measurements NO was built after the ammonia concentration fell below $(0{,}8 \pm 0{,}2)$ vol-% $NH_3$.

# Index

# Abbreviations

Table 1: Table of Abbreviation

| Chemical Directory | |
|---|---|
| Al | Aluminium |
| Ca | Calcium |
| $CH_4$ | Methane |
| CO | Carbon monoxide |
| $CO_2$ | Carbon dioxide |
| $e^-$ | Electron |
| $H^+$ | Proton |
| $H_2$ | Hydrogen |
| $H_2O$ | Water |
| Li | Lithium |
| $N_2$ | Nitrogen |
| $NH_3$ | Ammonia |
| Ni | Nickle |
| NO | Nitrogen oxide |
| $NO_2$ | Nitrogen dioxide |
| $NO_x$ | Nitrogen oxides in general |
| $O_2$ | Oxygen |
| Ru | Ruthenium |

| Symbol Directory | | |
|---|---|---|
| bara | Absolute pressure | [bar] |
| barg | Over pressure | [bar] |
| $c_p$ | Heat capacity | [J/kgK] |
| d | Gradient | [-] |
| $\Delta E^{\pm}$ | Change of activation energy | [kJ/mol] |
| $\Delta E^{\pm}$ | Change of adsorption energy | [kJ/mol] |
| G /ΔG | Gibbs energy or free enthalpy / change of Gibbs energy | [kJ/mol] |
| H / ΔH | Enthalpy / change of enthalpy | [kJ/mol] |
| $\Delta H^0$ | Standard enthalpy of reaction | [kJ/mol] |
| I | Inaccuracies of the FTIR | [%] |
| K | Equilibrium constant | [-] |
| $\Delta K_{Gili}$ | Reading accuracy of the gilibrator | [%] |

| | | |
|---|---|---|
| $K_{Gili}$ | Calibration constant of the gilibrator | [Nl/hV] |
| $\dot{m}$ | Mass flow | [kg/h] |
| mol | $6{,}022*10^{23}$ particles | [-] |
| $\Delta\dot{m}_p$ | Reading accuracy of the pump | [%] |
| n | Amount of mol | [mol] |
| Q | Reaction quotient | [-] |
| $\dot{Q}_{el}$ | Electrical energy/heat flow | [W/h] |
| R | Ideal gas constant | [J/molK] |
| r | Reaction rate | [kmol/m³ s] |
| S / ΔS | Entropy / change of entropy | [kJ/molK] |
| T | Temperature | [K] |
| $U_{MFC}$ | Measured value of the MFC | [V] |
| $\Delta U_{MFC}$ | Output accuracy of the MFC | [%] |
| $\dot{V}$ | Volume flow | [m³/h] |
| X | Mol fraction | [-] |
| x | Set point | [-] |
| $\Delta\vec{X}_{FTIR}$ | Error vector of the FTIR | [%] |
| $\Delta X_{NH3,dry}$ | Error of the corrected dry ammonia concentration | [%] |

## General Abbreviations

| | |
|---|---|
| AVL | Anstalt für Verbrennungskraftmaschinen List |
| CAT 1 | Catalyst 1 |
| CAT 2 | Catalyst 2 |
| CAT 3 | Catalyst 3 |
| CAT 4 | Catalyst 4 |
| CV | Control Volume |
| DoE | Design of Experiment |
| FTIR | Fourier Transformation Infrared Spectrometer |
| GHSV | Gas Hourly Space Velocity |
| IR | Infrared |
| MFC | Mass Flow Controller |
| SCR | Selective Catalytic Reduction |
| SNCR | Selective Non-Catalytic Reduction |
| SV | Space Velocity |
| TOF | Turn Over Frequency |

# 1 Introduction

Even though the first version of a fuel cell (FC) was already discovered by Christian Friedrich Schönbein in 1838 and further improved by Sir William Grove in the same year [1], it has not reached general importance in our daily life yet. Due to cheaply available fossil fuels this technology always fell behind. Now that global warming and sustainable energy sources are being widely discussed a slow but steady rethinking towards alternatives is taking place. The fuel cell represents one of these alternative technologies. By just considering the electrochemical reaction of hydrogen and oxygen to water, the energy production with fuel cells would be completely $CO_2$ emission free.

The announcement that Japan is planning to power their entire Olympia town in 2020 with fuel cells in combination with their plan to provide 100 busses run by fuel cells is just one example of the new momentum this technology is gaining [2]. Another example is the already existing fuel cell car *Mirai* from the Japanese company *Toyota*, or the *h-tron quattro* from the German company *Audi*, who are also planning to louche serial production. Beside the mobile sector, fuel cells are more and more reaching out to replace the current electricity production in residential areas (ENE-FARM program in Japan) or being installed as energy back-up-systems for big servers. For this stationary purpose especially high temperature fuel cells, called Solid Oxide Fuel Cells (SOFC), are used. Due to their high operation temperature, around 900 °C, this FC type has the benefit that a combination of heat and power production is possible. That way an overall efficiency of 95 % and an electrical efficiency of 60 % can be achieved [3]. This is the reason why further investigations on different types of stationary FC systems are of big interest for the industry.

The biggest challenge regarding this technology is still the storage of hydrogen that is currently used as fuel. By looking for alternatives ammonia has outstanding benefits. It is easier to handle than hydrogen, better in terms of its volumetric energy density and since ammonia is already being used as refrigerant and as basic material for the global fertilizer production, it is one of the most produced substances. This makes an investigation of a FC system entirely run by ammonia as a hydrogen carrier and therefore as fuel, extremely interesting.

# 2 Problem Definition and Target

Currently the biggest challenge for fuel cell application is the storage of hydrogen. It is the smallest element and therefore able to diffuse through nearly all materials, what can cause a continuous hydrogen loss [4]. The two common ways to store hydrogen are either at -252 °C as a liquid in insulated and cooled tanks or compressed to 700 bar as a gas in pressure tanks, what is the preferred solution of the automotive industry. Both solutions are energy intense and not easy to handle in an everyday situation.

Much easier is the storage of ammonia. In its liquid form ammonia is either stored in atmospheric tanks at a temperature of -33 °C or in pressurised tanks at a pressure of 8 bara. Another benefit of ammonia as a hydrogen carrier is that in its liquid state it is able to store 1,7 times more hydrogen, than liquid hydrogen does itself [5]. A variety of studies that compared ammonia with hydrogen came to the result that beside the toxicity of ammonia it is better suited as a fuel for fuel cells than pure hydrogen [4], [6] - [7]. And even the toxicity can be reduced to a level lower than the one of gasoline by storing ammonia in metal amines [4].

Furthermore, studies that are investigating if ammonia can be used as fuel in SOFC systems, also came to positive results [8] - [9]. To reduce the thermal stress, the anode of the SOFC is confronted with by the endothermically dissociation of ammonia, a pre-reformer was designed. With the test results of the reformer the best relation of $NH_3$-dissociation inside the reformer to $NH_3$-dissociation directly on the anode of the fuel cell can be determined.

The task of this master thesis was to find commercially available catalyst materials for the ammonia dissociation and to compare them against each other in a suitable test facility. The temperature and the space velocity that are needed to reach full dissociation of ammonia and the influence of steam are the main parameters that were investigated.

# 3 Fundamentals

In this chapter the theoretical background to understand the discussion in Chapter 6 is presented. Furthermore, just the fundamentals that are directly linked to this master thesis or those, that were necessary to explain certain findings are covered within this section. In Chapter 6 references are linking the findings with the necessary background information of this chapter.

Content that is covered in this chapter are, the general properties of ammonia, Le Châtelier's Principle, the synthesis of ammonia with a general explanation of the Haber-Bosch process and a more detailed explanation of its catalytic mechanism. Then heterogenous catalysis and its kinetic mechanism are shown to gain a general overview of the reaction that is happening inside the reformer. The next subchapter is dealing with the theoretical background of the Gibbs energy and the reason why the theoretically estimated equilibrium composition is not that easy to reach under real conditions. Then selective catalytic and none-catalytic reduction is explained, what is becoming important later with regard to $NO_x$ emissions. And finally, because the measurement of ammonia in gas phase was way harder than initially expected a general overview of the FTIR's working principle is given. This Information is necessary to understand the cross-sensitivity and therefore the measuring error that is discussed in Chapter 6.

The Haber-Bosch process was not part of the master thesis, but due to its importance a variety of investigations have been carried out to understand its catalytic reaction steps in detail. This knowledge was used in revers order for this thesis, since detailed studies on the catalytic reaction steps of the ammonia dissociation have not been of big importance yet, and therefore detailed studies are hard to find.

## 3.1. Properties of Ammonia

In Table 2 the physical and chemical properties as well as the hazards of ammonia are listed. The data are based on the safety data sheet of the company Air Liquide, who was also the supplier for the ammonia used in this master thesis.

Table 2: Chemical and Physical Properties of Ammonia [10].

| $NH_3$ - Ammonia | | | |
|---|---|---|---|
| **Physical and Chemical Properties** | | | |
| physical state at 20°C / 1bar | : | gas | |
| colour | : | colourless | |
| molar mass | : | 17 | [g/mol] |
| melting point | : | -77,7 | [°C] |
| boiling point | : | -33 | [°C] |
| critical temperature | : | 132 | [°C] |
| flammability range | : | 15,4 to 33,6 | [vol% in air] |
| vapour pressure at 20 °C | : | 8,6 | [bara] |
| relative density, gas (air = 1) | : | 0,6 | |
| relative density, liquid (water = 1) | : | 0,7 | |
| solubility in water | : | 517000 | [mg/l] |
| auto-ignition temperature | : | 630 | [°C] |
| **Hazards** | | | |
| health hazards | | - toxic if inhaled<br>- causes severe skin burns and eye damage<br>- corrosive to respiratory tract | |
| physical hazards | | - flammable gas<br>- gases under pressure - liquified gas may explode if heated | |
| environmental hazards | | - very hazardous to the aquatic environment with long lasting effects | |
| **Pictograms** | | | |
|  GHS06 | |  GHS05 |  GHS04  GHS09 |

## 3.2. Le Châtelier's Principle

Henry-Lous Le Châtelier (1850-1936), a French physicist formed a law, called the "*Le Châtelier's Prinziple*", that explains how a chemical system at equilibrium reacts under the influences of constraints. This law helps to predict which conditions are beneficial for a certain outcome of a reaction, by shifting its equilibrium either to the product, or the educt side. This principle can be expressed as following:

> *"When any system at equilibrium is subject to change in concentration, temperature, volume, or pressure, then the system readjusts itself to counteract (partially) the effect of the applied change and a new equilibrium is established."* [22]

Put simply, there are three ways to influence the chemical equilibrium: (1) By adding or removing an educt or product (2) changing the pressure or (3) changing the temperature.

$$N_2 + 3\,H_2 \rightleftharpoons 2\,NH_3 \qquad \Delta H = -92{,}5\,\frac{kJ}{mol} \tag{3.1}$$

### Concentration Changes

A chemical equilibrium is a dynamic state of forth-and-back reactions between products and educts. When one component gets withdrawn the system, due to energy minimisation, is compensating the loss by reproducing the withdrawn component. The opposite happens when there is an abundance of one component. In the specific situation of the ammonia synthesis (formula 3.1), that would mean that a constant withdrawal of $NH_3$ would force the left side to form more $NH_3$ to re-establish the equilibrium. This method is successfully used in the Haber-Bosch-Process (see Chapter 3.3.1).

In the reactor of this master thesis the reverse process of the Haber-Bosch-Process was realised. With an excess of $NH_3$ it was tried to shift the equilibrium to $N_2$ and $H_2$.

### Pressure Changes

If the pressure of a system gets increased, by decreasing the volume, *Le Châtelier's Prinziple* says that the system reacts on that force via shifting its equilibrium towards a state of lower

pressure. The same is true the other way around. A system energetically minimises the constraint of pressure by reducing the total number of gas molecules and likewise readjusts to under pressure by adding more gas molecules. In equation 3.1 the number of mol on the educt side is 4, whereas the number of mol on the product side is just 2. That means an increase of the pressure would facilitate the production of $NH_3$, whereas a decrease of the pressure would be beneficial for the reaction towards the educts.

### Temperature Changes

The synthesis of ammonia from nitrogen and hydrogen is an exothermic process. That means heat is released during the production of $NH_3$. For the reverse reaction, the dissociation of $NH_3$ into its elementary constituents, energy is needed and therefore it is an endothermic reaction. The *Le Châthelier's Principle* says that the system is always balancing the force it is compelled with, by doing the opposite. If heat is added to the reaction shown in formula 3.1 the system will balance it by shifting towards its left, endothermic, side. By doing so the added energy gets consumed through the dissociation of $NH_3$. If the reaction gets cooled $N_2$ and $H_2$ are compensating this force through the exothermic reaction by building $NH_3$.

## 3.3. $NH_3$ Synthesis

The fertilization to obtain the worlds food supply is mainly based on nitrogen. More than 99% of the free nitrogen exists as biologically inactive $N_2$ in our atmosphere. Therefore, the reduction of $N_2$ to ammonia, the most important bioavailable nitrogen compound, is of extreme significance. The biological process to convert $N_2$ into $NH_3$ is restricted to a few microorganisms and done by an enzyme called Nitrogenase.

$$N_2 + 8\,H^+ + 8\,e^- \xrightarrow[Nitrogenase]{1\,bara,\ 20\,°C} 2\,NH_3 + H_2 \tag{3.2}$$

The non-biological fixation of nitrogen is done for over 100 years by the Haber-Bosch-Process.

$$N_2 \; + \; 3\,H_2 \xrightarrow[Fe-catalyst]{150-250\,bara,\;\; 460-550\,°C} 2\,NH_3 \tag{3.3}$$

The production volume of ammonia in 2006 was approximately 150× $10^6$ t, what ranks it second, behind sulphuric acid, under the most produced organic basic chemicals [11]. Therefore, 2 % of the worldwide natural gas production and 1 % of the world energy production was used. Around 85 % of the produced ammonia is used for fertilizers. Based on this data it can be said that the synthesis of ammonia is one of the most important chemical processes worldwide.

### 3.3.1. Haber–Bosch Process

The $N_2/H_2$ gas that is used for the ammonia synthesis is mainly produced from natural gas, air and water. Based on this educts hydrogen is produced by catalytic steam reforming over nickel catalysts.

$$CH_4 \; + \; H_2O \;\; \rightarrow \;\; 3\,H_2 \; + \; CO \qquad \Delta H^0 = 206\,\frac{kJ}{mol} \tag{3.4}$$

Parallel to this reaction the carbon monoxide conversion, better known as water-gas shift reaction, is taking place.

$$CO \; + \; H_2O \;\; \rightarrow \;\; H_2 \; + \; CO_2 \tag{3.5}$$

In a primary reformer at 700-900 °C and 20-40 bara a part of the methane is transformed. Then in a secondary reformer with the same nickel catalyst, another part of the gas mixture is burned under controlled air supply. This reaction is exothermic, and the temperature rises to 1200 °C. The endothermic steam reforming reaction is cooling the system down again to 1000 °C. Under this condition a residual methane content of 0,5 % is reached [11]. The air demand for the second reformer is determined by the $N_2/H_2$ ratio required by the subsequent ammonia synthesis. CO, $CO_2$ and sulfuric compounds need to get separated completely because they are catalyst poisons for the following Haber-Bosch catalyst.

The ammonia synthesis out of its elementary constituents is exothermic and slightly exergonic under standard conditions (20 °C, 1 bara).

$$\frac{1}{2}N_2 + \frac{3}{2}H_2 \rightarrow NH_3 \qquad \Delta H^0 = -46\frac{kJ}{mol}, \Delta G^0 = -16\frac{kJ}{mol} \tag{3.6}$$

Based on *Le Châtelier's Principle* it can be said that low temperature and high pressure are leading to a high equation concentration of ammonia. Additionally, the constant drain of liquid $NH_3$ is also shifting the equilibrium towards a higher production of ammonia. As it is shown in Figure 1 the clean $N_2/H_2$ mixture, coming from the preconnected process is entering the Haber-Bosch facility at the inlet. The gas is then heated up to 550 °C and gets contacted with several catalyst stacks. Between the catalyst stacks there are cooling units to hold the exothermic process on a stable temperature level. After that the $NH_3$, $N_2$ and $H_2$ gas mixture is expanded and additionally cooled, which leads to a condensation of $NH_3$. The ammonia condensate is then collected in a refrigerant unit and the not reacted $N_2$ and $H_2$ is recycled and mixed again with the inlet stream. With this process it is possible to reach an overall ammonia conversion of 97 %, even though one single cycle just converts about 15 % $NH_3$ [12].

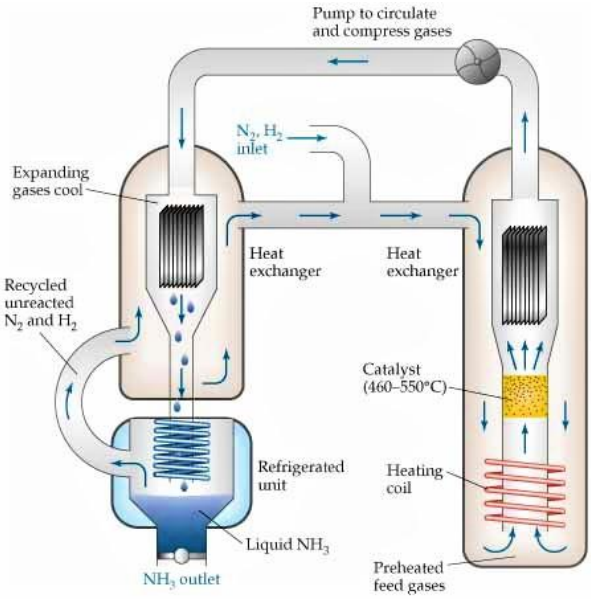


Figure 1: Schematic description of the Haber-Bosch Process – Here the three ways, change of pressure, temperature or concentration, a chemical equilibrium can get affected by according to Le Châtelier's Principle are seen [22].

### 3.3.2. Catalytic Mechanism of the Ammonia Synthesis

$N_2$ is relatively inert. The only element that is reacting with nitrogen at room temperature is the highly reactive lithium. However, at higher temperatures a variety of other materials, especially transition metals, react with nitrogen as well. The high thermodynamic stability can be explained by the triple bond of $N_2$. The binding and dissociation energy of $N_2$ is 945 kJ/mol [11]. As reference, the binding and dissociation energy of $H_2$ is 436 kJ/mol and from $O_2$ it is 495 kJ/mol [13].

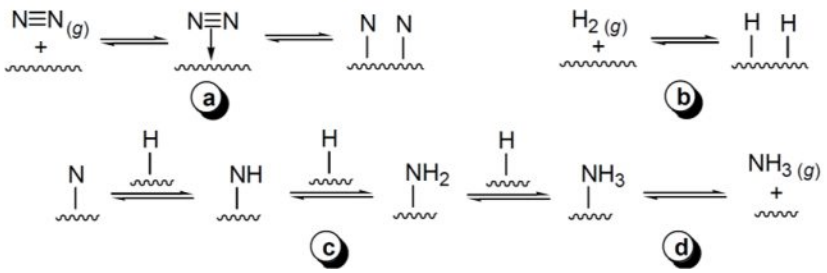


Figure 2: Mechanism of the Catalytic Ammonia Synthesis – (a), (b) Nitrogen and hydrogen are adsorbed to the catalysts surface by dissociative chemisorption. (c) Ammonia is formed by successive combination of a nitrogen atom with three hydrogen atoms. (d) The newly formed ammonia molecule desorbs from the catalyst surface [3].

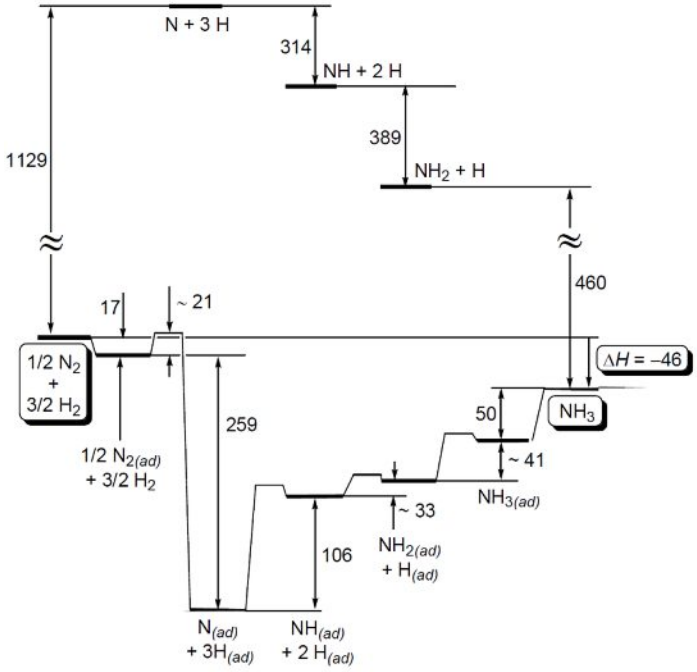


**Figure 3: The Energy Profile Diagram for the Ammonia Production – Here the Energy that is needed to build $NH_3$ out of $N_2$ and $H_2$ is shown. The upper part of the diagram symbolises the energy demand without a catalyst and the lower curve with the iron catalyst [20].**

A detailed investigation on the catalytical mechanism was carried out by G. Ertl, who was honoured for his work with the Nobel Prize in Chemistry in 2006 [14]. The four-step mechanism is shown in Figure 2. The first step (a) is the dissociative chemisorption of $N_2$ on the surface of the iron catalyst. That includes the adsorption of the $N_2$ molecule, the dissociation of the N-N-bond and the bonding of the two separate N-atoms onto the surface of the iron catalyst. This was determined to be the rate limiting step of the whole reaction. $H_2$ is then adsorbed to the surface through dissociative chemisorption as well (b). The hydrogenation occurs through

stepwise reaction of the bound N-atoms with three H-atoms (c). The reaction is ended by the desorption of the $NH_3$ (d).

The energy profile diagram of the ammonia production with an iron catalyst is shown in the lower half of Figure 3. The energetically highest state is the transition state for the reaction $½\ N_{2(ad)} + 2/3\ H_2 \rightarrow N_{ad} + 3\ H_{ad}$. The energetically most stable state is where all four atoms are bound to the surface of the iron catlyst ($N_{ad} + 3\ H_{ad}$). From that moment the energy is increasing, but the reaction as a total is with -46 kJ/mol exothermic. Completely different is the energetically profile of the homogenous non-catalytical reaction in the upper curve of Figure 3. The state of four separate atoms (N + 3 H) is the most unstable or highest-energy state of the reaction [15]. Every following step decreases the overall energy. This extremely high activation energy is the reason why this reaction cannot be realised under reasonable chemical conditions without a catalyst. Even at 1000 K (1 bara) the degree of dissociation for $N_2$ and $H_2$ would be around $10^{-22}$ and $10^{-9}$, so that the non-catalytical way is not a practicable approach [11].

## 3.4. Heterogeneous Catalysis

Catalysis is the key to many chemical transformations. Most industrial syntheses and nearly all biological reactions require catalysts. A definition due to Ostwald (1895), that is still valid today is: "a catalyst accelerates a chemical reaction without affecting the position of the equilibrium." [16] That means a catalyst is a substance that promotes a reaction but is not being used by the reaction. The graph in Figure 4 shows the principle of a catalytically supported reaction. By reducing the activation energy, a catalyst is providing a less energy intense way for the reaction to take place, without affecting the equilibrium itself.

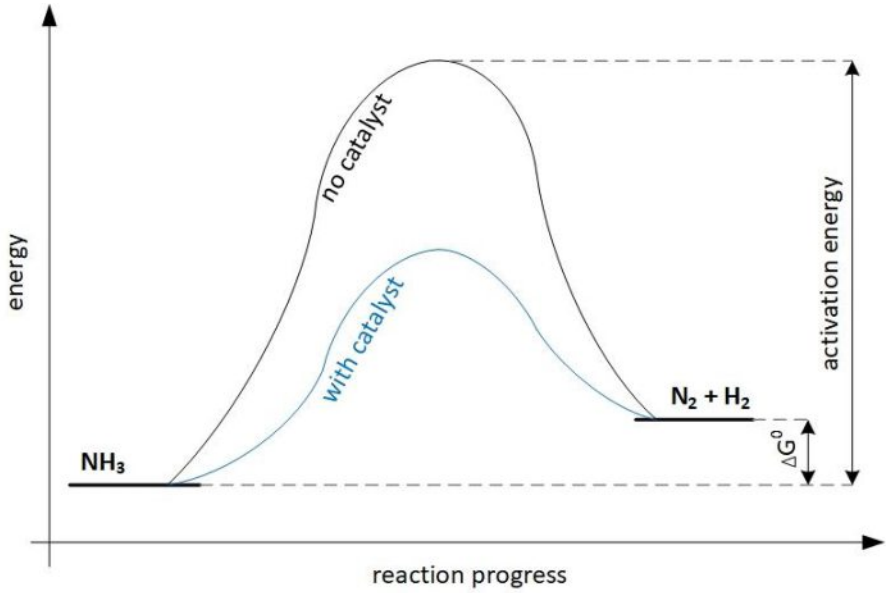


Figure 4: Principle of a Catalyst – The reduction of the activation energy through a catalyst is shown for the endothermic and endergonic reaction of ammonia to nitrogen and hydrogen.

For the endergonic and endothermically splitting of ammonia into nitrogen and hydrogen, that means less energy in form of heat is needed for the reaction to start, resulting in higher dissociation rates at lower reactor temperatures.

In general, catalysts can be classified into the three categories, homogenous, heterogenous and biological catalysts. When the starting materials, the catalyst and the reactants are present in the same phase it is called homogenous catalysis. Biological catalysts are called enzymes and can be found in nearly every biological reaction. In this master thesis the focus lies on heterogeneous catalysis, where the catalyst, educts and products are appearing in different phases. Therefore, phase boundaries are always present on which the catalytically enhanced reaction is taking place. This means, that different to homogenous catalysis, where in theory every atom can be catalytically active, in heterogenous catalysis only the surface atoms are active. This type of catalysis most commonly occurs between a solid catalyst and reacting agents that are in gas phase. This is also the case for the ammonia reforming covered in this thesis.

### 3.4.1. Kinetic Mechanism

As it is already mentioned in the Chapter 3.3, in heterogenic catalysis just the surface atoms of the catalyst are active. A restricted approaching direction of the active sites, or the effect that neighbouring active centres are blocking each other, are the consequence. Therefore, it is important for heterogenous catalysts to have a large surface area to maximise the number of active sites. This circumstance has a complex reaction process as consequence, consisting of several physical and chemical reaction steps. Beside the actual chemical reaction, for the overall process, adsorption, desorption and diffusion are of importance. In Figure 5 it is shown for the simplest case of catalytic gas reaction, how the starting materials need to get transported to the active site, before the actual catalytic reaction is able to take place.

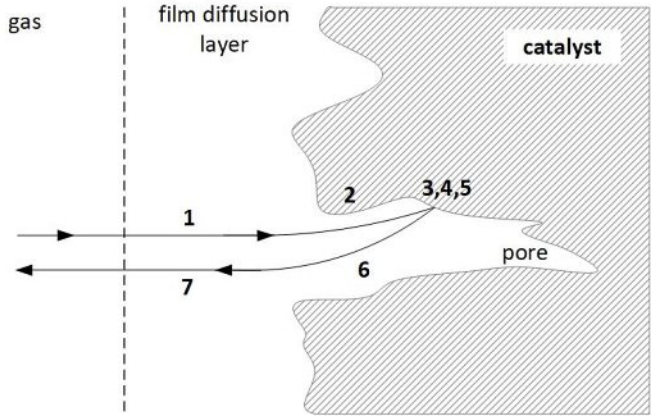


Figure 5: Heterogeneously Catalysed Gas-Phase Reaction – The individual steps of the heterogenous catalysis, consist of diffusion, adsorption, chemical reaction, desorption and diffusion.

The kinetic mechanism of heterogeneous catalysis is a step-wise process, describing the particles path onto and off the catalyst surface including the chemical reaction (see Figure 5):

1. diffusion of the starting materials through the boundary layer to the surface of the catalyst (film diffusion)
2. diffusion into the pores (pore diffusion)
3. adsorption of the reactants on the catalyst material
4. actual chemical reaction on the catalyst surface
5. desorption of the product from the catalyst surface
6. diffusion out of the pores
7. diffusion back into the gas phase and away from the catalyst

Step 1,2, 6 and 7 are physical reaction steps and part of the macrokinetics, whereas step 3, 4 and 5 are chemical reaction steps and part of the microkinetics. Whatever step is the most inhibited and therefore the slowest is also the rate-determining one. If the physical steps determine the reaction the capacity of the catalyst is not fully exploited. This effect can be decreased by a higher gas velocity and therefore a smaller film diffusion layer [16]. What all steps have in common is that they become faster with increasing temperature. For the ammonia synthesis adsorption and desorption are the rate limiting steps [17]. Especially the desorption of nitrogen was determent to be the most energy intense step [18].

## 3.5. Gibbs Energy

Reforming reactions as investigated in this thesis ideally happen under constant pressure and temperature conditions. To calculate chemical equilibria of gases under these circumstances, minimization of Gibbs Energy (G) is used

$$G = H - TS \tag{3.7}$$

with the gases enthalpy (H), temperature (T) and entropy (S). The change of the Gibbs energy ($\Delta$G) for a system originates in the changes of the enthalpy ($\Delta$H), and entropy ($\Delta$S)

$$\Delta G = \Delta H - T\Delta S \tag{3.8}$$

The mathematical sign of $\Delta$G determines whether a chemical reaction will proceed in the direction of the products ($\Delta G < 0$, exergonic) or the reactants ($\Delta G > 0$, endergonic). If $\Delta$G is zero, the reaction has reached its equilibrium state. The chemical equilibrium represents the minimum of the free enthalpy of a system as it can be seen in Figure 6. In case both $\Delta$H and -T$\Delta$S terms are having the same sign, the Gibbs energy is either always positive or always negative for all temperatures. For the reaction with differing signs at $\Delta$H and -T$\Delta$S it depends on the temperature if a reaction is taking place spontaneously or not. The reaction of nitrogen and hydrogen to ammonia and backwards, is an example of a system that is temperature dependent.

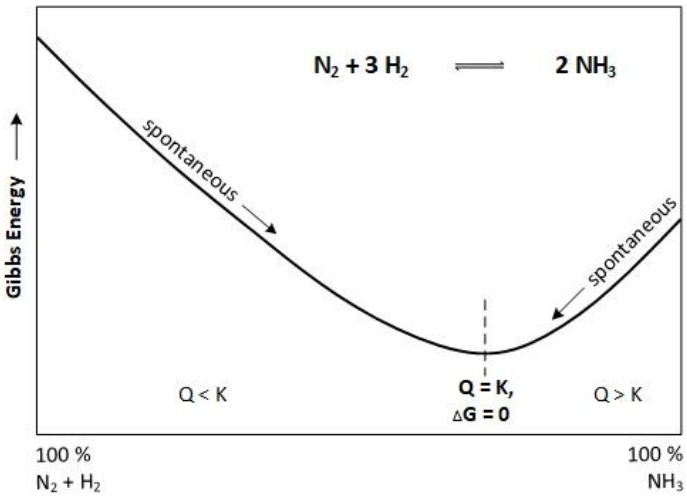


Figure 6: Gibbs Energy – Gibbs energy of the NH3 synthesis reaction as a function of the gas composition at fixed temperature. The chemical equilibrium is determined by the Gibbs energy minimum.

Another possibility to describe a systems deviation from equilibrium state is the reaction quotient (Q)

$$Q = \frac{[NH_3]^2}{[N_2] \cdot [H_2]^3} \tag{3.9}$$

where [NH3], [N2] and [H2] are either the species concentration, mol-fraction or partial pressure in a certain non-equilibrium state. Q is merging into the equilibrium constant (K) if the reaction has reached its minimal level of free energy, or in other words, if the reaction is in its equilibrium state. That means if Q < K the reactants are present in excess and the reaction is moving to the right until K is reached. If Q > K the products are abundant, and the reaction is moving to the left. This principle can also be seen in Figure 6.

There is a general connection of the free enthalpy and the reaction quotient given by

$$\Delta G = \Delta G^0 + RTlnQ \tag{3.10}$$

where $\Delta G^0$ is standing for the Gibbs Energy of the reaction at standard conditions, R is the ideal gas constant (8,314 J/molK) and T is the absolute temperature at which ΔG shall be calculated. For the equilibrium state of a reaction equation 3.9 changes to

$$\Delta G = \Delta G^0 + RTlnK = 0 \tag{3.11}$$

where Q is replaced by K and the change of Gibbs Energy has reached its minimum. Out of this correlation under the requirement, that the Gibbs Energy for the standard condition is

known, a general formula to predict the equilibrium constant and therefore also the equilibrium constitution of the reactants and products can be derived.

$$K = e^{-\frac{\Delta G^0}{RT}} \tag{3.12}$$

With these relations (3.7 -3.12), the tabled values of the entropy and the enthalpy at standard conditions and the information about the chemical equation, it is possible to predict the chemical composition of a system at different temperatures. The assumption that $\Delta G^0$ is not temperature dependent and therefore also $\Delta H^0$ and $\Delta S^0$, is valid for most reactions under the condition that the pressure stays the same and lower than 10 bar [13].

It is important that the Gibbs Energy and its direct conclusion of whether the reaction is endergonic or exergonic, does not say anything about the speed of a reaction. The Gibbs energy is just comparing the stability of the starting substance with the stability of the reaction products. It says nothing about the activation energy of a reaction, that needs to be overcome by the reactants during the reaction. The higher this activation energy is the slower is the reaction and at really high activation energies it basically stops completely.

## 3.6. Selective Catalytic and None-Catalytic Reduction

The selective catalytic reduction (SCR) is a technique used in industrial facilities, waste incineration plants, gas turbines, furnaces and combustion engines, to reduce the amount of $NO_x$ in the exhaust gas. This reaction is selective, which means mainly NO and $NO_2$ are reduced on the surface of the catalyst. For this reaction ammonia is injected and mixed into the off gas. The products of the reaction are $N_2$ and water:

$$4\,NO + 4\,NH_3 + O_2 \rightarrow 4\,N_2 + 6\,H_2O \tag{3.13}$$

$$2\,NO_2 + 4\,NH_3 + O_2 \rightarrow 3\,N_2 + 6\,H_2O \tag{3.14}$$

$$NO_2 + NO + 2\,NH_3 \rightarrow 2\,N_2 + 3\,H_2O \tag{3.15}$$

At temperatures below 700 °C this reaction is just taking place when a catalyst is around to promote the reduction [19]. Catalysts for the SCR are titanium oxide, vanadium oxide and activated carbon.

This technique is also used directly inside the combustion chamber at a higher temperature range of 900 to 1050 °C. At this energy level the reduction works even without a catalyst and is called selective non-catalytic reduction (SNCR). Below this temperature interval the SNCR's conversion rate is too low and above 1050 °C formation of nitrogen oxides is taking place again. Therefore, it is important to stay within 900 to 1050 °C for the SNCR [19].

Under the name AdBlue® [20] or BlueTec® [21] the SCR can be found in cars, trucks and heavy-duty vehicles. The only difference to the technique mentioned above is that here a 32,5 % urea solution diluted with distilled water is used instead of pure ammonia. That is necessary because of the hazardous properties of $NH_3$ (see Chapter 3.1).

Because of the similarities between the techniques described in the current chapter and the working conditions of the $NH_3$-reformer of this thesis, it was expected that the reformers exhausted gas is going to be completely $NO_x$ free.

## 3.7. Infrared Spectroscopy

The covalent bonds between atoms are in a continuous state of swinging movement along their axes, as well as in a certain angle towards them, depending on their degree of freedom. Deformation vibration are changing the angles, stretch vibrations are changing the length between chemical bonds and rotational movements are twisting the bond along its axis. With the complexity of the molecule the number of the possible swinging movements is increasing tremendously. The chemical bond of a molecule can be stimulated at its characteristic frequency. In order for a molecule to be infrared-active, this stimulation occures with a change of the dipole moment. It does not require a constant dipole, though. If a molecule is symmetrical, like $N_2$ or $H_2$ for example, its vibrational band is not observed in the IR spectrum. Infrared spectroscopy is using electromagnetic radiation with a wave numbers between 4000 and 600 $cm^{-1}$. This spectrum has the right energy to stimulate deformation and stretch

vibrations of organic molecules. The electromagnetic radiation in this spectrum is within the range of infrared radiation. If a molecule is confronted with a photon which's frequency corresponds to one of the molecules oscillation modes, then the photon gets absorbed. During this process, the photons energy is being transferred to the swinging modes of the absorbing molecule. If more radiation energy is absorbed the amplitude, but not the frequency of the molecule's vibration, increases. Based on the wave number that is absorbed by certain chemical bonds it is possible to predict the type of bond of a chemical connection. Therefore, a beam of infrared light gets passed through a sample and the spectrum of the transmitted light reveals how much energy was absorbed at each wave number. The examination of the samples characteristic spectrum reveals its chemical composition.

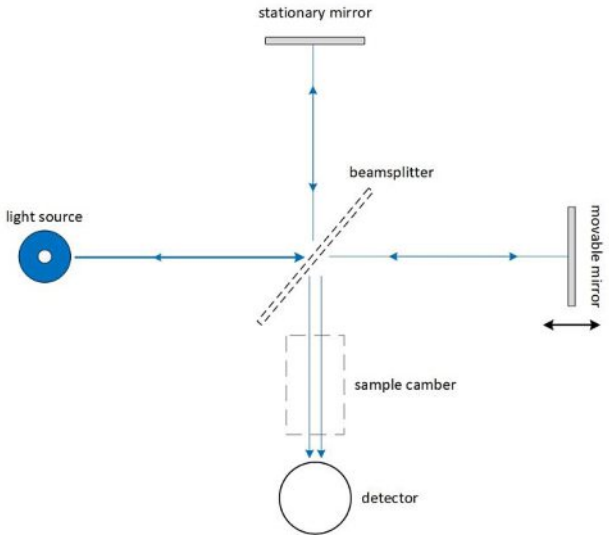


figure 7: Schematic setup of an Interferometer – This graphic shows how the IR light is split and the variation of the pathlengths between the mirrors inside a FTIR to produce an interferogram.

For this master thesis a Fourier-Transformation-Infrared-Spectrometer (FTIR) with a detector cooled by a Peltier cooler was used (see Chapter 4.1.). The basic principle of an infrared spectrometer is shown in figure 7. A light source is emitting IR light onto a beamsplitter, where half of the light gets reflected and half is transmitted. The split light is hitting either the stationary mirror or the movable mirror where it gets reflected again. When it comes back to the beamsplitter, again, half of the light transmits and half of it gets reflected. The radiation from the stationary and from the movable mirror are brought together before they go through the sample chamber. The two paths between the mirrors and the beamsplitter differ in length, so that the waves are not in phase. Depending on the position of the movable mirror they interfere either constructively or destructively. Constructive interference occurs when they are in phase, destructive interference occurs if they are out of phase by half a wavelength, in which case they completely cancel each other. For any other variation they partially cancel. This difference in pathlength is called retardation and causes that the beam going through the sample chamber has a different spectrum each moment the movable mirror has a different position. This data

(light absorption for each mirror position), called interferogram is saved for each moment and combined by a Fourier Transformation to the final spectrum (light absorption for each wave length) of the sample. This spectrum gets then compared to a data bank of reference measurements for certain substances, to determine which chemical components are part of the sample.

Before a FTIR can get used a calibration measurement is carried out with a not IR-active gas like $N_2$. Due to its symmetry this gas lets the whole spectrum of the interferometer's light source pass. This measurement, where no absorption is taking place, is then saved as the reference spectrum of the measuring device. During the actual measurements the calibration gas is turned off and just the sample gas is streaming through the measuring chamber. The spectrum that is recorded with the sample gas are always referenced to the calibration measurement with no absorption, to determine which wave numbers were absorbed by the sample gas and to what extent. To exclude decreasing accuracy of the FTIR due to a decreasing quality of the light source a calibration measurement should be done as often as possible.

# 4 Material and Methods

## 4.1. List of Equipment

The reformer as well as the test stand that were used for this master thesis were manufactured by AVL. The following list of equipment (Table 3) gives an overview of the most important parts of the setup.

Table 3: List of Equipment - This table shows the used equipment for the experimental setup of this master thesis. Just the main components are displayed, all the other material like tubes, insulation etc. are not part of this table. The used catalysts are presented in Table 4.

| no. | Component | Manufacturer | Information |
|---|---|---|---|
| | | Hardware | |
| 1 | MFC | Vögtlin | red-y smart controller<br>Type: GSC-C5ST-BB12<br>Medium: air<br>Measuring range: 1-50 nl/min |
| 2 | Evaporator | Adrop | Athros (1 kg/h evaporating rate) |
| 3 | Heating Wire | Horst GmbH | Type: HSQ |
| 4 | Water Pump | KNF Lab | Stepdos O3 RC |
| 5 | Gilibrator | Sensidyne | Gilibrator-2 Calibrator |
| 6 | Reformer | AVL | Self-made component |
| 7 | FTIR | Gasmet | DX4000 plus system parts |
| 8 | Thermocouple | FuelerSysteme eNET | TE Type K (NiCr-Ni) 1,5 mm |
| | | Software | |
| 9 | LabVIEW | National Instruments | Version 2014 SP1 |
| | | Chemicals | |
| 10 | $N_2$ | Air Liquide | ALPHAGAZ STICKSTOFF 1<br>($N_2$ 99,999%) |
| 11 | Forming Gas | Air Liquide | ARCAL F5, $N_2/H_2$ 95/5 |
| 12 | $NH_3$ | Air Liquide | AMMONIA N38<br>($NH_3$ 99,98 Vol.%)<br>$H_2O < 100$ ppmw<br>Oil $< 5$ ppmw |

Additionally, several basic components like tubes, insulation material etc. were used during the tests without being listed in Table 3. The gilibrator was used to calibrate the MFC, which was made out of ammonia resistant material, but was pre-calibrated on air. A pre-calibration with

$NH_3$ is something that is hardly done by companies, because of the high chance to damage their laboratory equipment with $NH_3$ gas. The heating wires needed to get changed on a regular basis, because the high temperature made them brittle. This fact in combination with the frequent mounting and dismounting of the reformer to change the catalyst material, made them break easily. The same type of wire was used in different length from 2 to 5 meters with an electrical power from 350 W to 850 W.

## 4.2. Test Stand

Parts of the setup were already existent before the start of this master thesis and got extended to the whole setup that is shown in Figure 8. The reformer was designed and produced by AVL.

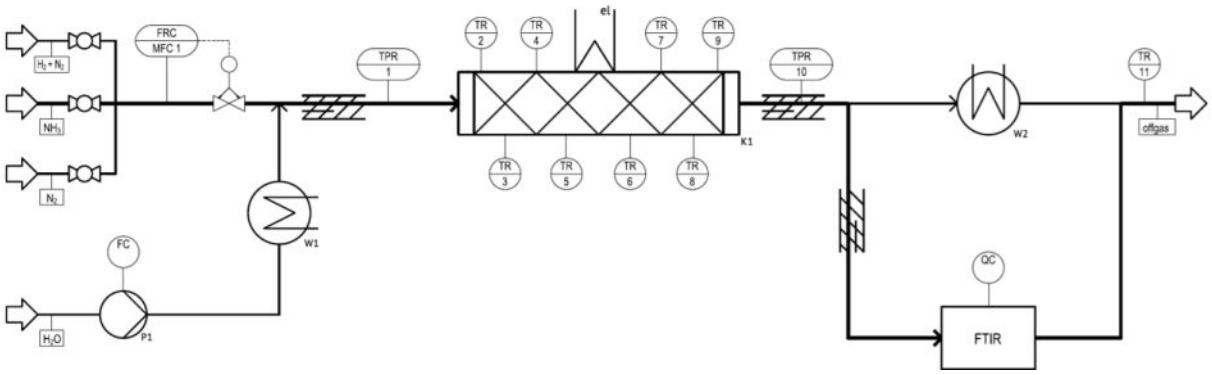


Figure 8: Flowsheet of the test stand – This flowsheet describes the general setup of the test facility that is shown in Figure 9. Ammonia is the main feed and goes through a heated tube into the reformer (K1) that is filled with the catalyst. The reformer is heated by an electrical heating wire up to 900 °C. After the reformer the off gas goes through an FTIR where its composition is determined before it leaves the facility into the exhaust system of the laboratory. The part of the off gas that was not used by the FTIR was cooled to room temperature in the second heat exchanger (W2) before it was mixed again with the off gas from the FTIR. The pump (P1) and the vaporiser (W1) were used for moist measurements to dose 20 vol% of H2O steam into the ammonia stream. 11 temperature sensors (TR) or temperature and pressure sensors (TPR) are monitoring the temperature distribution within the facility.

As shown in Figure 8 the core part of the test facility was the reformer. This reformer, as it can be seen in Figure 9 was made from stainless steel, with an inner diameter of 29,7 mm, a tube length of 760 mm and a total filling volume of 500 $cm^3$. It was filled with a catalyst and heated with electrical heating wires that were controlled by temperature controllers. At the

beginning and the end of the reformer a small wad of metal wool was fixing the catalyst material. Eight connectors for thermocouples where welded onto the reformer with eight Type K temperature sensors attached to them. The thermocouples were positioned directly in the middle of the tube. The whole reformer was insulated on the outer side with a band of glass wool to protect the heating wires and then put into a bed of thermo-granulate for a better insulation. In Figure 9 the reformer and its setup are shown.

The test stand's control cabinet was connected to a PC where the LabVIEW based control software and the data logging were executed. Parallel to the measurement of the computer a separate FTIR was used to measure the gas composition after the reformer. Both measurements were then brought together manually into one log data file. The FTIR was calibrated for an $NH_3$ range of 0 to 10 vol% and therefore measurement accuracy decreases above the level of 10 vol% $NH_3$.

In front of the reformer an $H_2O$ pump in combination with a vaporiser were installed additionally to the ammonia supply. That enabled the facility to also measure an ammonia and steam mixture. From the point steam and ammonia were mixed within the facility, all the tubes were heated and insulated to prevent condensation of water and therefore also $NH_3$ going into solution.

The test stand was connected to three different gas supplies (Figure 8). Ammonia, nitrogen and forming gas, which is a mixture of 95 % $N_2$ and 5 % $H_2$. Forming gas was used to activate the Ni catalyst by reducing the initial Ni oxides. The Ni based catalysts (Table 4) were delivered in their oxidised form and needed to get reduced to their metallic form to reach their full catalytic potential. Nitrogen was used to flush the test facility to prevent left over $NH_3$ gas from condensing. During the measurements all the other gas supplies where turned off and only ammonia and for the moist measurements ammonia in combination with the water supply were used. Depending on if just dry ammonia or a mixture of ammonia and steam was needed, the vaporiser and the pump were turned off or on. Before every measurement the reformer was heated up to 400 °C with the $NH_3$ supply turned off. From the moment the reformer reached 400 °C the ammonia supply was turned on. The reformer then was heated up to the highest reachable temperature or, if possible to 900 °C. Failures due to short-circuits between the heating wires and the reformer's metal surface caused initial problems, that were solved by

removing the insulation layer between the reformer and the heating wire. In Chapter 6.1 this initial problem is discussed in more detail.


Figure 9: Test Stand – Image (a) shows the reformer and how it was integrated into the test facility. During the measurements, the box around the reformer, was filled with a thermo granulate for a better insulation. The flow direction is indicated by white arrows. Image (b) shows the whole test stand. Image (c) shows the reformer without any insulation. Image (d) shows the position of the thermocouples inside the empty reformer before it was filled with a catalyst material.

## 4.3. Used Catalysts

In this chapter the catalysts that were used in this master thesis are presented. The manufacturers just gave a rough information about the catalysts composition which is shown in Table 4.

Table 4: list of the used catalysts – This table gives a detailed information about the catalysts based on the details the manufactures were willing to disclose.

| no. | Name | Manufacturer | Information |
|---|---|---|---|
| 1 | CAT 1 | Manufacturer 1 | 540°C calcined basis<br>Ni 6.0 ± 1.0 wt. %<br>Ca 5.3 ± 2.1 wt. %<br>Al 3.5 ± 1.5 wt. %<br>loss on ignition at 540 °C ≤ 1.0 wt. %<br>magnesium oxide balance |
| 2 | CAT 2 | Manufacturer 2 | aluminium oxide coated with Ru |
| 3 | CAT 3 | Manufacturer 3 | coated 5% Ru alumina spheres |
| 4 (bonus) | CAT 4 | Manufacturer 1 | NiO 56.5 wt. %<br>support and promoter balance |


Figure 10: Picture of the Catalysts – (a) CAT 1, (b) CAT 2, (c) CAT 3, (d) CAT 4

# 5 Measurement Results

## 5.1. DoE

The aim was to dissociate ammonia in an electrically heated reformer filled with different catalysts at different temperatures while measuring the residual ammonia concentration at the outlet. For this reason, the temperature was increased dynamically from 400 °C up to 900 °C for each measurement.

The base setting for the measurements was chosen, regarding the gas hourly space velocity (GHSV written as SV in the following document) a state of the art AVL natural gas reformer would have, if it was operated with ammonia instead of natural gas at the same calorific power. The SV of this reformer would be 1300 $h^{-1}$. M. Wang [23] performed ammonia reforming tests with a similar SV of 1320 $h^{-1}$ with a reactor volume of 0,05 l. The similarity to the basic space velocity made this result a benchmark for the reformer test. In Table 5 a linear interpolation starting at the 0,05 l reformer from M. Wang, up to the natural gas reformer of the company AVL is shown. To realise this interpolation the $NH_3$ feed, the AVL natural gas reformer plus SOFC would need to produce 6 kW electrical power, was calculated based on the values shown in Table 6. The result of this estimation was an $NH_3$ feed of 55,4 Nl/min. This resulted, based on the direct comparison with the 0,05 l reactor, in a reactor volume of 2,52 l. The test reformer that was used for the reformer test was 5 times smaller and had 0,5 l. The linear interpolation for this reactor volume is also shown in Table 5.

Table 5: Estimation for DoE based on literature – In the following table the reference values out of a literature source are shown with two compared estimations. One estimation assumes that 12 kW $NH_3$ for our SOFC Stack is needed, and the other estimation is based on the actual reactor volume of 0,5 l of our test reactor. The calculation beneath shows how the $NH_3$ feed to reach 12 kW energy with $NH_3$ was determined.

| | factor 1 | | factor 10 | | factor 50 | |
|---|---|---|---|---|---|---|
| | Dates from Paper [23] | | Estimation Basis 0,5l Reactor Volume | | Estimation Basis 55,4 Nl/min $NH_3$ Feed | |
| reformer volume | 0,05 | $dm^3$ | 0,50 | $dm^3$ | 2,52 | $dm^3$ |
| $NH_3$ feed | 1,1 | Nl/min | 11 | Nl/min | 55,4 | Nl/min |
| $NH_3$ conversion | 99,9 | % | 99,9 | % | 99,9 | % |
| $H_2$ yielding rate | 1,7 | Nl/min | 16,5 | Nl/min | 83,1 | Nl/min |
| estim. el. power | 158 | W | 1580 | W | 7958 | W |
| cracking temp. | 600 | °C | 600 | °C | 600 | °C |
| face velocity | 88 | cm/s | 88 | cm/s | 88 | cm/s |
| space velocity | 1320 | $h^{-1}$ | 1320 | $h^{-1}$ | 1320 | $h^{-1}$ |
| $N_2/H_2$ product gas(600°C) | 6,5 | Nl/min | 64,5 | Nl/min | 324,6 | Nl/min |

Table 6: Estimated $NH_3$ Feed – The shown values from the database of the VDI [24] were used to estimate the $NH_3$ consumption a state of the art natural gas reformer of the company AVL would have to produce 6 kW electrical power out of 10 kW ammonia. To be on the safe side 2 kW were added for all the unexpected energy losses. In total the ammonia flow rate to carry 12 kW of energy was determined to be 55,4 Nl/min.

| Given Values | | | Result | | |
|---|---|---|---|---|---|
| heating value of $NH_3$ | 5,2 | kWh/kg | $NH_3$ Feed | 55,4 | Nl/min |
| density of $NH_3$ at 25°C | 0,6942 | $kg/m^3$ | | | |
| needed power | 12 | kW $NH_3$ | | | |

Knowing these findings, a Design of Experiment (DoE) was chosen to investigate a range of different SVs above and below the base SV of 1320 $h^{-1}$. The limiting factor was the heat input from the reformer. It turned out that 1920 $h^{-1}$ is the highest SV the reformer can handle and therefore a symmetric range from 720 $h^{-1}$ to 1920 $h^{-1}$ was set. Additionally, to the measurements with 100 vol% dry $NH_3$, 20 vol% of steam was added for moist measurements. That means all together 3 different catalysts (+ 1 bonus catalyst) where investigated, in each case 3 dry and 3 moist measurements. Originally it was planned to investigate 4 different catalysts. But during the first measurements a lot of unexpected problems occurred, what made the results of the first catalyst unusable. Just two test measurements of this catalyst delivered useful datasets,

therefore the decision was made to use these two measurements as bonus, even though their SV differed to the others. An overview of the DoE is shown in Table 7.

Table 7: Design of Experiment – Overview of all measured parameters. The space velocity is always referred to a 100 % $NH_3$ feed and calculated based on the reformer volume of 0,5 l. During the moist measurements 20 vol % of steam was added to the dry $NH_3$ stream what led to a 20 % higher space velocity for moist measurements.

| | Catalysts | | | | | | | |
|---|---|---|---|---|---|---|---|---|
| | Cat 1 | | Cat 2 | | Cat 3 | | Cat 4 (Bonus) | |
| $NH_3$ SV [$h^{-1}$] | dry (100 % $NH_3$) | moist (+ 20 % $H_2O$) | dry (100 % $NH_3$) | moist (+ 20 % $H_2O$) | dry (100 % $NH_3$) | moist (+ 20 % $H_2O$) | dry (100 % $NH_3$) | moist (+ 20 % $H_2O$) |
| 720 | 720 $h^{-1}$ | 864 $h^{-1}$ | 720 $h^{-1}$ | 864 $h^{-1}$ | 720 $h^{-1}$ | 864 $h^{-1}$ | 492 $h^{-1}$ | 590 $h^{-1}$ |
| 1320 | 1320 $h^{-1}$ | 1584 $h^{-1}$ | 1320 $h^{-1}$ | 1584 $h^{-1}$ | 1320 $h^{-1}$ | 1584 $h^{-1}$ | | |
| 1920 | 1920 $h^{-1}$ | 2304 $h^{-1}$ | 1920 $h^{-1}$ | 2304 $h^{-1}$ | 1920 $h^{-1}$ | 2304 $h^{-1}$ | | |

## 5.2. Results

In this chapter the results of the measurements are presented. The discussion of these results is done in Chapter 6 separately. Due to the fact, that the catalyst was filled by hand into the reformer and because of the specific reformer design, it was not always possible to fill the whole tube completely. These inaccuracies and the changes of the SV derived from the changes of catalyst volume, are displayed in a table of each individual reformer section.

Each measurement is presented in a separate plot (Figure Figure 11 - Figure 30). The first diagram of each plot shows the FTIR measurement of the $NH_3$ concentration after the reformer, based on the temperature T9 at the end of the reformer. The second diagram shows the $NO_x$ concentration and additionally the $H_2O$ concentration for moist measurements, also based on temperature T9. And the third diagram shows the course of all temperature sensors during the measurement. The x-axes of the last plot also shows how long it took to reach the final temperatures. The measurements were taken for the temperature range of 400 °C to 900 °C. During the measurements the temperature inside the reformer was increased steadily until the highest possible temperature was reached.

### 5.2.1. Catalyst 1

Table 8: Specification of the Catalyst CAT 1 – The pellets of this catalyst were originally too large to fit into the reformer tube and therefore had to be crushed. The low filling volume of 0,3 l of this catalyst shows, even with the crushed catalyst, that it was hard to fill the whole reformer. Therefore, the SVs are higher than the calculated SV based on the reformer volume of 0,5 l. A more detailed description of the chemical composition of the catalyst is given in Table 4. The weight of the used catalyst was measured before and after the test.

| CAT 1 | | | | | |
|---|---|---|---|---|---|
| catalyst | | | reformer | | |
| volume: | 0,3 | l | volume: | 0,5 | l |
| weight: | | | | | |
| before | 394,3 | g | | | |
| after | 380,6 | g | | | |
| dry (100% $NH_3$) | | | moist (+20% $H_2O$) | | |
| feed flow rate | SV reformer | SV real | feed flow rate | SV reformer | SV real |
| [l/h] | [$h^{-1}$] | [$h^{-1}$] | [l/h] | [$h^{-1}$] | [$h^{-1}$] |
| 360 | 720 | 1200 | 432 | 864 | 1440 |
| 660 | 1320 | 2200 | 792 | 1584 | 2640 |
| 960 | 1920 | 3200 | 1152 | 2304 | 3840 |

CAT 1, SV 1200 $h^{-1}$, dry

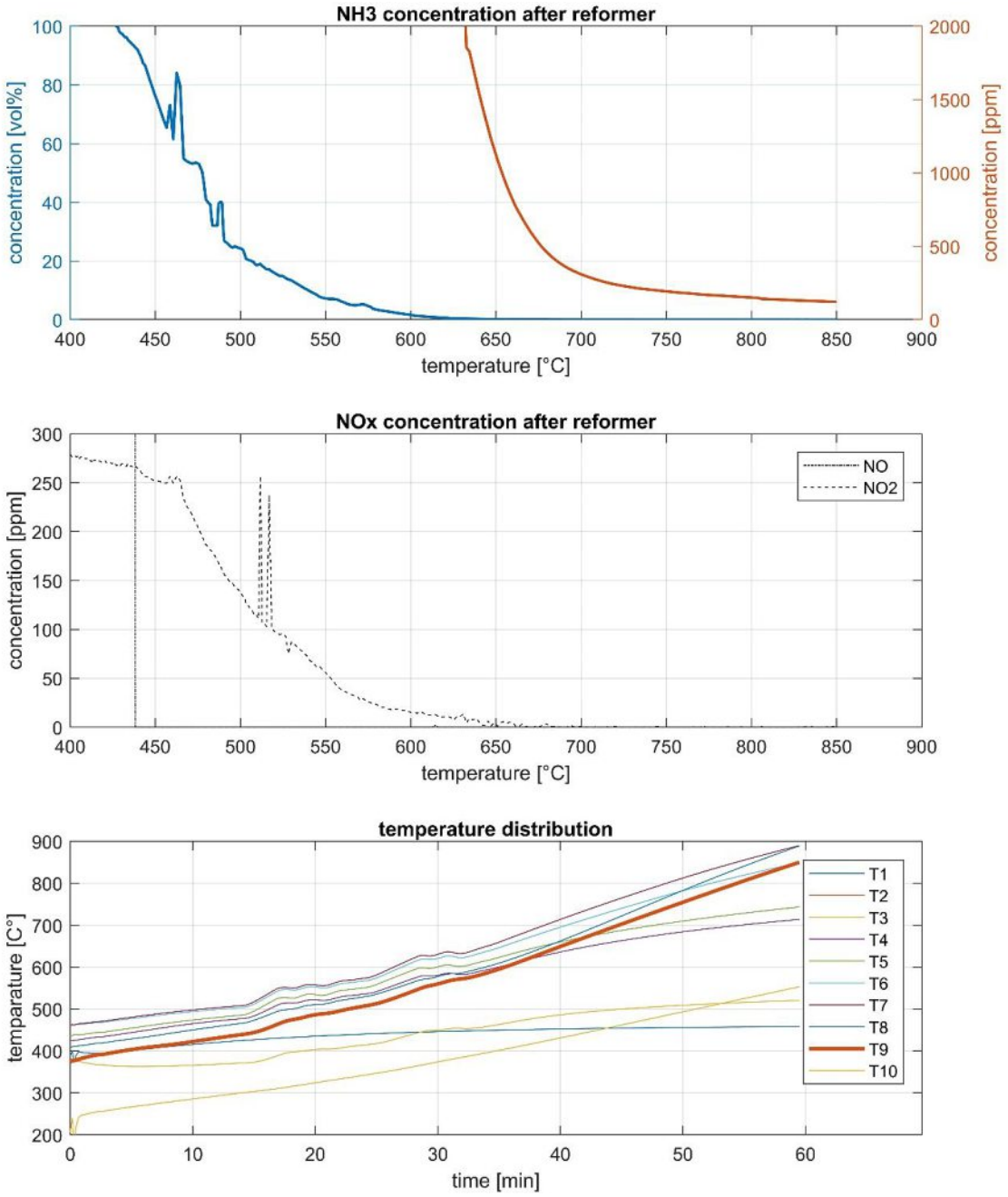


Figure 11: CAT 1, SV 1200 $h^{-1}$, dry – All fluctuations of the $NH_3$ curve above 20 % can be explained by measurement inaccuracies, caused by excess of the calibrated range. The used FTIR was calibrated for 0 – 10 vol% of $NH_3$ gas. T9 represents the last temperature measurement at the end of the $NH_3$ reformer and was used as reference temperature for the plots.

CAT 1, SV 1440 $h^{-1}$, moist

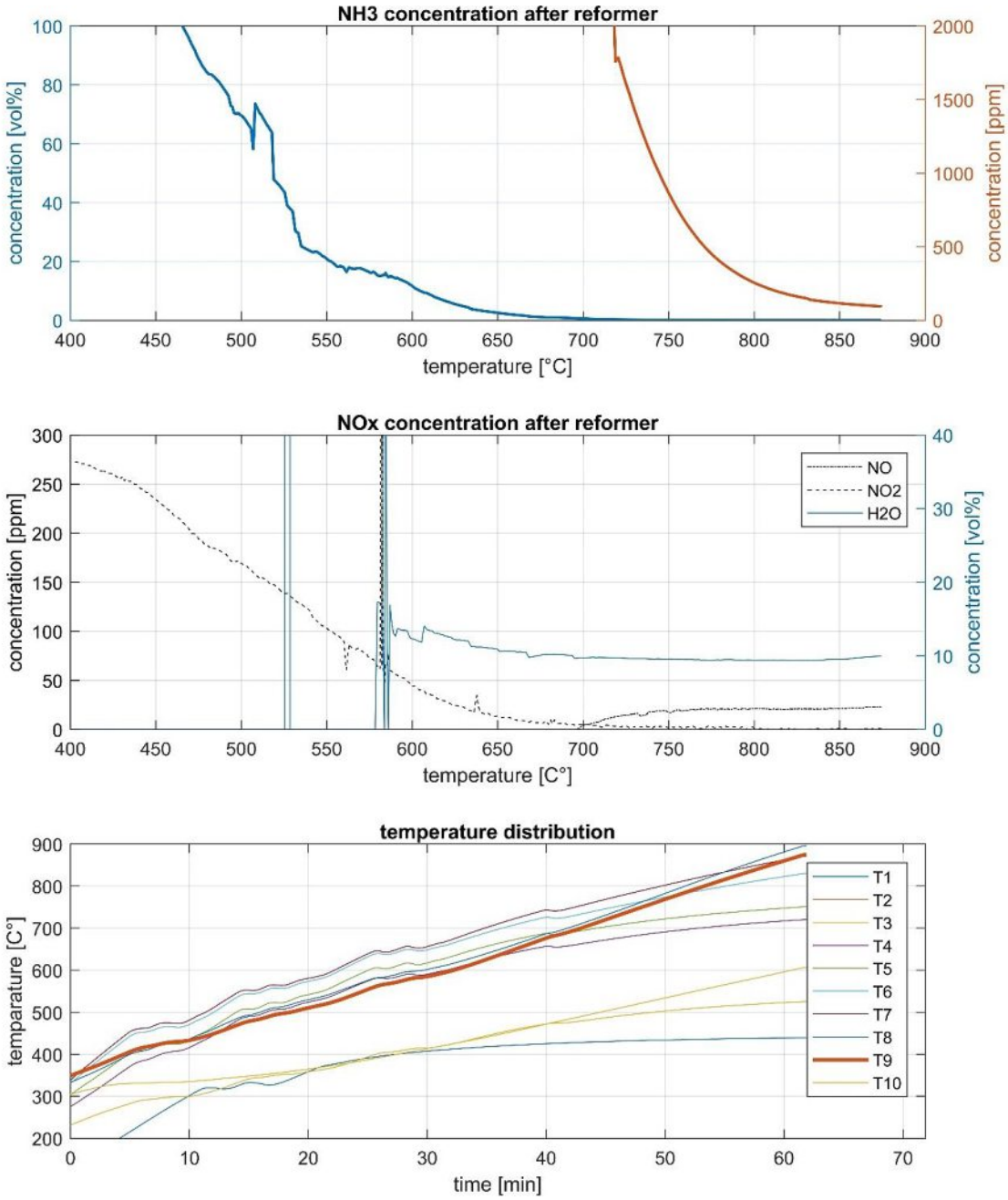


Figure 12: CAT 1, SV 1440 $h^{-1}$, moist – All fluctuations of the $NH_3$ curve above 20 % can be explained by measurement inaccuracies, caused by excess of the calibrated range. The used FTIR was calibrated for 0 – 10 vol% of $NH_3$ gas. The $H_2O$ curve also started to be representative from the moment $NH_3$ was below 15 %, every movement before can be ignored. T9 represents the last temperature measurement at the end of the $NH_3$ reformer and was used as reference temperature for the plots.

CAT 1, SV 2200 $h^{-1}$, dry

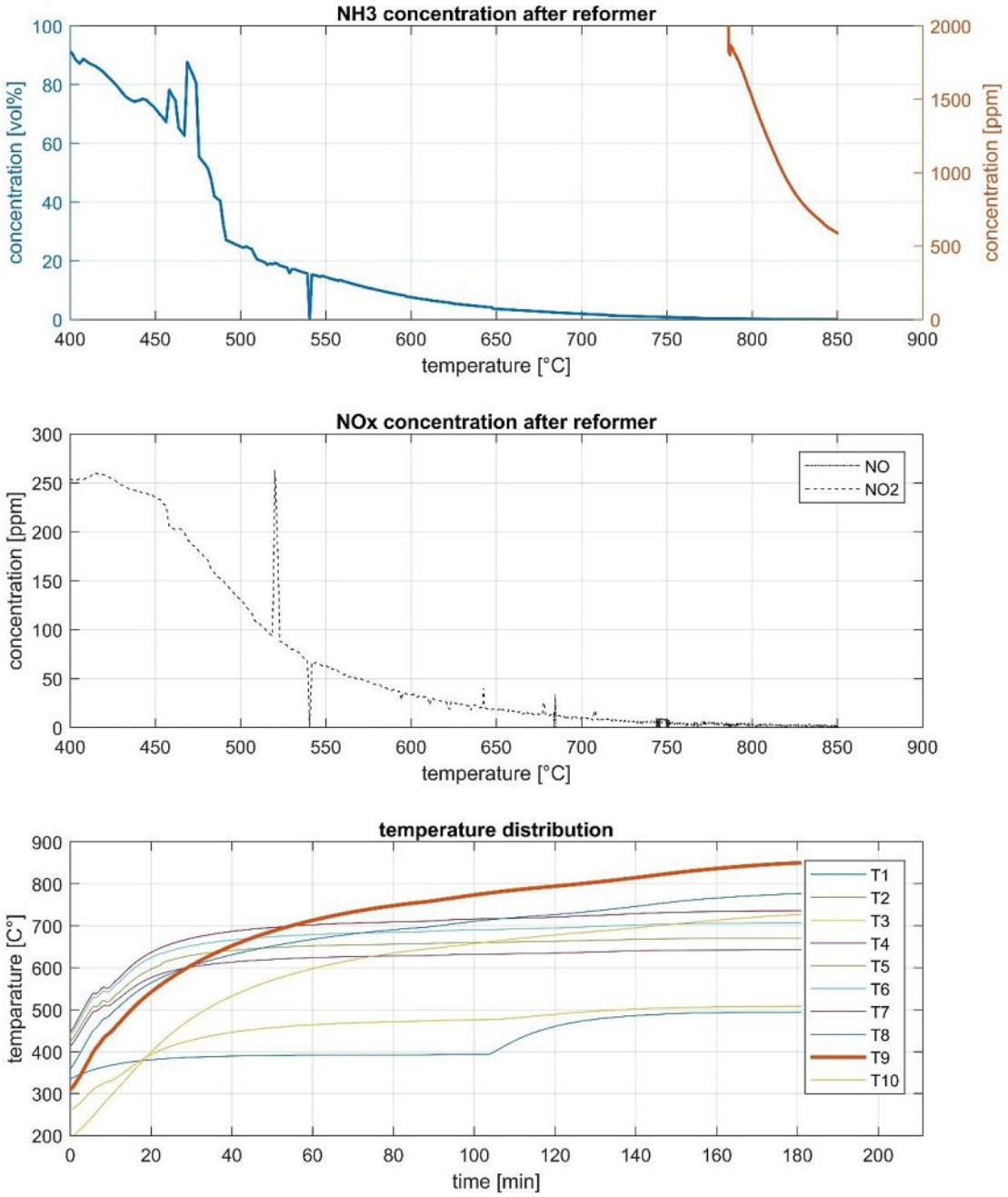


Figure 13: CAT 1, SV 2200 $h^{-1}$, dry – All fluctuations of the $NH_3$ curve above 20 % can be explained by measurement inaccuracies, caused by excess of the calibrated range. The used FTIR was calibrated for 0 – 10 vol% of $NH_3$ gas. T9 represents the last temperature measurement at the end of the $NH_3$ reformer and was used as reference temperature for the plots.

CAT 1, SV 2640 $h^{-1}$, moist

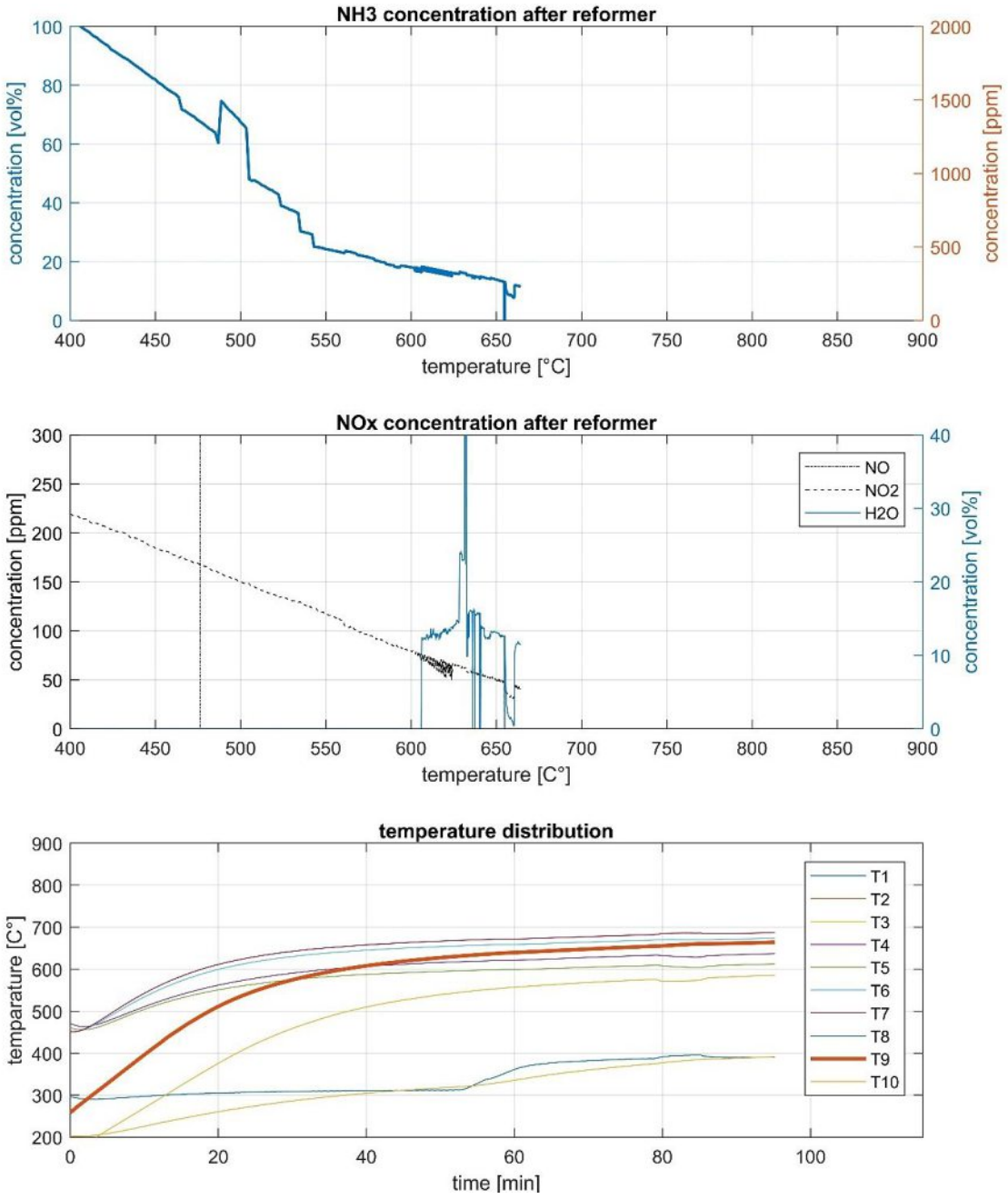


Figure 14: CAT 1, SV 2640 $h^{-1}$, moist – All fluctuations of the $NH_3$ curve above 20 % can be explained by measurement inaccuracies, caused by excess of the calibrated range. The used FTIR was calibrated for 0 – 10 vol% of $NH_3$ gas. The $H_2O$ curve also started to be representative from the moment $NH_3$ was below 15 %, every movement before can be ignored. T9 represents the last temperature measurement at the end of the $NH_3$ reformer and was used as reference temperature for the plots.

CAT 1, SV 3200 $h^{-1}$, dry

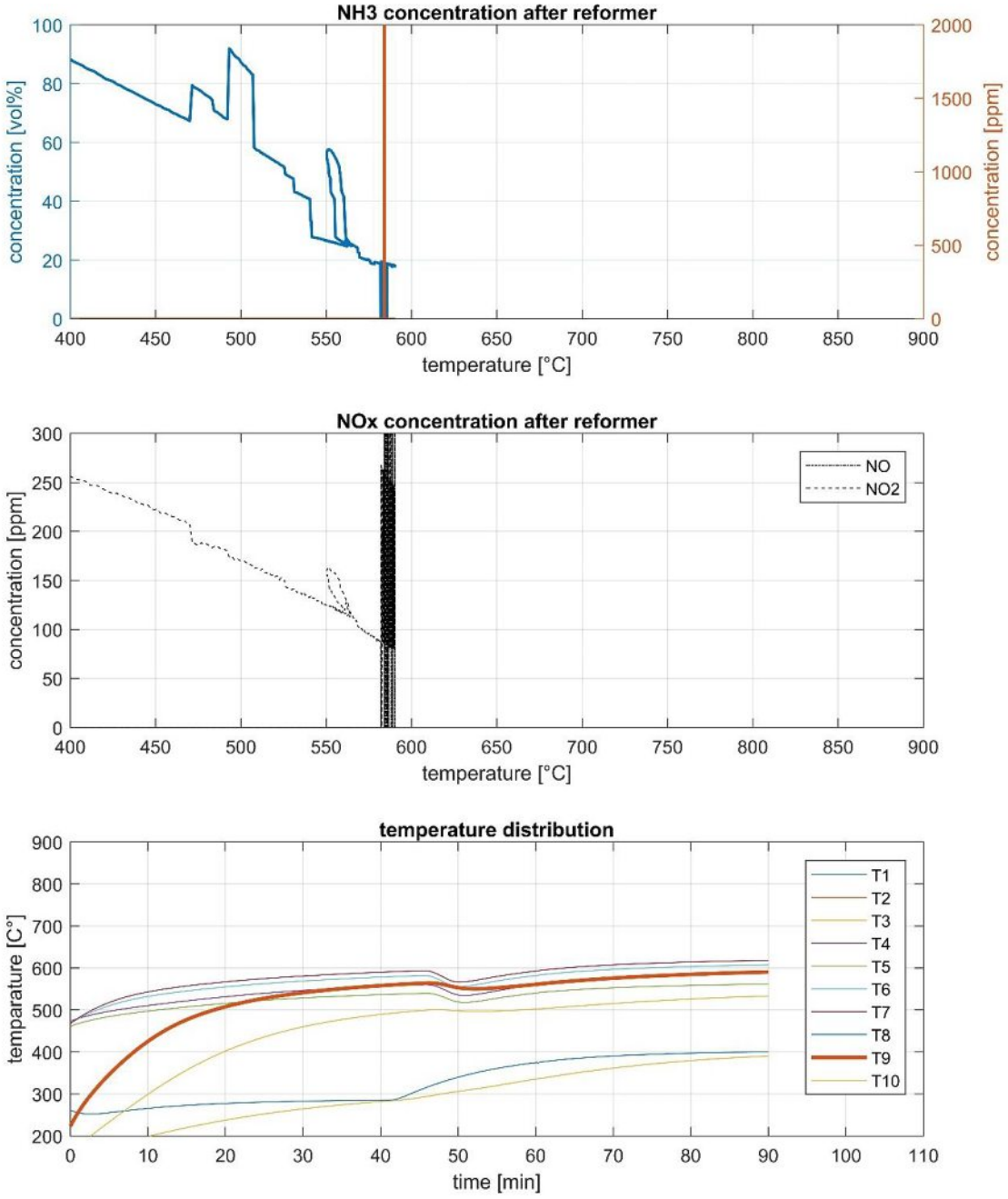


Figure 15: CAT 1, SV 3200 $h^{-1}$, dry – All fluctuations of the $NH_3$ curve above 20 % can be explained by measurement inaccuracies, caused by excess of the calibrated range. The used FTIR was calibrated for 0 – 10 vol% of $NH_3$ gas. T9 represents the last temperature measurement at the end of the $NH_3$ reformer and was used as reference temperature for the plots.

CAT 1, SV 3840 $h^{-1}$, moist

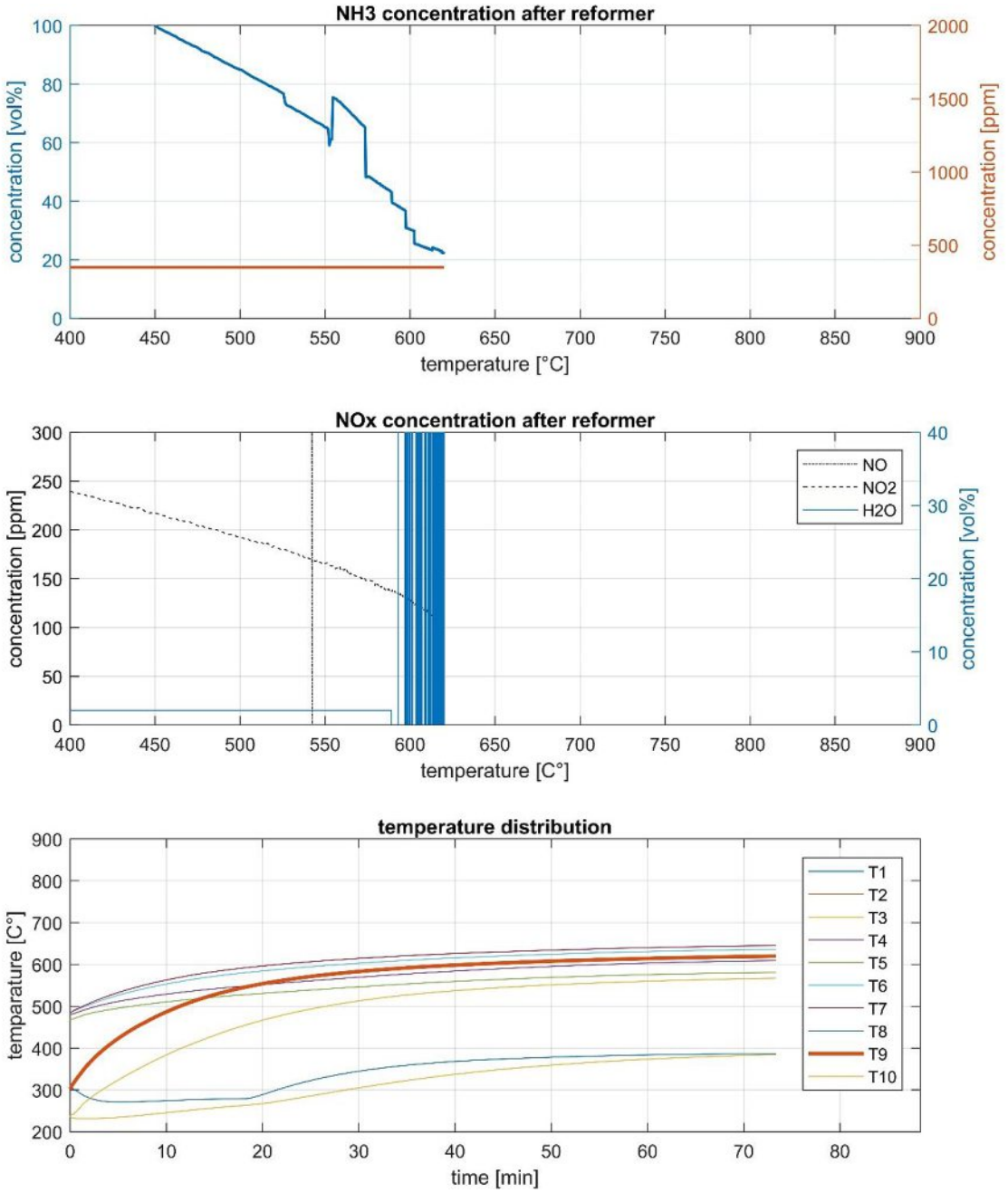


Figure 16: CAT 1, SV 3840 $h^{-1}$, moist – All fluctuations of the $NH_3$ curve above 20 % can be explained by measurement inaccuracies, caused by excess of the calibrated range. The used FTIR was calibrated for 0 – 10 vol% of $NH_3$ gas. The $H_2O$ curve also started to be representative from the moment $NH_3$ was below 15 %, every movement before can be ignored. T9 represents the last temperature measurement at the end of the $NH_3$ reformer and was used as reference temperature for the plots.

### 5.2.2. Catalyst 2

Table 9: specification of the catalyst Cat 2 – Different to the first catalyst the pellets of the Cat 2 were a lot smaller and therefore it was a lot easier to fill the reactor tube. That is why the real SVs based on the actual catalyst volume do not differ too much from the SVs based on the reformer volume. A more detailed description about the chemical structure of the catalyst is given in Table 4. The weight of the used catalyst was measured before and after the tests.

| Cat 2 | | | | | |
|---|---|---|---|---|---|
| catalyst | | | reformer | | |
| volume: | 0,45 | l | volume: | 0,5 | l |
| weigh: | | | | | |
| before | 389,2 | g | | | |
| after | 383,1 | g | | | |
| dry (100% $NH_3$) | | | moist (+20% $H_2O$) | | |
| feed flow rate | SV reformer | SV real | feed flow rate | SV reformer | SV real |
| [l/h] | [$h^{-1}$] | [$h^{-1}$] | [l/h] | [$h^{-1}$] | [$h^{-1}$] |
| 360 | 720 | 800 | 432 | 864 | 960 |
| 660 | 1320 | 1467 | 792 | 1584 | 1760 |
| 960 | 1920 | 2133 | 1152 | 2304 | 2560 |

CAT 2, SV 800 $h^{-1}$, dry

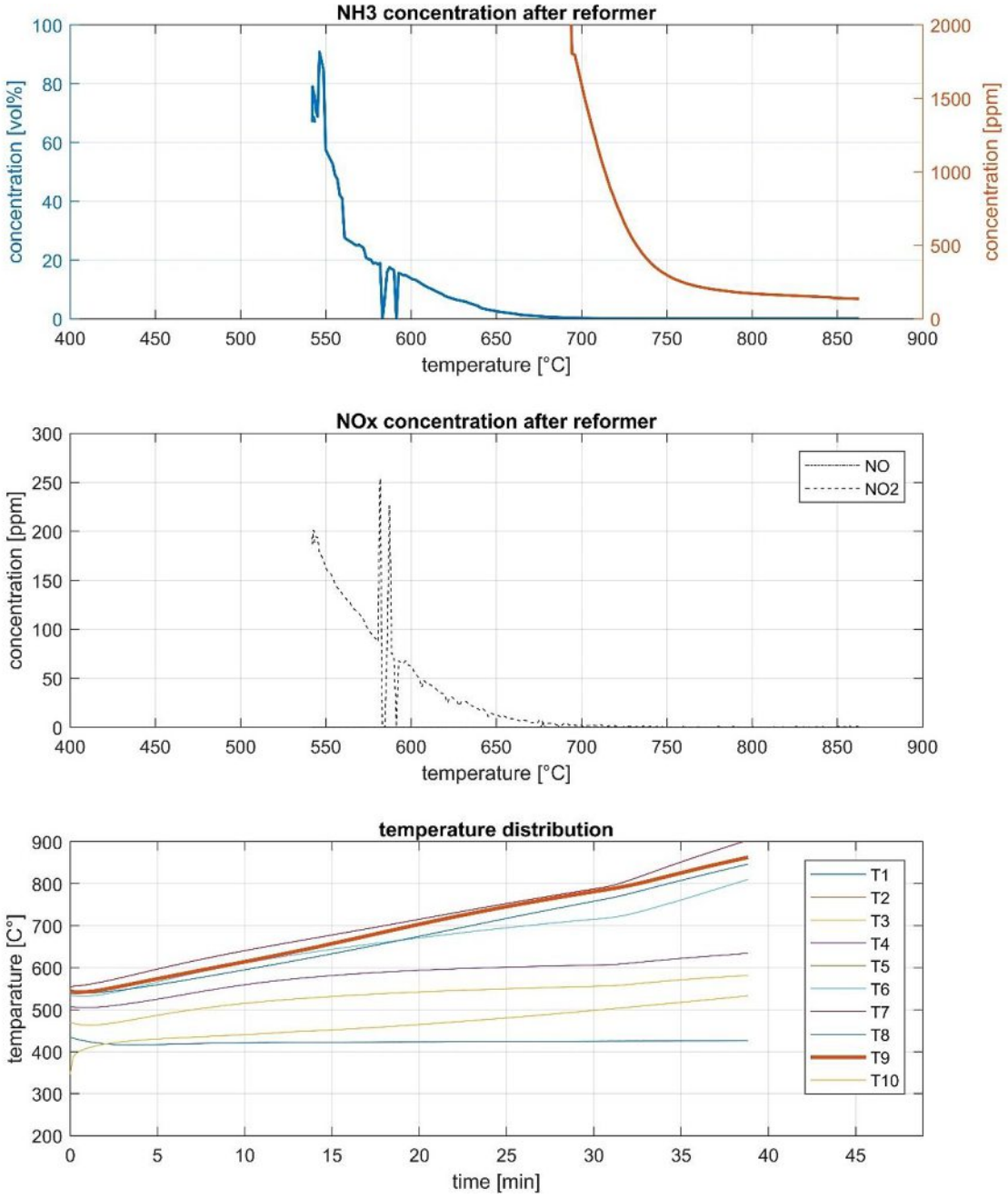


Figure 17: CAT 2, SV 800 $h^{-1}$, dry – All fluctuations of the $NH_3$ curve above 20 % can be explained by measurement inaccuracies, caused by excess of the calibrated range. The used FTIR was calibrated for 0 – 10 vol% of $NH_3$ gas. T9 represents the last temperature measurement at the end of the $NH_3$ reformer and was used as reference temperature for the plots.

CAT 2, SV 960 $h^{-1}$, moist

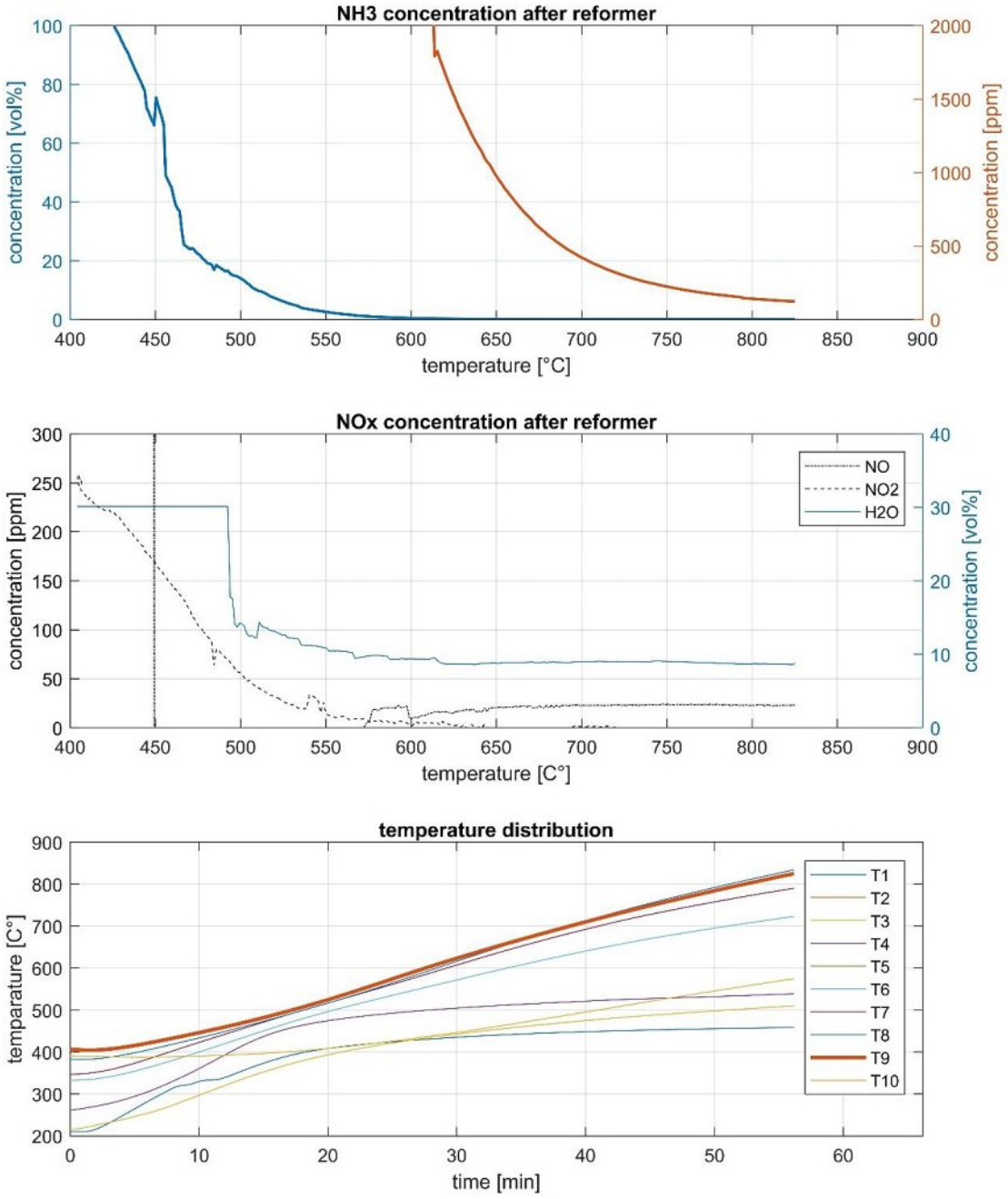


Figure 18: CAT 2, SV 960 $h^{-1}$, moist – All fluctuations of the $NH_3$ curve above 20 % can be explained by measurement inaccuracies, caused by excess of the calibrated range. The used FTIR was calibrated for 0 – 10 vol% of $NH_3$ gas. The $H_2O$ curve also started to be representative from the moment $NH_3$ was below 15 %, every movement before can be ignored. T9 represents the last temperature measurement at the end of the $NH_3$ reformer and was used as reference temperature for the plots.

CAT 2, SV 1467 $h^{-1}$, dry

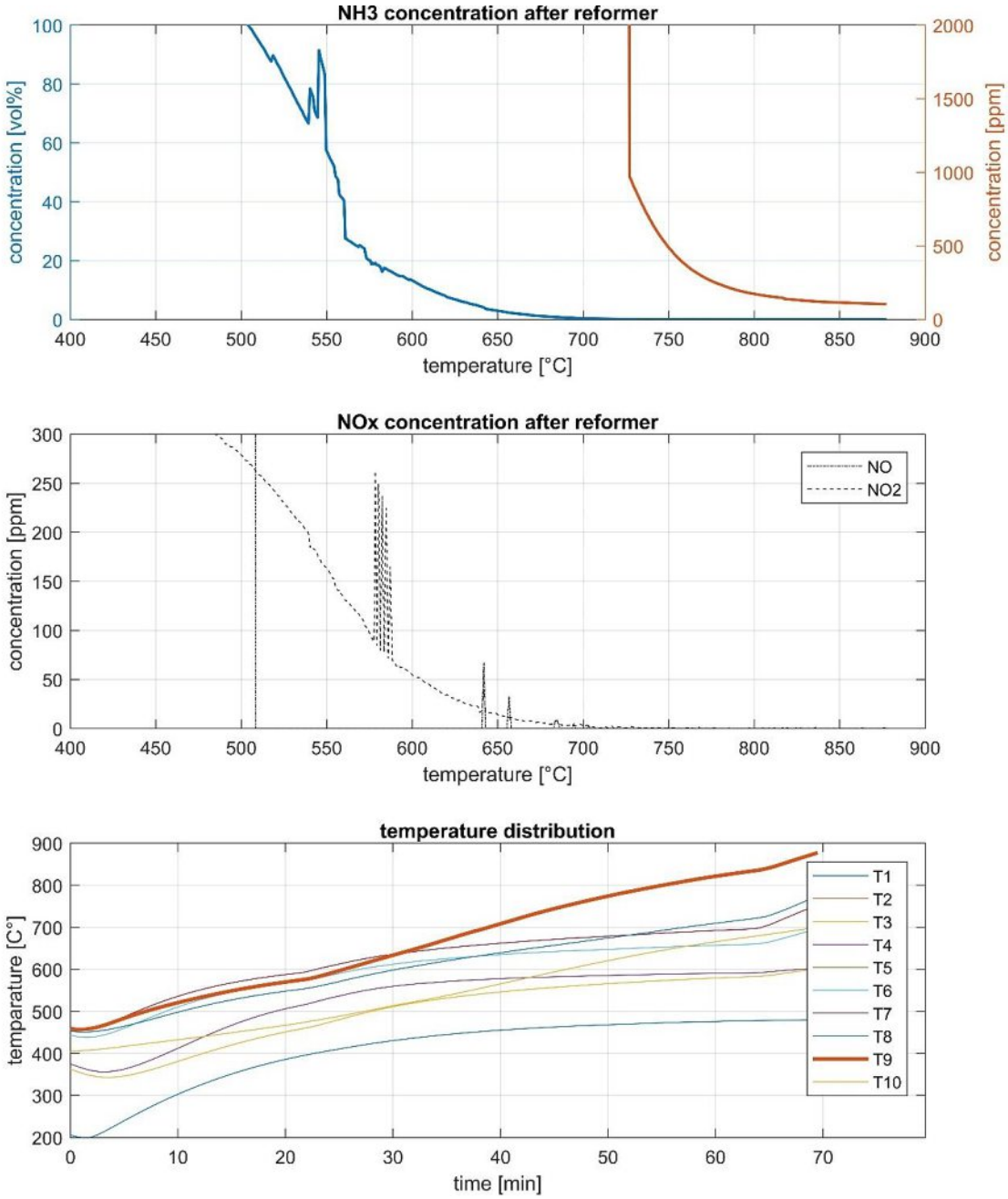


Figure 19: CAT 2, SV 1467 $h^{-1}$, dry – All fluctuations of the $NH_3$ curve above 20 % can be explained by measurement inaccuracies, caused by excess of the calibrated range. The used FTIR was calibrated for 0 – 10 vol% of $NH_3$ gas. T9 represents the last temperature measurement at the end of the $NH_3$ reformer and was used as reference temperature for the plots.

CAT 2, SV 1760 $h^{-1}$, moist

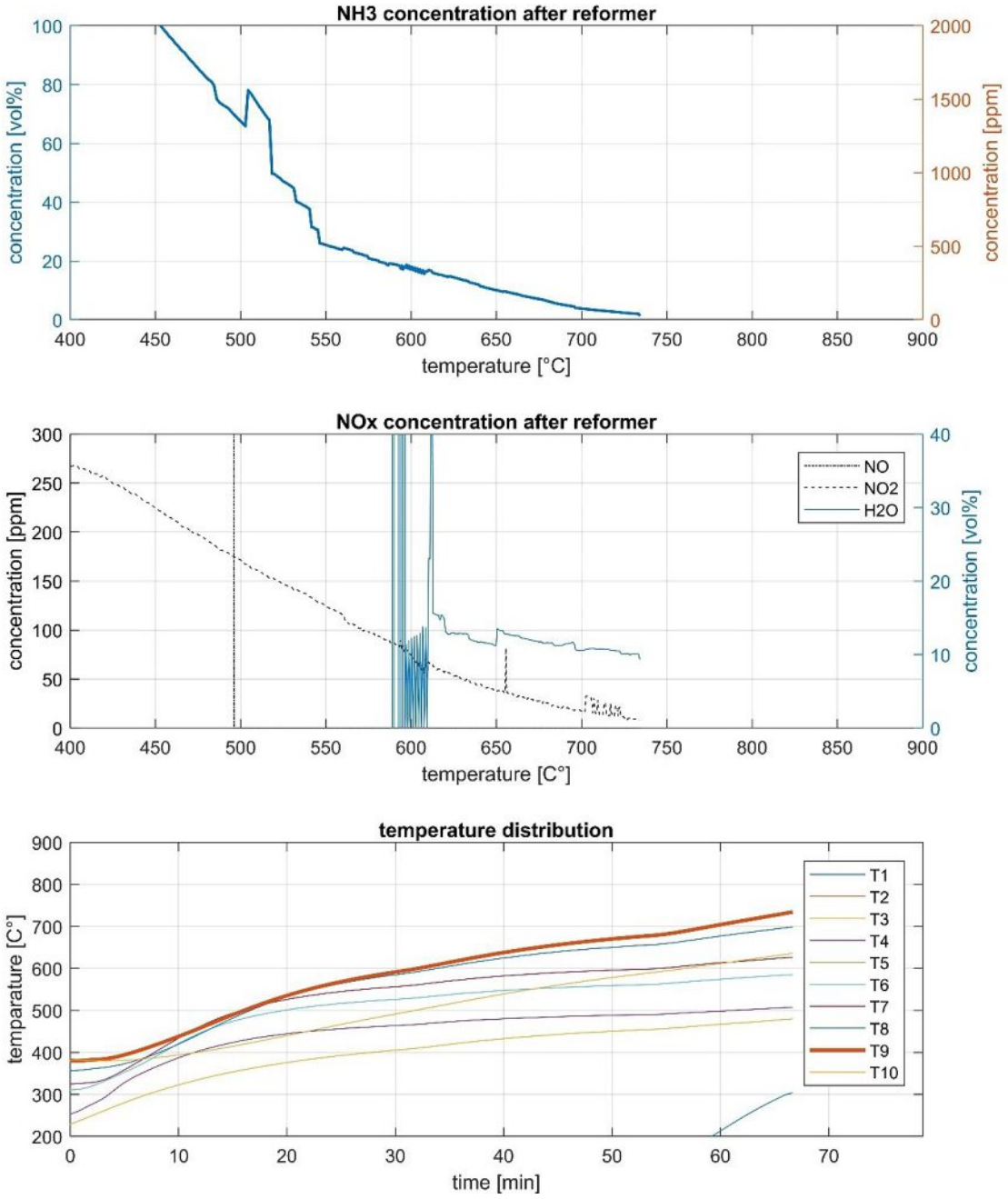


Figure 20: CAT 2, SV 1760 $h^{-1}$, moist – All fluctuations of the $NH_3$ curve above 20 % can be explained by measurement inaccuracies, caused by excess of the calibrated range. The used FTIR was calibrated for 0 – 10 vol% of $NH_3$ gas. The $H_2O$ curve also started to be representative from the moment $NH_3$ was below 15 %, every movement before can be ignored. T9 represents the last temperature measurement at the end of the $NH_3$ reformer and was used as reference temperature for the plots.

CAT 2, SV 2133 $h^{-1}$, dry

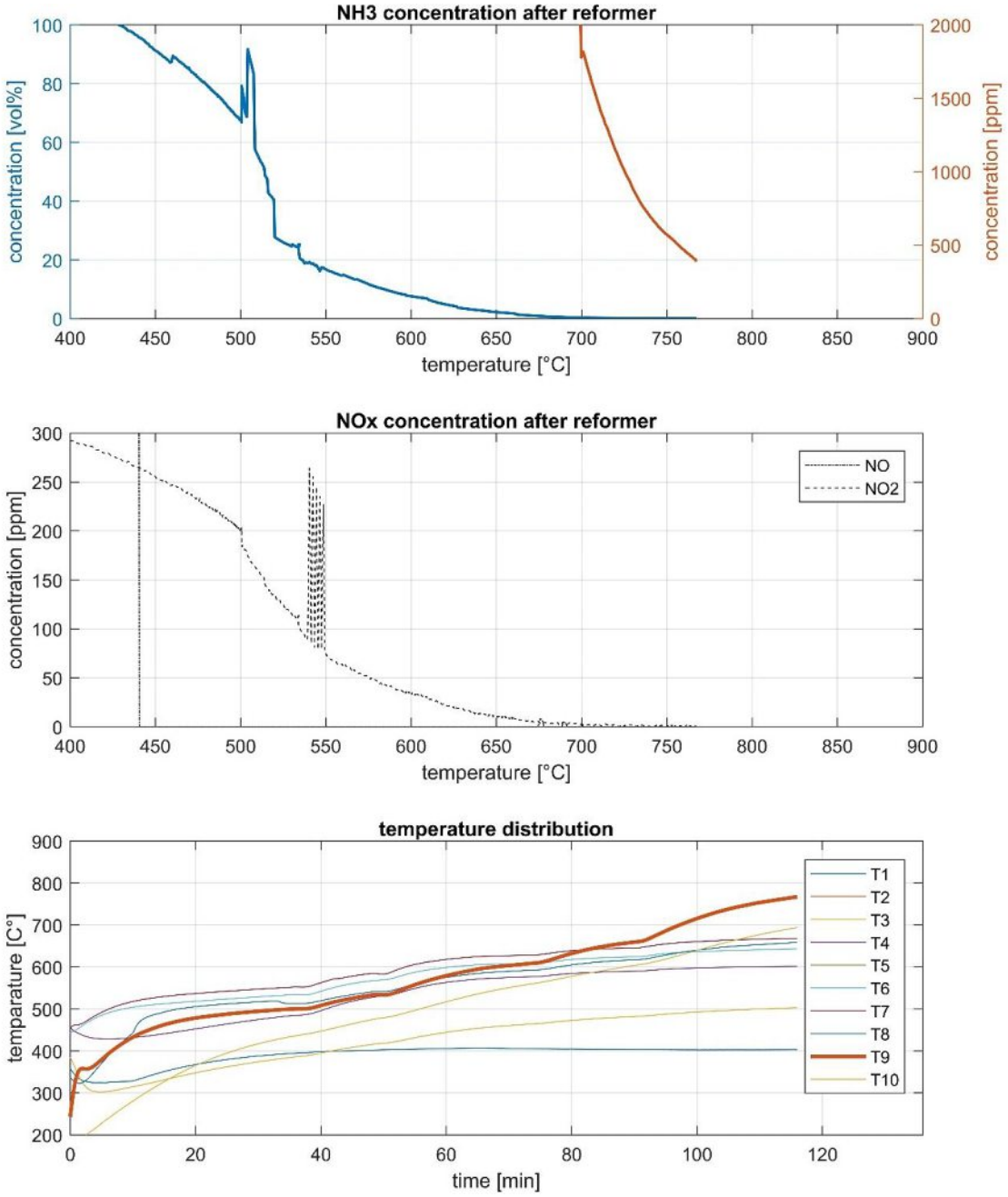


Figure 21: CAT 2, SV 2133 $h^{-1}$, dry – All fluctuations of the $NH_3$ curve above 20 % can be explained by measurement inaccuracies, caused by excess of the calibrated range. The used FTIR was calibrated for 0 – 10 vol% of $NH_3$ gas. T9 represents the last temperature measurement at the end of the $NH_3$ reformer and was used as reference temperature for the plots.

CAT 2, SV 2560 $h^{-1}$, moist

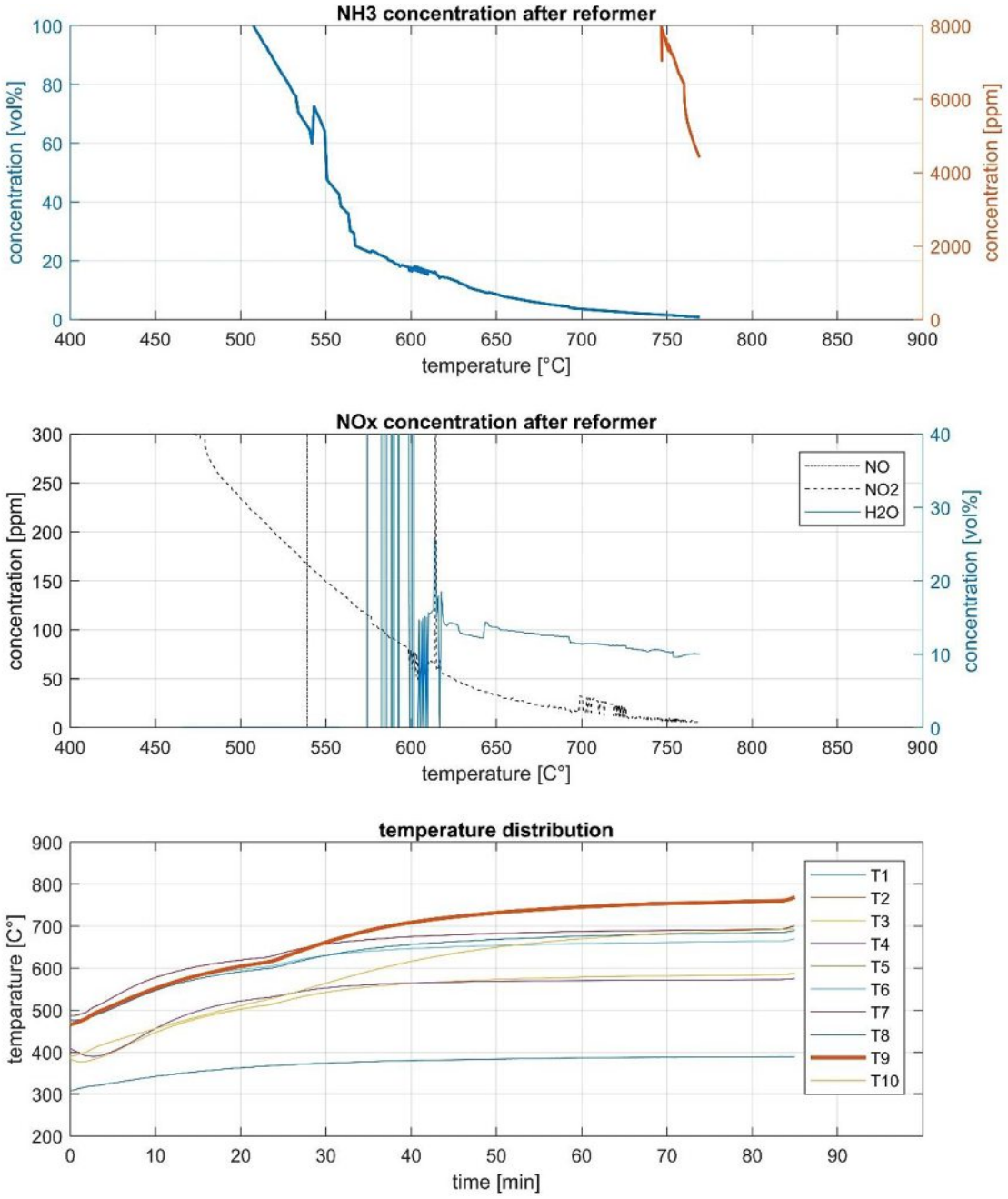


Figure 22: CAT 2, SV 2560 $h^{-1}$, moist – All fluctuations of the $NH_3$ curve above 20 % can be explained by measurement inaccuracies, caused by excess of the calibrated range. The used FTIR was calibrated for 0 – 10 vol% of $NH_3$ gas. The $H_2O$ curve also started to be representative from the moment $NH_3$ was below 15 %, every movement before can be ignored. T9 represents the last temperature measurement at the end of the $NH_3$ reformer and was used as reference temperature for the plots.

### 5.2.3. Catalyst 3

Table 10: specification of the catalyst CAT 3 – With this catalysator it was possible to fill the reformer tube completely. Because of that the real SV does not differ from the SV based on the reformer volume. The missing weight of the catalyst before the measurements can be explained with a mistake that happened. Unfortunately, it is not possible to determine the weight of the catalyst in hindsight. A more detailed description about the chemical structure of the catalyst is given in Table 4.

| CAT 3 | | | | | |
|---|---|---|---|---|---|
| catalyst | | | reformer | | |
| volume: | 0,5 | l | volume: | 0,5 | l |
| weigh: | | | | | |
| before | - | g | | | |
| after | 331,5 | g | | | |
| dry (100% $NH_3$) | | | moist (+20% $H_2O$) | | |
| feed flow rate | SV reformer | SV real | feed flow rate | SV reformer | SV real |
| [l/h] | [$h^{-1}$] | [$h^{-1}$] | [l/h] | [$h^{-1}$] | [$h^{-1}$] |
| 360 | 720 | 720 | 432 | 864 | 864 |
| 660 | 1320 | 1320 | 792 | 1584 | 1584 |
| 960 | 1920 | 1920 | 1152 | 2304 | 2304 |

CAT 3, SV 720 $h^{-1}$, dry

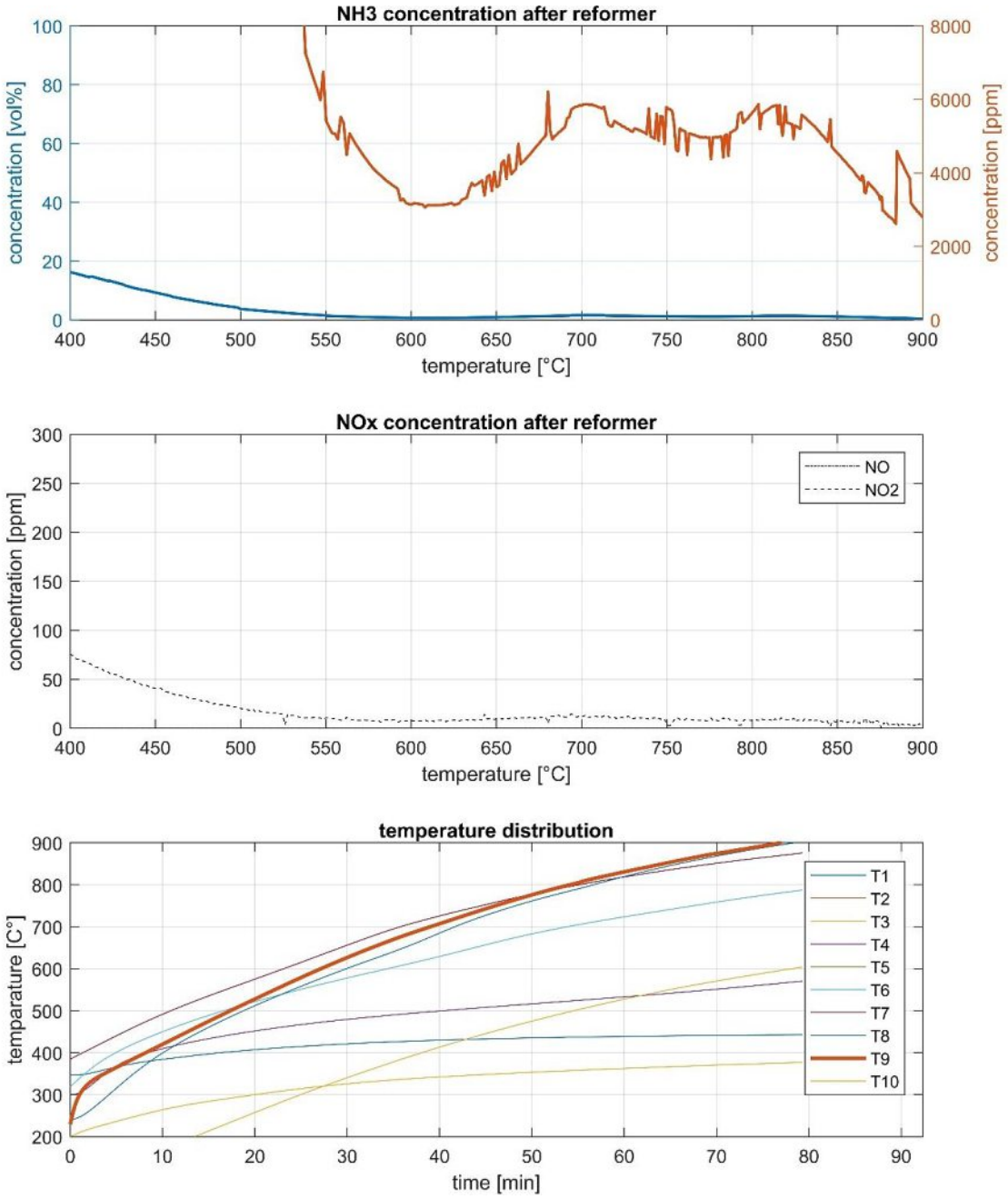


Figure 23: CAT 3, SV 720 $h^{-1}$, dry – All fluctuations of the $NH_3$ curve above 20 % can be explained by measurement inaccuracies, caused by excess of the calibrated range. The used FTIR was calibrated for 0 – 10 vol% of $NH_3$ gas. T9 represents the last temperature measurement at the end of the $NH_3$ reformer and was used as reference temperature for the plots.

CAT 3, SV 864 $h^{-1}$, moist

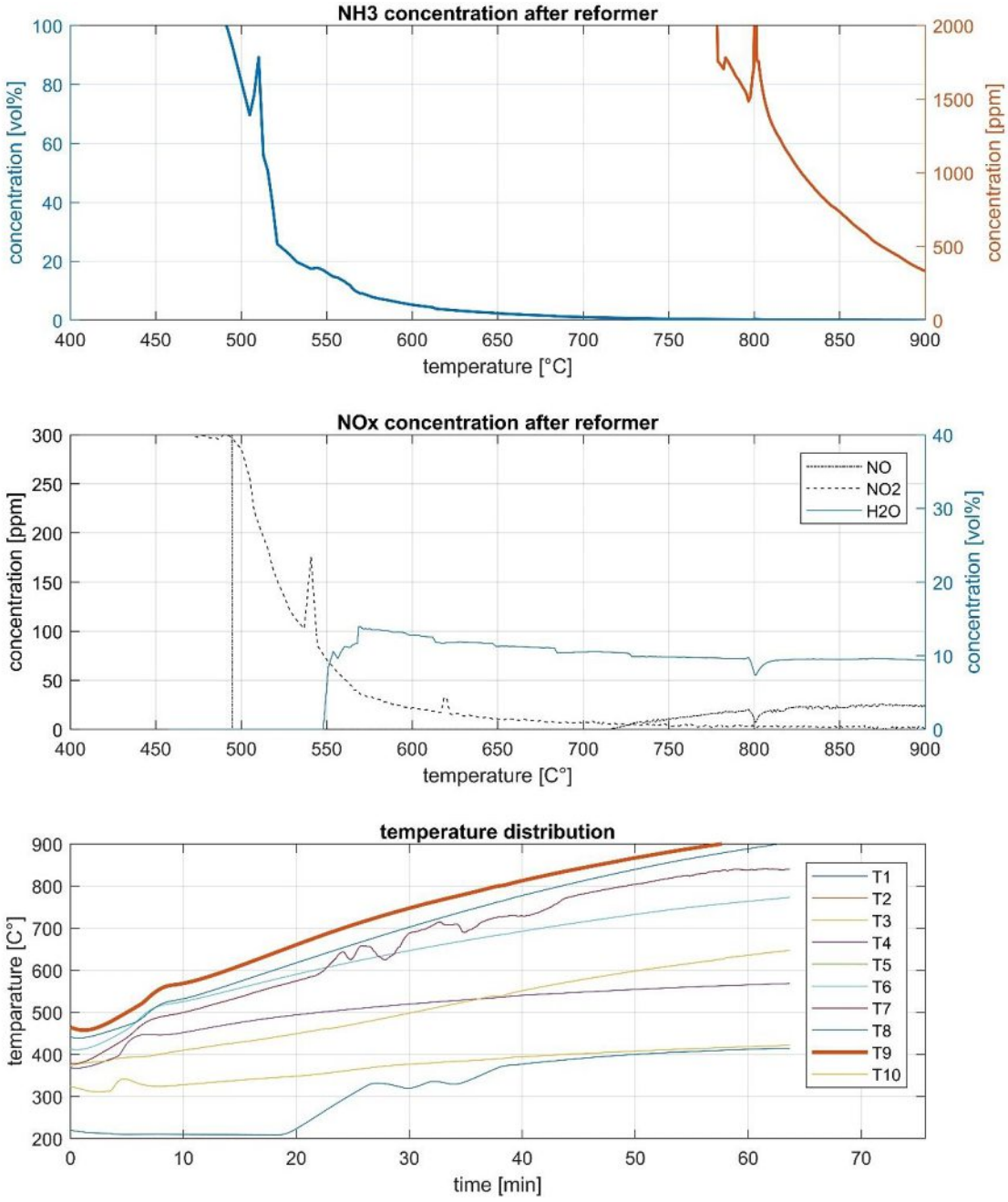


Figure 24: CAT 3, SV 864 $h^{-1}$, moist – All fluctuations of the $NH_3$ curve above 20 % can be explained by measurement inaccuracies, caused by excess of the calibrated range. The used FTIR was calibrated for 0 – 10 vol% of $NH_3$ gas. The $H_2O$ curve also started to be representative from the moment $NH_3$ was below 15 %, every movement before can be ignored. T9 represents the last temperature measurement at the end of the $NH_3$ reformer and was used as reference temperature for the plots.

CAT 3, SV 1320 $h^{-1}$, dry

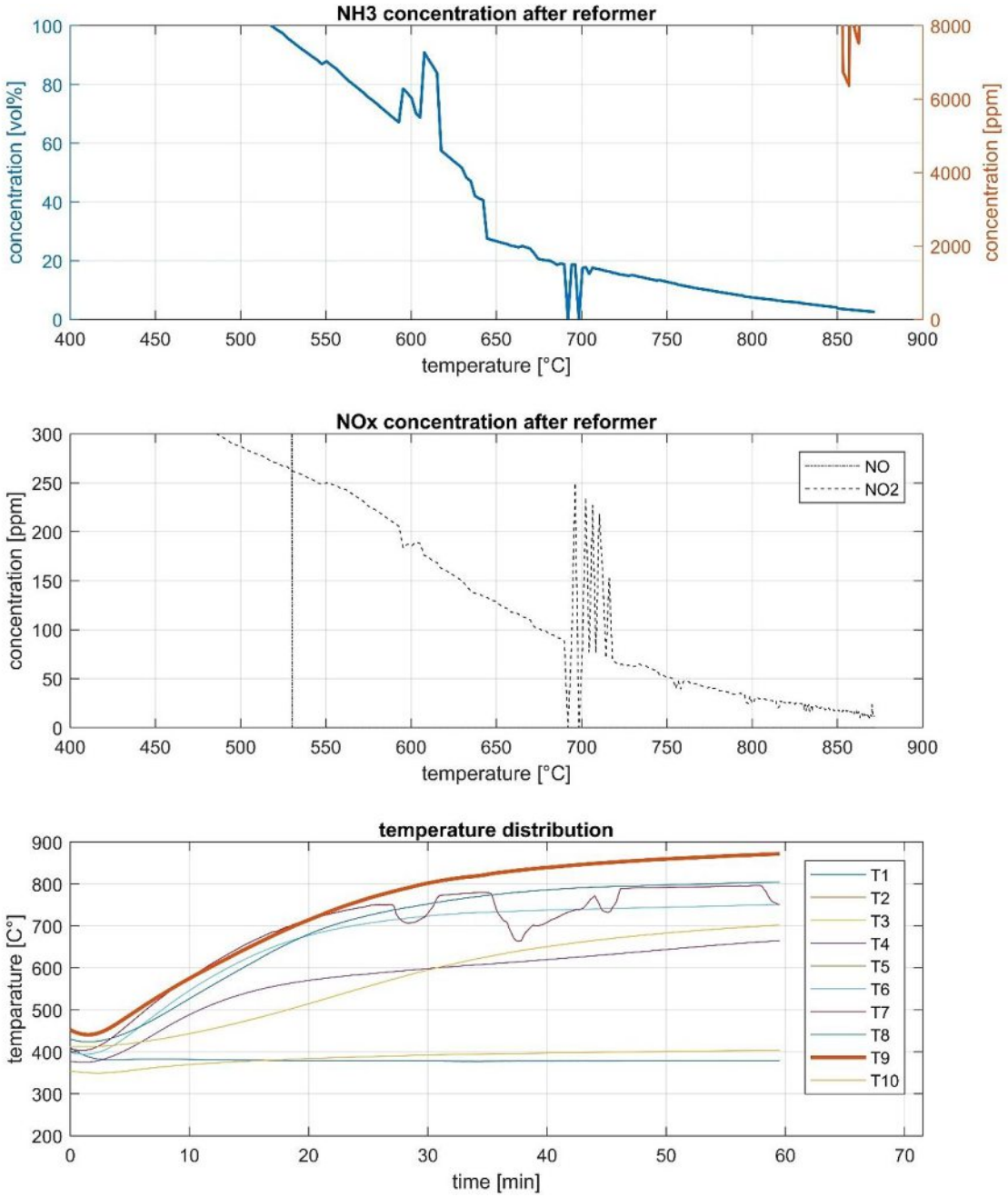


Figure 25: CAT 3, SV 1320 $h^{-1}$, dry – All fluctuations of the $NH_3$ curve above 20 % can be explained by measurement inaccuracies, caused by excess of the calibrated range. The used FTIR was calibrated for 0 – 10 vol% of $NH_3$ gas. T9 represents the last temperature measurement at the end of the $NH_3$ reformer and was used as reference temperature for the plots.

CAT 3, SV 1584 $h^{-1}$, moist

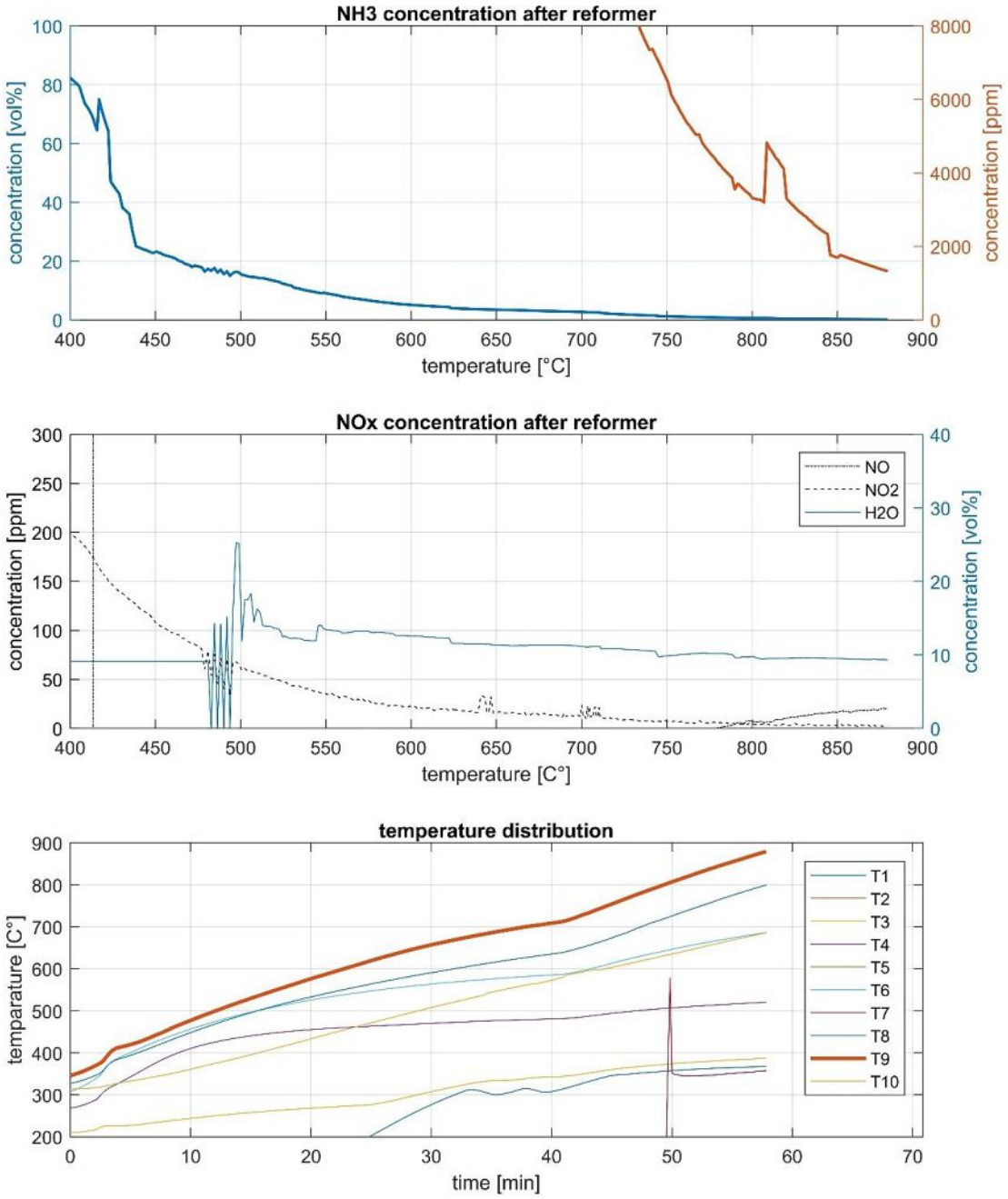


Figure 26: CAT 3, SV 1584 $h^{-1}$, moist – All fluctuations of the $NH_3$ curve above 20 % can be explained by measurement inaccuracies, caused by excess of the calibrated range. The used FTIR was calibrated for 0 – 10 vol% of $NH_3$ gas. The $H_2O$ curve also started to be representative from the moment $NH_3$ was below 15 %, every movement before can be ignored. T9 represents the last temperature measurement at the end of the $NH_3$ reformer and was used as reference temperature for the plots.

CAT 3, SV 1920 $h^{-1}$, dry

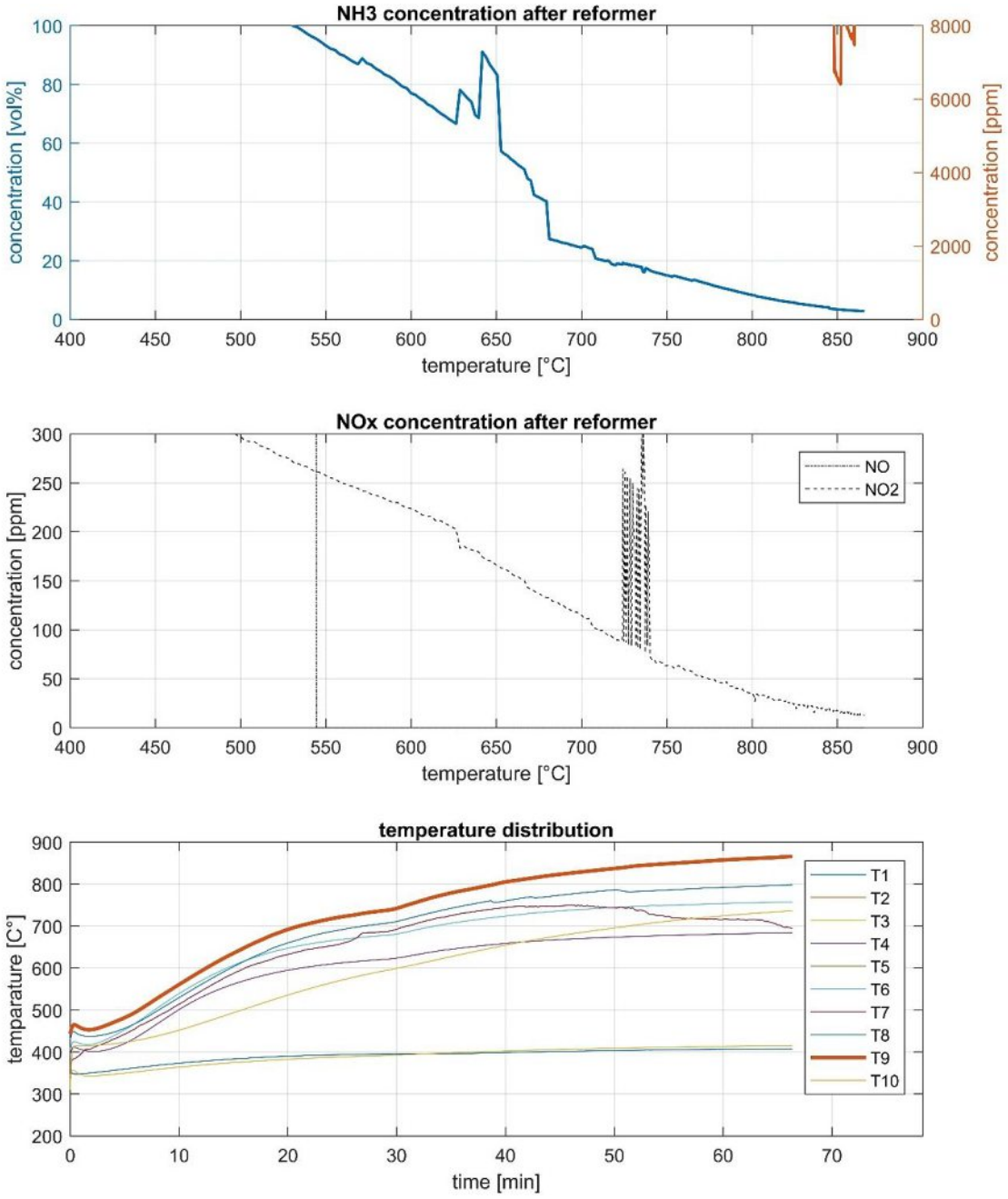


Figure 27: CAT 3, SV 1920 $h^{-1}$, dry – All fluctuations of the $NH_3$ curve above 20 % can be explained by measurement inaccuracies, caused by excess of the calibrated range. The used FTIR was calibrated for 0 – 10 vol% of $NH_3$ gas. T9 represents the last temperature measurement at the end of the $NH_3$ reformer and was used as reference temperature for the plots.

CAT 3, SV 2304 $h^{-1}$, moist

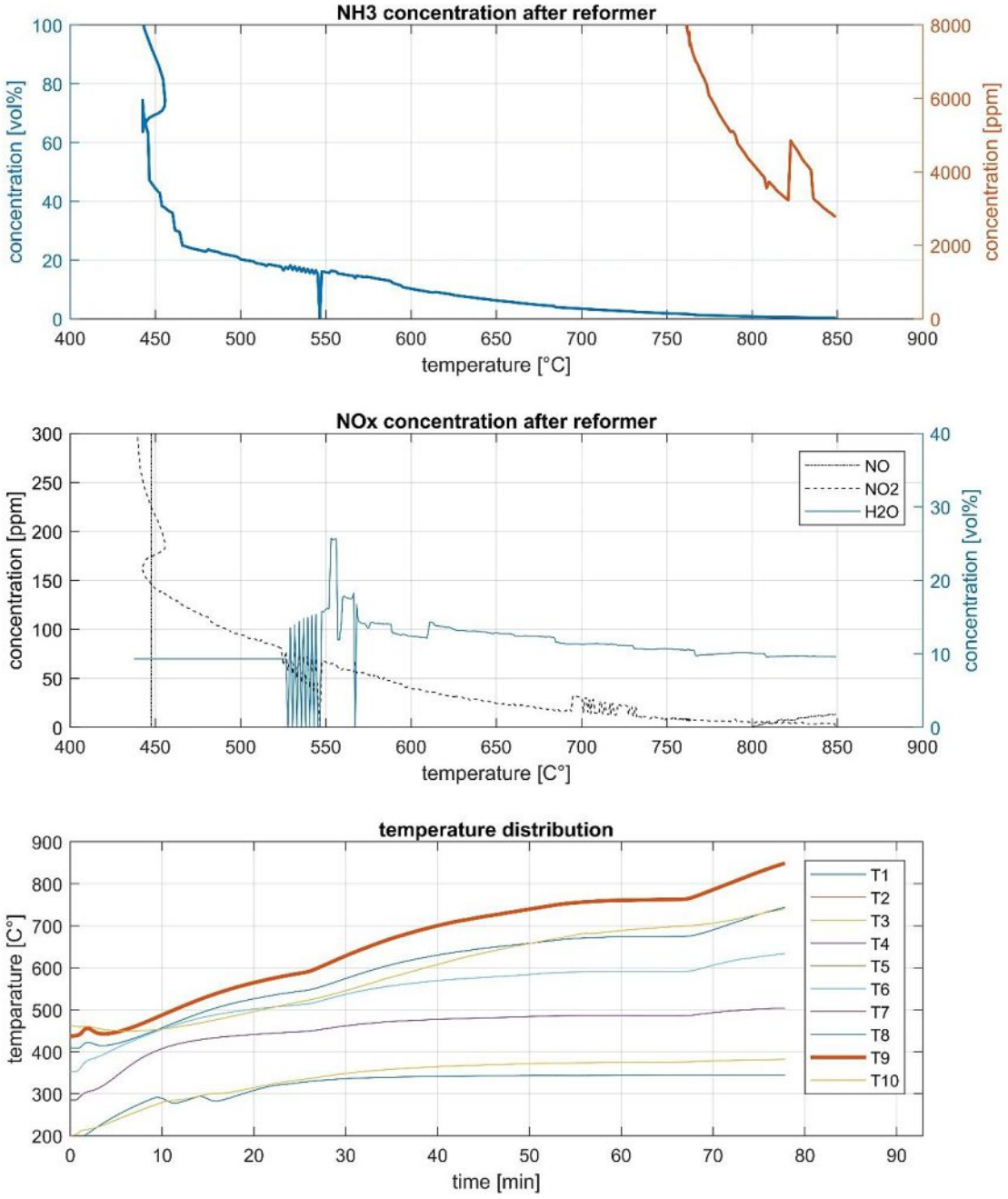


Figure 28: CAT 3, SV 2304 $h^{-1}$, moist – All fluctuations of the $NH_3$ curve above 20 % can be explained by measurement inaccuracies, caused by excess of the calibrated range. The used FTIR was calibrated for 0 – 10 vol% of $NH_3$ gas. The $H_2O$ curve also started to be representative from the moment $NH_3$ was below 15 %, every movement before can be ignored. T9 represents the last temperature measurement at the end of the $NH_3$ reformer and was used as reference temperature for the plots.

### 5.2.4. Catalyst 4 – Bonus

Table 11: specification of the catalyst CAT 4 – Since it wasn't planned to do measurements with this catalysator it needs to be seen as bonus measurement and is therefore also not complete. Different to the CAT 1 the CAT 4 has a very small pellet size what made it easier to fill the reformer tube. Nevertheless, due to the complex design of the reformer it wasn't possible to fill it completely. A detailed description about the chemical structure of the catalyst is given in Table 4:

| CAT 4 | | | | | |
|---|---|---|---|---|---|
| | | | | | |
| catalyst | | | reformer | | |
| volume: | 0,4 | l | volume: | 0,5 | l |
| weigh: | | | | | |
| before | - | g | | | |
| after | 536 | g | | | |
| | | | | | |
| dry (100% $NH_3$) | | | moist (+20% $H_2O$) | | |
| feed flow rate | SV reformer | SV real | feed flow rate | SV reformer | SV real |
| [l/h] | [$h^{-1}$] | [$h^{-1}$] | [l/h] | [$h^{-1}$] | [$h^{-1}$] |
| 246 | 492 | 615 | 295,2 | 590,4 | 738 |
| - | - | - | - | - | - |
| - | - | - | - | - | - |

CAT 4, SV 615 $h^{-1}$, dry

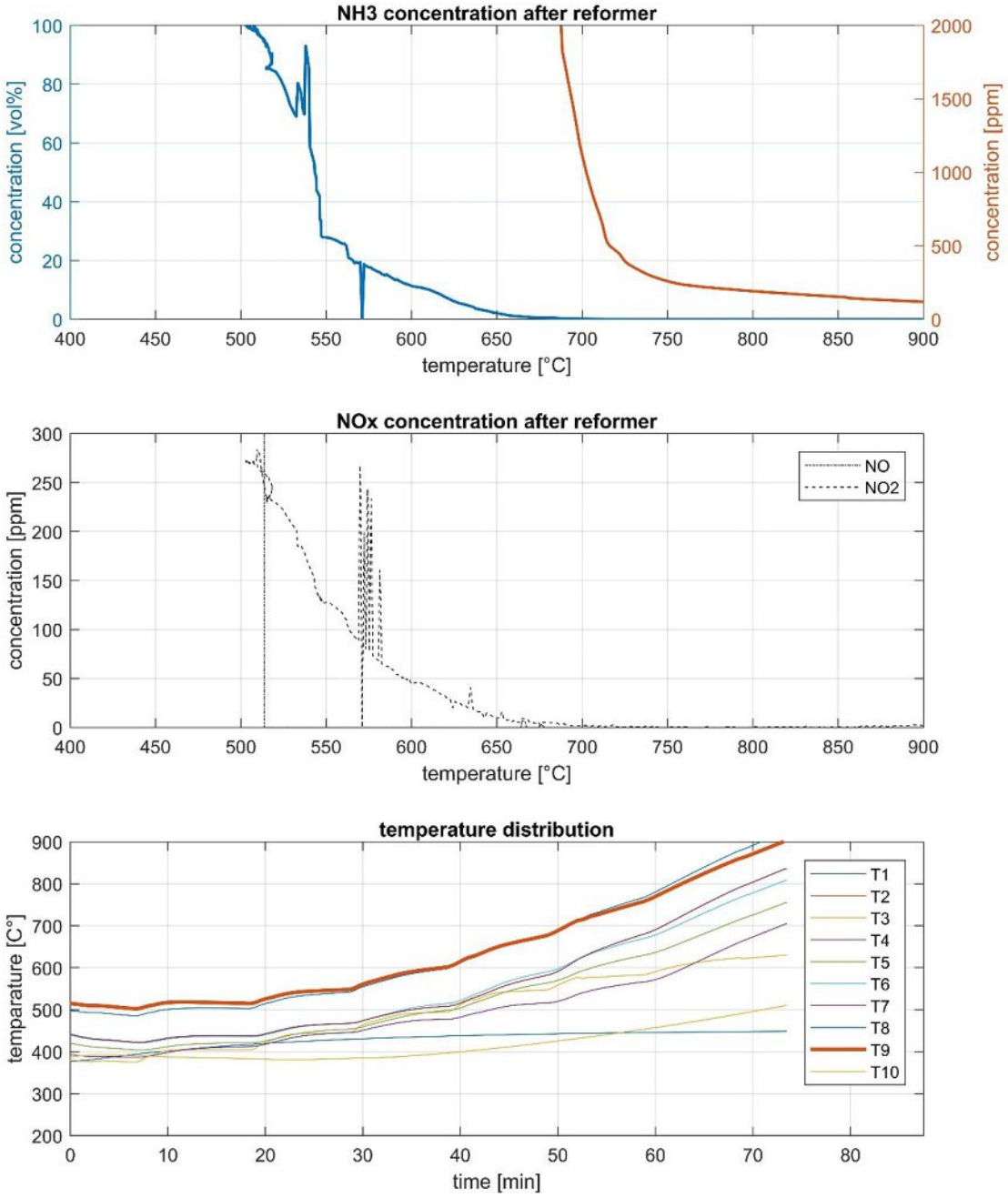


Figure 29: CAT 4, SV 615 $h^{-1}$, dry – All fluctuations of the $NH_3$ curve above 20 % can be explained by measurement inaccuracies, caused by excess of the calibrated range. The used FTIR was calibrated for 0 – 10 vol% of $NH_3$ gas. T9 represents the last temperature measurement at the end of the $NH_3$ reformer and was used as reference temperature for the plots.

CAT 4, SV 738 $h^{-1}$, moist

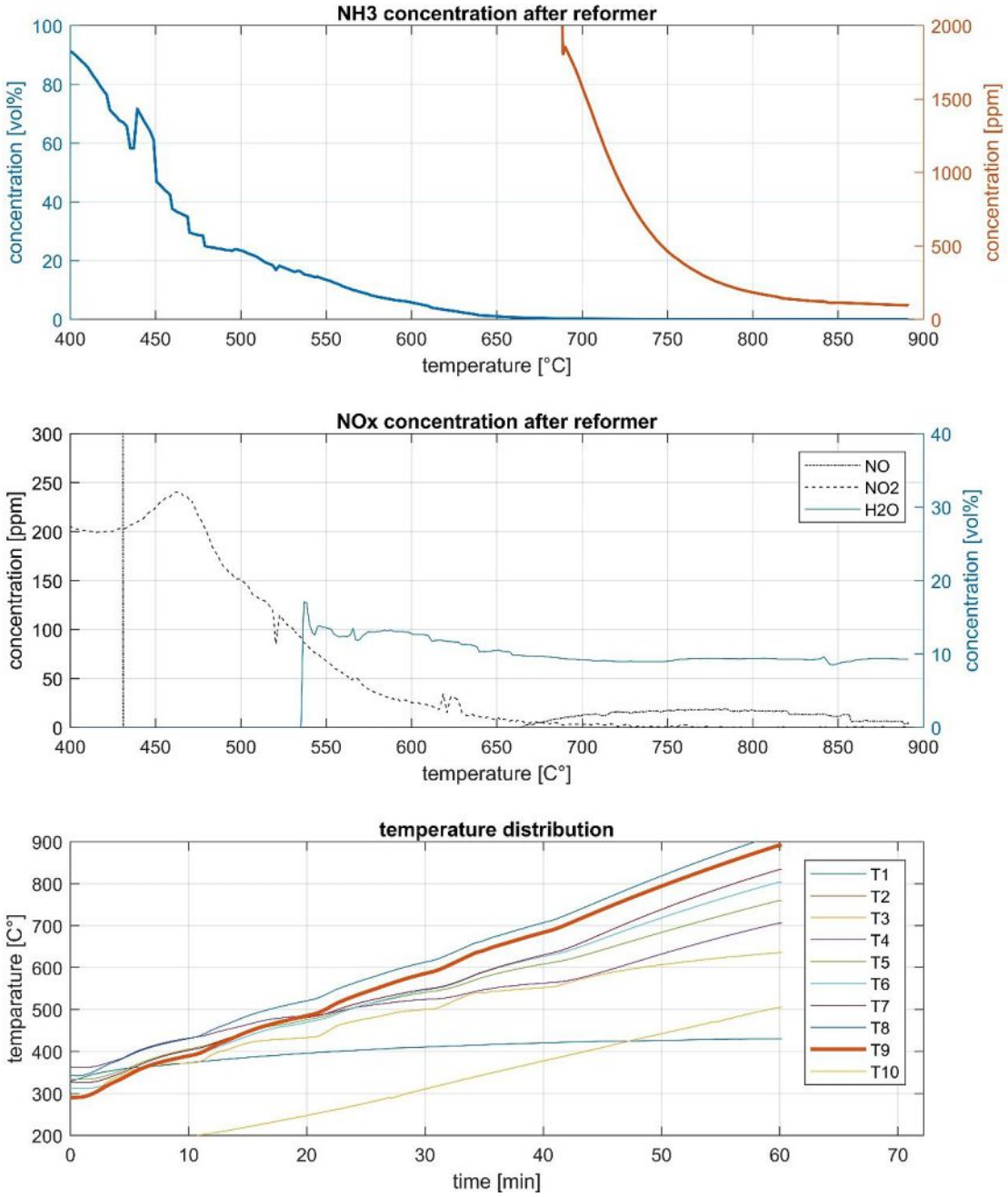


Figure 30: CAT 4, SV 738 $h^{-1}$, moist – All fluctuations of the $NH_3$ curve above 20 % can be explained by measurement inaccuracies, caused by excess of the calibrated range. The used FTIR was calibrated for 0 – 10 vol% of $NH_3$ gas. The $H_2O$ curve also started to be representative from the moment $NH_3$ was below 15 %, every movement before can be ignored. T9 represents the last temperature measurement at the end of the $NH_3$ reformer and was used as reference temperature for the plots.

# 6 Discussion

This chapter is dealing with the most important issues that were solved or investigated during this master thesis. Every finding that had an influence on the reformer tests or led to an important solution is presented in a separate subsection. First the already known facts like the energy demand and the equilibrium composition of the $NH_3$ dissociation are compared to the measured results. Then the measured results are discussed and compared in their raw form, based on the plots from Chapter 5.2. After the discussion of the raw results the important findings like, the effect $H_2O$ has on the reaction, the catalyst that worded the best, $NO_x$ emissions and the change of the catalysts during the tests are presented in detail. A final error estimation is concluding the discussion.

## 6.1. Energy Demand

One of the initial tasks was to adjust the heat management to the requirements of the reaction. As it can be seen in Figure 14 - Figure 16 the power input was too low to reach the required temperature of 850 °C inside the reformer. That can be explained by two circumstances. First the heating wires and the surface of the reformer produced a short circuit at higher temperatures and second the first setup did not have enough electrical power. Against initial assumptions the problem of the short was solved by eliminating the glass wool band between the heating wire and the reformer tube. In Figure 31 the glass wool band is shown that was wrapped around the reformer to insulate it against the wire. The first attempt was that an additional insulation between the wire and the reformer would increase the electrical resistance and therefore enable the reformer to reach higher temperatures. After several trial and error approaches the solution was to put the heating wire directly onto the metal tube of the reformer. Why that brought the wanted solution can be explained by the fact, that due to too good insulation by the glass wool band, the heat transport was reduced. A local heat peak around

**Figure 31: Heating Wire – Glass wool band was a too good**

the heating wire was the consequence. This in comparison higher temperature led to a strong reduction of the electrical resistance and later to the short circuit. The effect that an additional insulation usually increases the electrical resistance, had a weaker impact than the reducing effect by the higher temperature. The trial to heat the facility up without the glass wool band showed, that a quicker heat transport from the heating wire into the reactor wall was possible and therefore the local temperature around the heating wire stayed on a lower level than with the glass wool band. As a consequence, a higher electrical resistance between the wire and the reformer occurred and no short was produced. This was also confirmed by measuring the resistance with a voltameter.

The second point that the facility did not have enough heating power was solved by adding additional electrical heating wires. The heat losses where bigger than initially expected and therefore this measure was necessary.

A general energy balance of the reformer is shown in Figure 32. The assumptions that were made to calculate this balance are:

- 100% $NH_3$ conversion
- adiabatic system
- no other reactions, like the formation of NO or $NO_2$ inside the reformer
- pressure of 1 bara

The control volume is marked blue (see Figure 32) and symbolises all streams that are considered. The inlet temperature is 300 °C for all feed streams and the outlet temperature is 900 °C for all product streams. As space velocity the highest possible one of 1920 $s^{-1}$ $NH_3$ plus a 20 vol% $H_2O$ steam was chosen. These settings are representing the highest energy demands of all measurements.

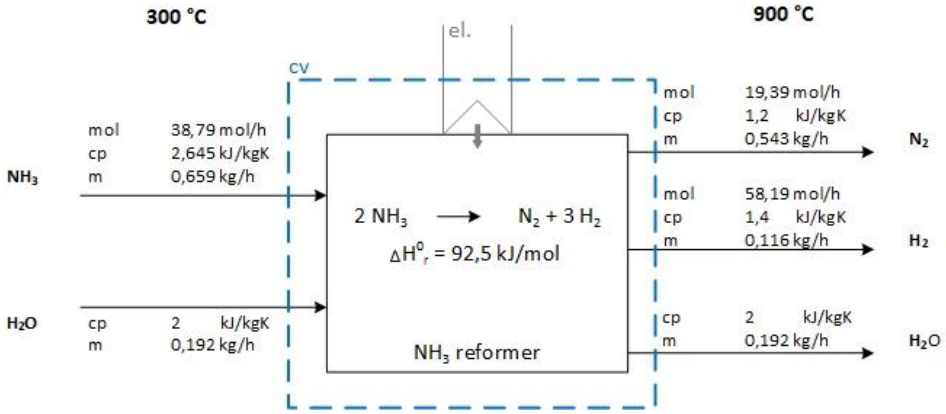


Figure 32: Energy Balance of the $NH_3$ Reformer – To calculate the energy consumption of the $NH_3$ reformer the inlet streams and the outlet streams where separated into their different components. Considered were the heat each individual stream was adding or withdrawing the system plus the reaction enthalpy, that was consumed by the dissociation of ammonia. The energy balance is based on the physical properties of the "VDI Wärematlas" [24] and takes as an assumption that the system is adiabatic and under a pressure of 1 bara.

The adiabatic energy demand was then calculated according to equation 6.1. The term $\dot{Q}_0$ is the thermodynamic power of the combined output stream, $\dot{Q}_i$ is the equivalent for the incoming stream, $\dot{Q}_R$ is the energy demand of the reaction and $\dot{Q}_{el}$ is the electrical energy from the heating wires. If a steady state is achieved the conversion to equation 6.2 is possible.

$$\frac{dQ}{dt} = \underbrace{\sum(\dot{m} \cdot c_p \cdot T)_{out}}_{\dot{Q}_0} - \underbrace{\sum(\dot{m} \cdot c_p \cdot T)_{in}}_{\dot{Q}_i} + \underbrace{r \cdot (-\Delta H_R) \cdot V}_{\dot{Q}_R} - \dot{Q}_{el} \tag{6.1}$$

$$\dot{Q}_{el} = \underbrace{1408\frac{kJ}{h}}_{\dot{Q}_0} - \underbrace{1220\frac{kJ}{h}}_{\dot{Q}_i} + \underbrace{1794\frac{kJ}{h}}_{\dot{Q}_R} = 550\ W \tag{6.2}$$

The calculated energy demand of 550 W is the result of the reaction energy plus the heating up of the whole gas phase for the highest possible flow. Not included are any heat losses, electrical efficiencies or parallel reactions like the formation of NOx.

In the beginning (Figure 14 to Figure 16) two heating wires (see Chapter 4.1) with 850 W each where used. After the first experiments it was clear that the electrical power was not sufficient. Therefore one heating wire with 850 W and 4 heating wires with 350 W each where wrapped around the reformer producing a total power of 2250 W. As it can be seen in all following measurements (Figure 17 to Figure 30), the initial problems with the heat intake were solved and the facility definitely had enough power.

## 6.2. Equilibrium Composition

Another point that was striking is the fact that the calculated temperature where ammonia is dissociated to a degree of 99 % and the temperature, most measurements reached this dissociation level, were different.

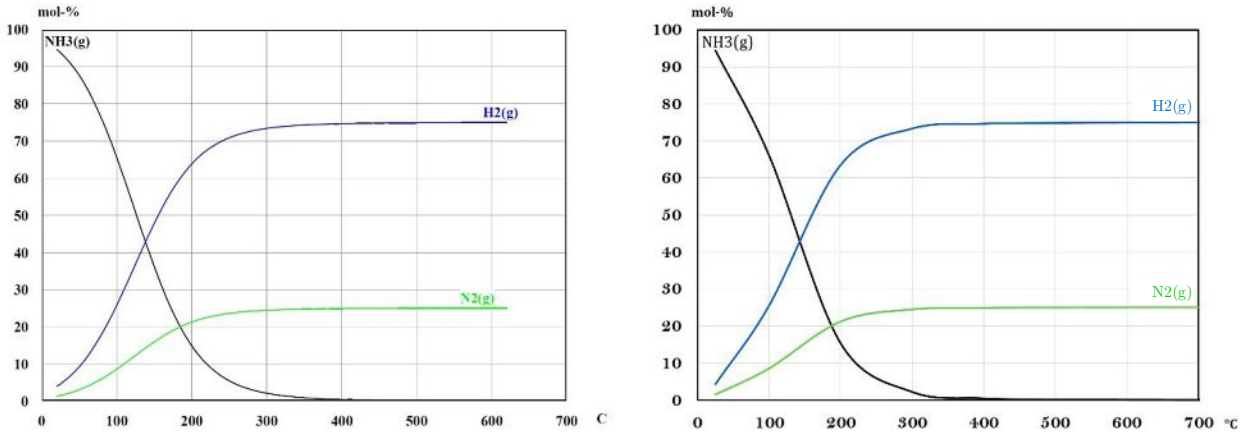


Figure 33: Gibbs Equilibrium – The left graph is showing the chemical composition of the ammonia synthesis calculated by the software HSC Chemistry and the right graph is showing the tabled values of ammonia dissociation over the temperature according to W. Schreiter [25].

The Gibbs Reactor of the software *HSC Chemistry* determines a 99 % dissociation of $NH_3$ at a temperature around 400 °C. This is congruent with equilibrium values from W. Schreiter [25] that are visualised in Figure 33. By looking at the measured results of this thesis, the same dissociation level was reached within a temperature range of 700 – 750 °C although a catalyst was used. That means the expected values of ammonia dissociation where not reached as quickly, even though temperatures of 900 °C where achieved under the influence of a Ni and Ru catalysts.

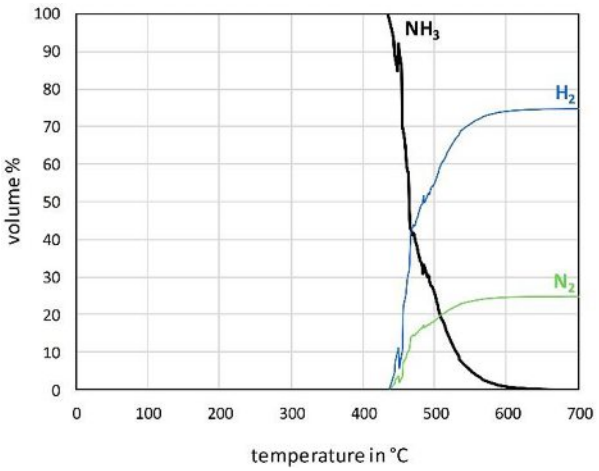


**Figure 34: Real Measurement – The graph shown above is from the measurement shown in Figure 18 (CAT 2, SV 960 $h^{-1}$, moist) and represents a direct comparison to the theoretical values from Figure 33. Only the NH3 curve is measured the other two are calculated curves based on the measurement. The small peaks around the temperature of 450 °C are due to measurement inaccuracies.**

In Figure 34 a real measurement, (its raw data are shown in Figure 18, *CAT 2, SV 960 $h^{-1}$, moist*), is directly compared to the result from the Gibbs reactor and the tabled values from W. Schreiter [25] that are shown in Figure 33. To

make the measured data directly comparable, the vol-% of water was cancelled out. Now the vol-% in Figure 34 can be directly compared to the mol-% of Figure 33, since in both cases pure $NH_3$ is compared to each other.

Why there is such a big difference between the measured values and the calculation based on the Gibbs energy can be explained by the theory, that is shown in Chapter *Gibbs Energy* (3.5). The Gibbs reactor is taking into consideration just the energetical situation of the products and the educts. This approach compares the energy level of two separate states, without focusing on the path that is lying in between. In Figure 3 of Chapter

*Catalytic Mechanism of the Ammonia* Synthesis (3.3.2) the energetical profile the nitrogen and hydrogen molecules need to overcome before they are able to form ammonia is shown. This graph shows that the nitrogen and hydrogen atoms need to climb a massive activation peak before the energetically lower state of ammonia can be reached. The same activation energy plus its exothermic energy need to be overcome by the reverse reaction of splitting ammonia. If just the beginning state of 100% ammonia and the final state of 75% hydrogen and 25% nitrogen are taken into consideration it might seem that the needed energy to make that endothermically reaction happen is only 92,5 kJ/mol. In fact, an initial amount of 1175 kJ/mol is needed to start the reaction that is ignored by the calculation of the Gibbs reactor. This extremely high activation energy is the reason why it is so crucial to use a catalyst to stabilise the transient states and therefore lower the energy consumption of the reaction as a total. The stabilisation of the transition states can also be seen in the energy profile of the ammonia synthesis in Figure 3 of Chapter

*Catalytic Mechanism of the Ammonia* Synthesis (3.3.2).

## 6.3. Results Comparison

A general overview and comparison of the measured results is shown in figure 35 and figure 36. As it was mentioned before the measurements with the catalyst *CAT 1* were taken before the additional heating wires were installed and therefore the heat intake was not sufficient. In section a) of figure 35 and figure 36 it can be seen, that during the measurements with higher

space velocities it was not possible to reach higher temperatures. Still, the SV range of 1200 - 1400 $h^{-1}$ delivered representative measurements.

Interesting to see was that the same interruption happened during the moist measurements of the catalyst CAT 2. This measurement was done after the facility's upgrade to more heating power and therefore a lack of heating energy can be excluded. Here the higher SVs (1760 $h^{-1}$ and 2560 $h^{-1}$) came to an abrupt end at about 750 °C and (2,0 ± 0,1) vol-% residual ammonia (figure 36, b). The fact that the same volume streams of the moist measurements with the catalyst CAT 3 (figure 36, c) did not have this problem gives the prove that it cannot be connected to an insufficient heat supply. An explanation could be, that the heat conduction of the CAT 2 catalyst was not as good as CAT 3 and therefore the heat transport within the catalyst did not happen quickly enough.

Another point that was outstanding is that the highest SV of the dry measurement with the catalyst from *CAT 2* enabled a quicker dissociation of ammonia, than it was achieved with the lower SVs. In Chapter *Kinetic Mechanism* (3.4.1) the explanation for this phenomenon is given. By increasing the flow, the film diffusion layer of the catalyst particles gets decreased [26] and therefore the limiting factor of this macrokinetical mass transfer step is reduced. The result is a faster dissociation of ammonia, due to a quicker transport to the active site of the catalyst, that can also be seen in the measured values (figure 35, b). Interesting is that the same tendencies cannot be seen at the moist measurements even though the volume streams are higher. An explanation here could be, that the additional water is reducing the partial pressure of $NH_3$ and therefore reducing the general reaction rate. Unfortunately, the amount of the measurements that were taken was not big enough to consider this approach as valid and therefore it must be seen as a possible explanation, that cannot be confirmed based on the current information.

In general, the tendency was that lower SVs showed a better dissociation rate of $NH_3$. Therefore, a longer residence time was beneficial for the splitting of ammonia. This finding can be directly transformed into the statement that the microkinetical steps of the reaction, adsorption, the chemical reaction on the catalyst surface and desorption are the reaction rate mitigating steps. Otherwise a higher SV would have been beneficial for the reaction, because a higher pressure accelerates the diffusion steps, as it is explained in Chapter *Kinetic Mechanism*

(3.4.1). This assumption gets reaffirmed by W. Tsai [18] who showed that the desorption of $N_2$ is the most energy intense step and therefore also the slowest.

Activation with forming gas was just done for the two Ni-based catalysts CAT 1 and CAT 4. The two Ru-based catalyst (CAT 2 and CAT 3) were used directly with ammonia without any activation. The atmosphere that was created by the dissociation of ammonia has a reducing effect on oxides and therefore an activation was not as important. As it is mentioned in Chapter 4.2 just the Ni catalysts were activated beforehand.

This assumption led to a mistake that was elucidated by the first measurement with the catalyst CAT 3 that was carried out at a SV of 720 $h^{-1}$ (figure 35, c). This measurement showed a completely different course to all the other measurements. First the dissociation happened at a lot lower temperature than compared to all the other measurements, and finally the $NH_3$ concentration started to increase again until it reached a value of (0,44 ± 0,02) vol-% $NH_3$ at 900 °C. One explanation could be that the catalyst was, not completely activated before the measurement and therefore showed this strange behaviour. Still interesting is that the dissociation started at that low temperatures, what should not be the case if the catalyst was not fully activated. At the beginning of the measurement a $H_2O$ concentration of (2,2 ± 0,1) vol-% was detected, what is normally an indication of a not complete activation. The catalysts are active in their metal state and deactivated when oxidised. Hydrogen reduces the metal oxides and produced water with the oxygen atom.

The higher SVs of the dry measurements (1320 $h^{-1}$ and 1920 $h^{-1}$) are also just reaching an ammonia concentration of (2,6 ± 0,1) vol-% and (2,8 ± 0,1) vol-%, while the moist measurements are reaching values near 0 vol-% at similar temperatures. That can either be explained again by the missing activation of the catalyst or by the circumstance that water has a positive effect on the $NH_3$ splitting. To have a better comparison and to decide if water has an influence or not it was subtracted from the general volume stream (see Chapter 6.4).

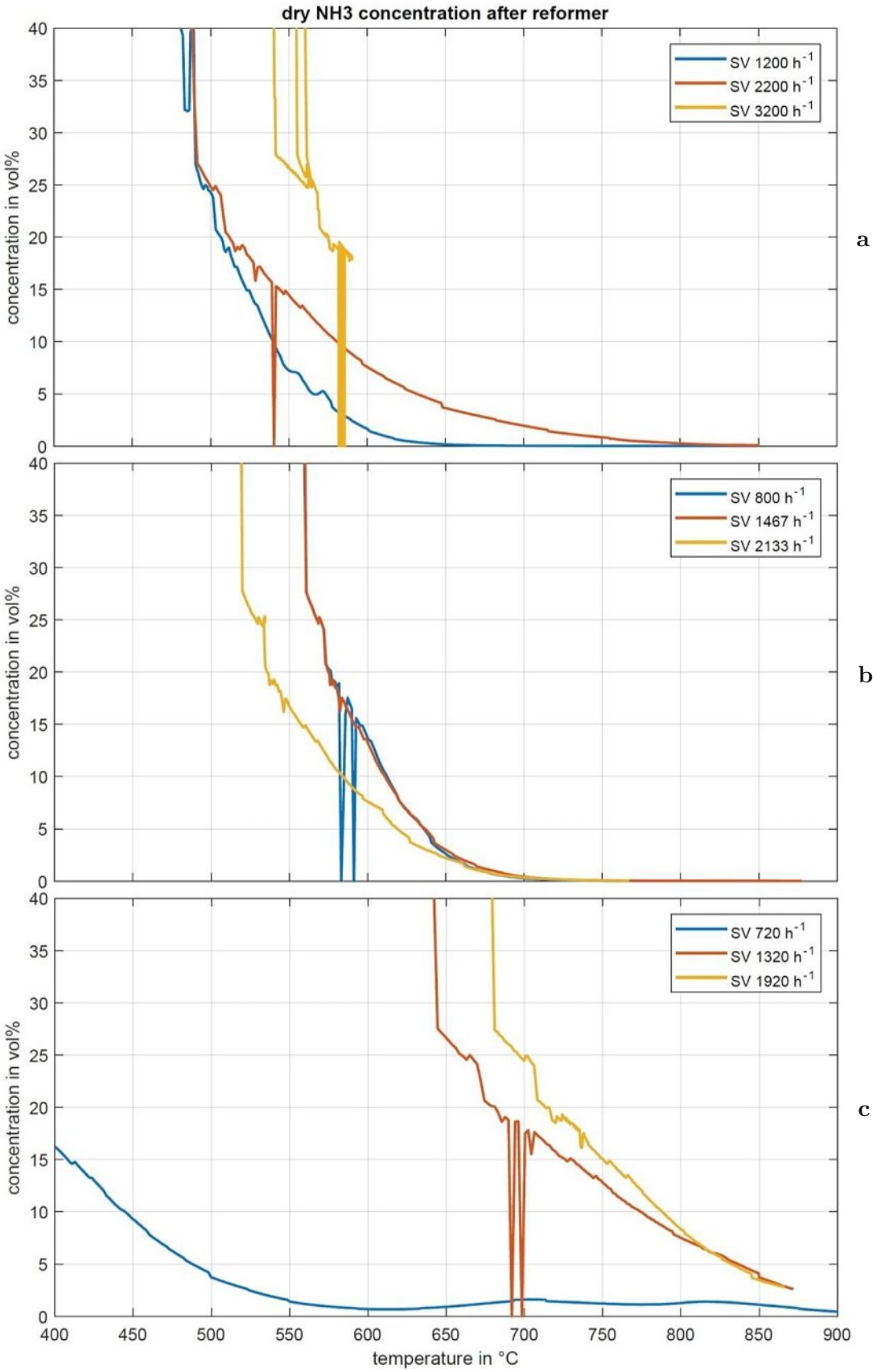


figure 35: Overview Dry Measurement – (a) represents the dry measurements with the Ni-based catalyst CAT 1. (b) shows the measurements with the Ru-based catalyst CAT 2 and (c) is again based on a Ru (CAT 3). The different SVs shown in the plot are due to the varying catalyst volume. The colour code in general represents the following $NH_3$ stream: blue for 360 l/h, red for 660 l/h and yellow for 960 l/h.

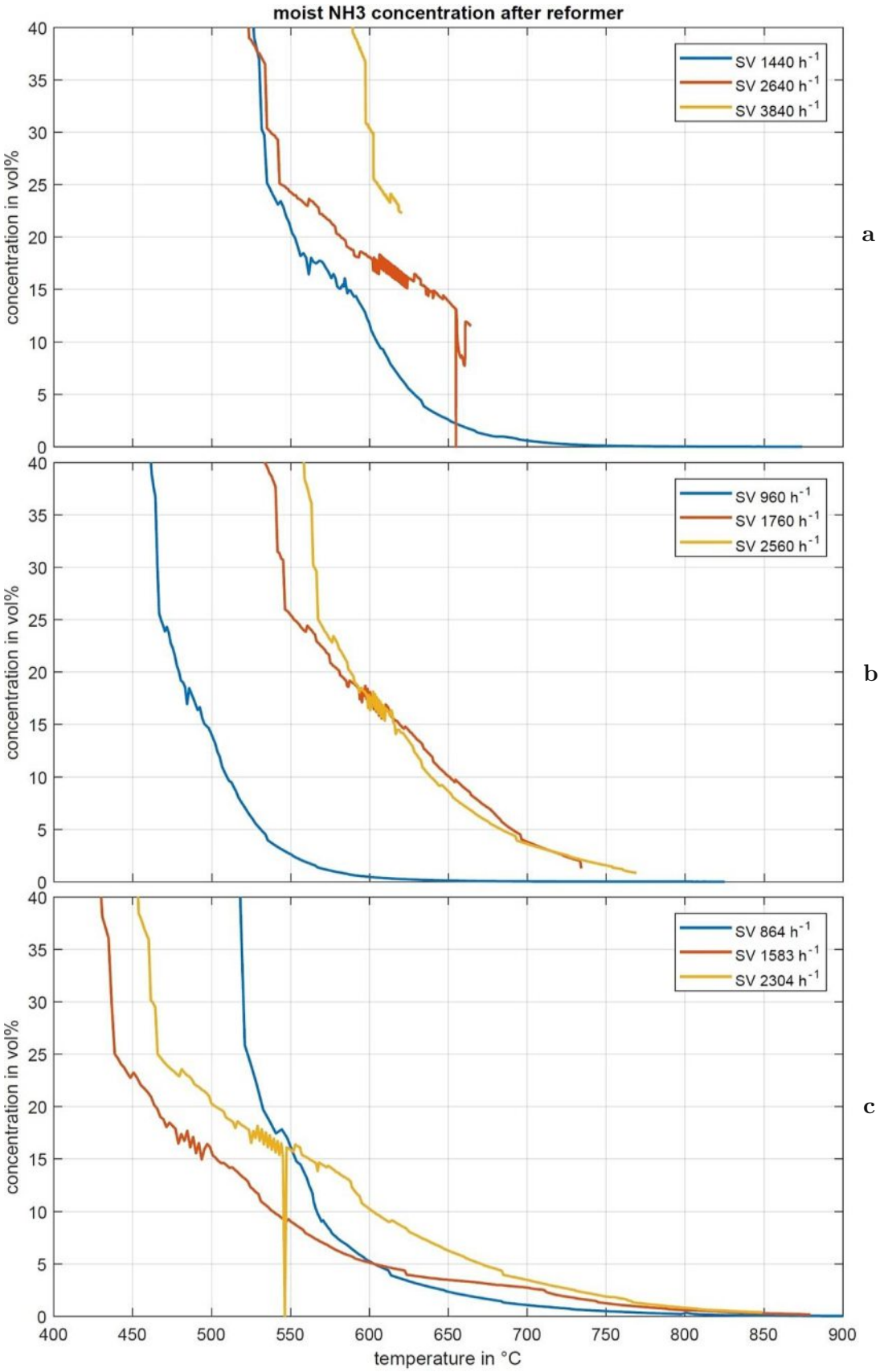


figure 36: Overview Moist Measurements – (a) represents the moist measurements with the Ni-based catalyst CAT 1. (b) shows the measurements with the Ru-based catalyst CAT 2, and (c) is again based on a Ru (CAT 3). The different SVs shown in the plot are due to the varying catalyst volume and the additional H2O steam. The colour code in general represents the pure NH3 stream: blue for 360 l/h, red for 660 l/h and yellow for 960 l/h.

## 6.4. Effect of $H_2O$

To figure out if steam has an influence on the dissociation rate of ammonia it was necessary to make sure that the moist and the dry measurements are referenced to the same conditions. For the dry measurements pure $NH_3$ gas was used. For the moist measurements water was added to produce 20 vol-% of steam at standard conditions. Before the steam was added to the $NH_3$ stream it was heated up to 300 °C. The moist measurements always had a higher volume flow than the dry ones. The ammonia feed was at room temperature at the point both streams were mixed. After this point every tube was heated to at least 150 °C to prevent condensation. The points were the volume flow was measured was at the gas inlet (MFC see Figure 8) and at the pump where the mass flow of liquid $H_2O$ was set before it went through the vaporiser. The calculation was based on mole fraction. Further, it was assumed that the amount of water molecules ($n_{H2O}$) stayed constant over the whole process time and that there were no other reactions than the dissociation of $NH_3$. With this assumption and the stochiometric knowledge of the reaction, it was possible to determine the $NH_3$ vol-% on dry basis ($X_{NH3,dry}$), just based on the measured value of $NH_3$ vol-% on moist basis ($X_{NH3}$). ($n_{NH3,in}$) represents the initial amount of ammonia molecules before the reaction.

$$X_{NH3,dry}\,(X_{NH3})\left[\frac{mol}{mol}\right] = \frac{X_{NH3}}{1 - X_{H2O}} = \frac{X_{NH3}}{1 - \frac{n_{H2O}[mol] \cdot (1 + X_{NH3})}{2 \cdot n_{NH3,in}[mol] + n_{H2O}[mol]}} \tag{6.3}$$

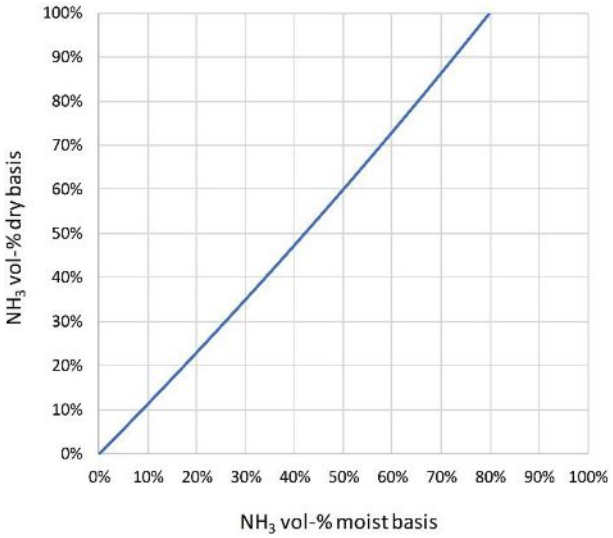


Figure 37: Comparison vol-% Dry-Moist – The x-axis "$NH_3$ vol-% moist basis" represents the values measured by the FTIR and the y-axis "$NH_3$ vol-% dry basis" are the calculated values based on the assumptions mentioned in the text.

In Figure 37 the general relation between $NH_3$ vol-% without water (calculation) and the $NH_3$ vol-% with $H_2O$ (measurement) is shown.

Now after the dilution of the steam is cancelled out, a statement of weather the steam has an effect on the dissociation of ammonia can be made. As it is illustrated in figure 38 all the graphs are now lying at slightly higher $NH_3$ concentrations than they were in figure 36. In general, it was expected that water does not have an effect on the reaction [27], other than a higher energy consumption, because of the additional power the heating up process of water requires. If there is an effect it should be slightly negative due to an increase of the space velocity and the dilution of the $NH_3$. That causes a reduction of the partial pressure of $NH_3$ what had a lower driving force for the reaction and therefore also a slower reaction rate as a consequence.

Looking at the measurements with the catalyst CAT 1 (section (a) in figure 35 and figure 38) these expectations are getting confirmed. There is a slight shift of the curves to the right, what can be explained by the lower partial pressure and that the general energy consumption of the moist streams is higher. The bigger heat consumption is shown by the fact that the higher SVs of the moist measurements are interrupted a lot earlier than the dry ones.

A different situation is presented when one compares the dry and the moist measurements that were carried out with the catalyst from *CAT 2* (section (b) in figure 35 and figure 38). Here two completely different statements are possible. The lower SVs, 800 $h^{-1}$ of the dry test and 960 $h^{-1}$ of the moist test, are giving the impression, that water has a positive effect on the dissociation rate. The moist curve is reaching the level of 0 vol-% $NH_3$ at lower temperatures than the dry one. Completely different is the behaviour of the higher SVs where the dissociation is better at dry conditions. While the biggest moist volume stream at 750 °C still has a $NH_3$ concentration of (3,28 ± 0,13) vol-%, the dry one reached (700 ± 28) ppmv at the same temperature. What can also be seen again is that the energy consumption of the moist streams is bigger.

Positive seemed to be the effect water had on the $NH_3$ dissociation of the measurement that were made with the catalyst CAT 3 (section (c) in figure 35 and figure 38). Even though the catalyst didn't work as well as the others, it can be seen, that the presence of steam is having a repeatedly positive effect. All moist measurements that were done are outperforming the dry ones. Just based on the measured results it can be said that for this catalyst steam had a

positive effect on the dissociation rate of $NH_3$. At this point it needs to be mentioned again, that it could also be due to a missing activation of the catalyst, what could also explain the strange graph of the lowest dry measurement.

The general impression was, that catalysts based on Ni are not or just slightly affected in a negative way by the presence of water while Ru-based catalyst are tending to have better dissociation rates if water is part of the reaction.

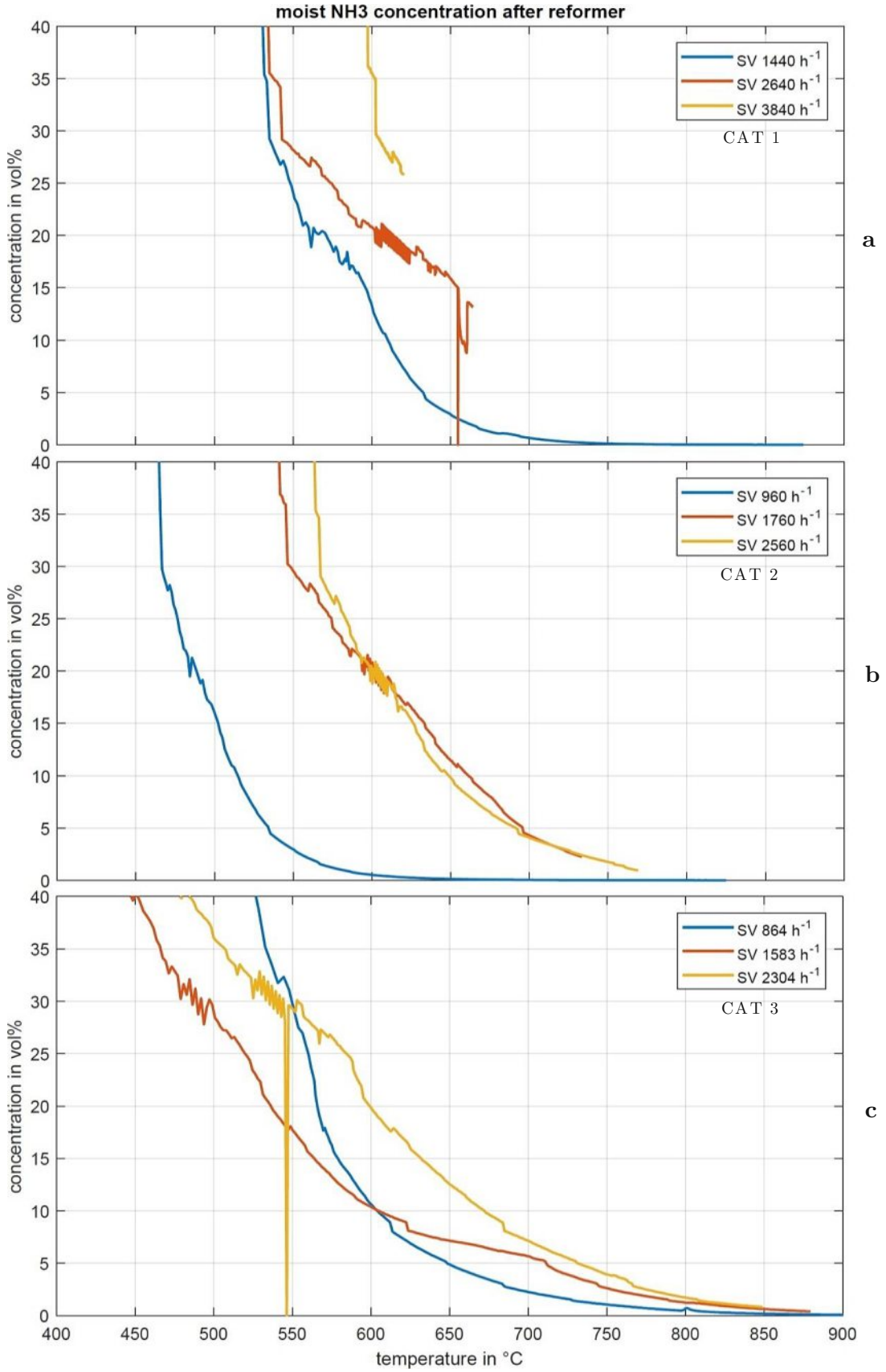


figure 38: Overview Moist Measurements $H_2O$ Correction – For this plot the volume stream of $H_2O$ was subtracted to present the measured $NH_3$ concentration in a comparable way to the dry measurement. As it can be seen when compared to figure 36 the tendencies and the general statement of the two plots do not change. What is changing is that especially at lower concentrations the $NH_3$ concentration is a lot higher than it was with the $H_2O$ included in the vol-%. What was not possible to correct is the higher SV that was caused by the additional water.

## 6.5. Catalyst Comparison

All four catalysts that were tested are compared to each other. The following figures show how the different catalyst materials performed.

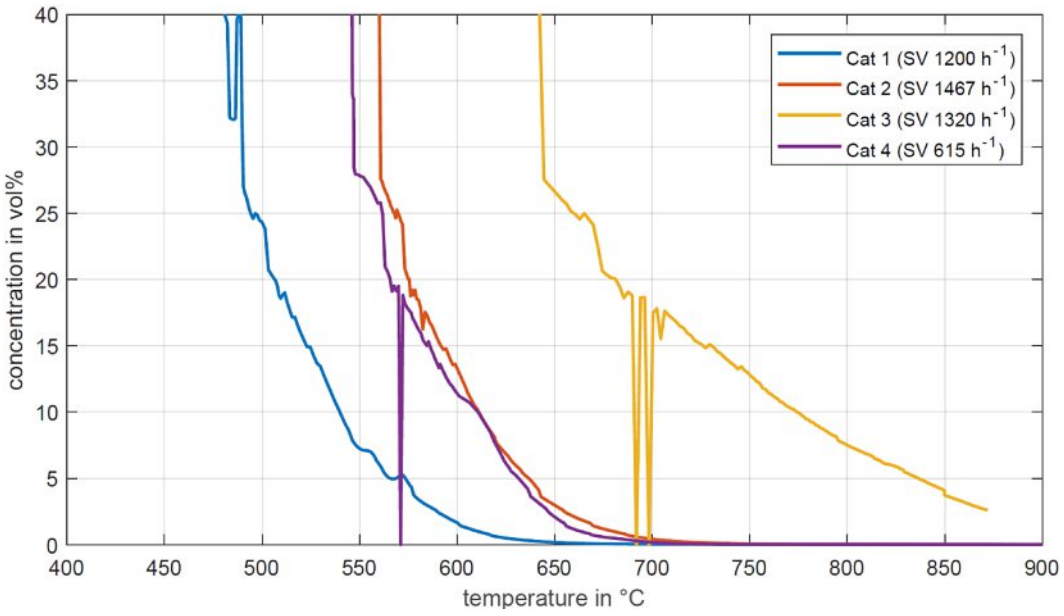


**figure 39: Catalyst Comparison Dry Measurements – In this plot the $NH_3$ concentration after the reformer is shown based on the different catalysts that were tested. It was tried to take similar space velocities to enable a representative comparison of the catalyst quality. The bonus catalyst was also selected to compare two Ni-based and two Ru-based catalysts with each other.**

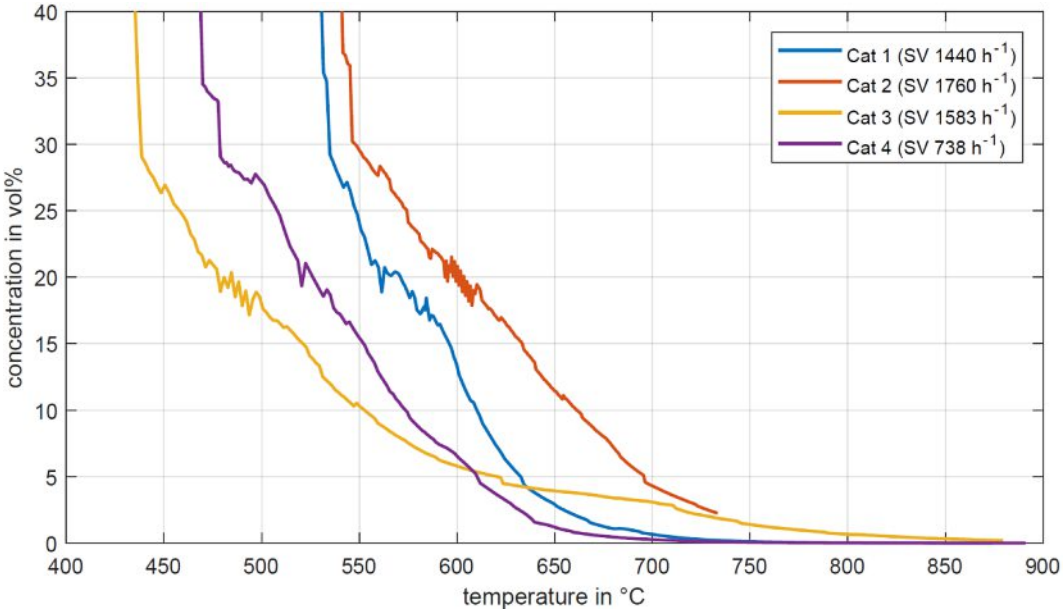


figure 40: Catalyst Comparison Moist Measurements - In this plot the corrected $NH_3$ concentration after the reformer is shown based on the different catalysts that were tested. It was tried to take similar space velocities to enable a representative comparison of the catalyst quality. The bonus catalyst was also selected to compare two Ni-based and two Ru-based catalysts with each other.

Based on figure 35, figure 36 and figure 38 that are shown before, it is hard to tell which catalyst worked the best in terms of dissociation rate and temperature. Therefore, the measurements with SVs around 1300 $h^{-1}$, which are the most interesting ones for the future system design (see Chapter 5.1) were chosen and directly compared to each other. This comparison is shown in figure 39 and figure 40. CAT 1 and CAT 4 are two Ni-based catalysts, whereas the catalysts from CAT 2 and CAT 3 are Ru-based (see Chapter 4.3).

By comparing figure 39 and figure 40 the general impression arises that water has a slightly negative effect on the temperature, that is needed to dissociate $NH_3$. Just the moist measurement with the catalyst CAT 3 shows an improvement of the reaction rate, but that can also be connected to a missing activation of the catalyst as it is already discussed in the previous chapters. To summarise there is a slight tendency to better results with dry conditions, but the difference is too small to take it as a valid statement.

What can be said is, that the Ni-based catalysts CAT 1 and CAT 4 have significantly better dissociation rates in both, moist and dry conditions, than the two Ru-based catalysts from CAT 2 and CAT 3 have. This can be explained with the higher binding strength between Ru and N-atoms, than the one between Ni and N-atoms. In Figure 41 this principle is illustrated. The volcano curve on the left is normally used to predict the best catalyst material for a certain hetero catalytic reaction. In this case it is shown for the ammonia synthesis. For our purposes, just the x-axis with the binding energy is of interest. Here it is shown that Ru has a stronger binding strength between the metal and the N-atom, than Ni and is therefore of better use for the ammonia synthesis. For the dissociation of ammonia whereas, this effect has a negative impact as it can be seen on the right side of Figure 41.

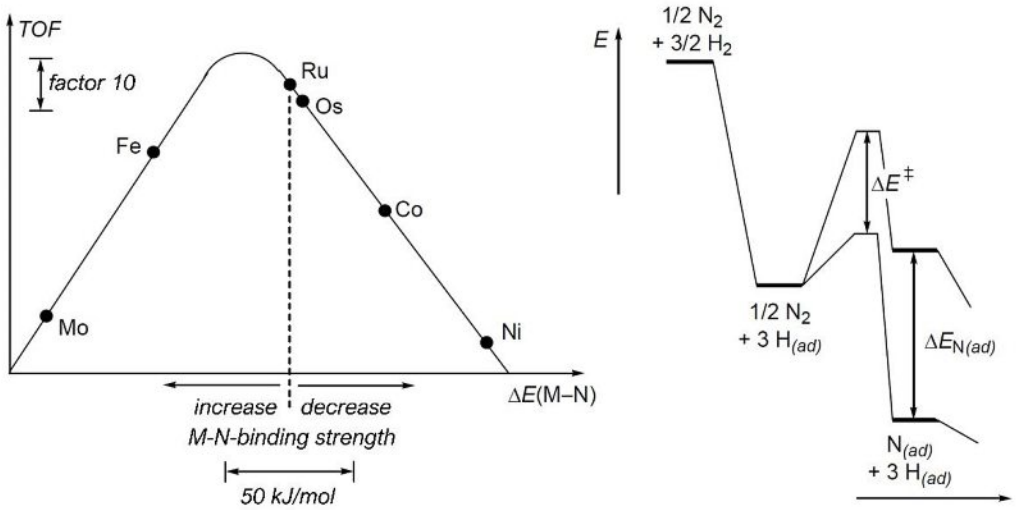


Figure 41: Binding Strength of Ru and Ni to N – In this figure the turn over frequency (TOF) for the ammonia synthesis at 400°C and 50 bar is shown as a function of the adsorption energy of different metals, also called "volcano curve" (graph on the left). On the right the energy profile of the dissociative chemisorption of $N_2$ at a metal with a high and a low M-N-binding energy is shown. $\Delta E^{\pm}$ is standing for the difference of the activation energy for the N-N-splitting and $\Delta E_{N(ad)}$ is standing for the difference of adsorption energy of nitrogen. This graph was directly taken from D. Steinborn [11].

The energy diagram for the dissociative chemisorption of ammonia shows two paths. The higher path is the one with lower binding energy (Ni for example) and therefore lower general energy level. The lower path is the one with higher binding energy (Ru for example) and has a higher general energy level. Compared to the information out of the energy diagram (Figure 3) that is shown in Chapter

*Catalytic Mechanism of the Ammonia* Synthesis (0), it means a lower energy difference between the state where all atoms are bound to the catalyst surface and the state where they are fully released again. The state where all atoms are bound to the catalyst surface is the biggest negative peak in Figure 3. This peak is smaller for a catalyst based on Ni than it is for a catalyst based on Ru. That means N-atoms are not as strongly bound to the surface of a Ni catalyst than they are bound to a Ru catalyst and therefore it is easier for them to desorb again. Summarised, that means Ni is the better catalyst for the splitting of ammonia due to a quicker desorption of nitrogen. This effect can also be seen by the measured values. The Ni-based catalysts have a better dissociation rate than the Ru-based ones.

## 6.6. $NO_x$ Emissions

Surprising was that every measurement no matter if dry or moist showed a significant amount of $NO_2$, detected by the FTIR in the reformer gas. This was especially surprising because of the fact, that ammonia gets used in industrial facilities to reduce the $NO_x$ emissions. This special technique of off gas treatment is described in Chapter

Selective Catalytic and None-Catalytic Reduction (3.6). Knowing that ammonia normally reduces the amount of $NO_2$ in combination with the similarity of the $NH_3$ with the $NO_2$ graph, it was obvious that this must be due to an error.

At first a deeper understanding of the way the FTIR works is necessary to understand the reason for this measurement inaccuracy. In Chapter *Infrared Spectroscopy* (3.7.) a detailed description of the FTIRs operating mode is given. This information in combination with the adsorption spectra that are shown in figure 42 led to the conclusion, that there exists a cross-sensitivity between the measurement of $NH_3$ and $NO_2$. The adsorption spectra are unique for individual substances. The FTIR uses these reference spectra to calculate the concentration of the corresponding species. By looking at figure 42 it can be seen, that the spectrum of $NO_2$ has a peak around the wave number of 1500 $cm^{-1}$. Parallel the $NH_3$ curve has a peak at the same wave number and whenever $NH_3$ gets detected, an $NO_2$ peak gets detected as well. This cross-sensitivity can be corrected by a subsequent adjustment of the FTIRs settings. The different parts of the spectra that are used by the infrared spectrometer can be chosen that way that an overlapping is avoided.

By looking at the reference spectra in figure 42 it can also be explained why the water measurement did not show reasonable values until a $NH_3$ concentration around 15 vol-% was reached. A belated check of the FTIRs settings showed, that the part of the $NH_3$ spectrum (3000 to 3500 $cm^{-1}$) that was used to determine the higher concentrations, slightly overlapped with the part of the $H_2O$ spectrum (3300 to 4000 $cm^{-1}$) that was used as well. For this reason, the water measurement showed an error whenever the adsorption due to ammonia was high. By choosing the reference spectra ranges, that are used from the FTIR to determine the gas composition, that way that no overlapping is possible cross-sensitivities could be avoided.

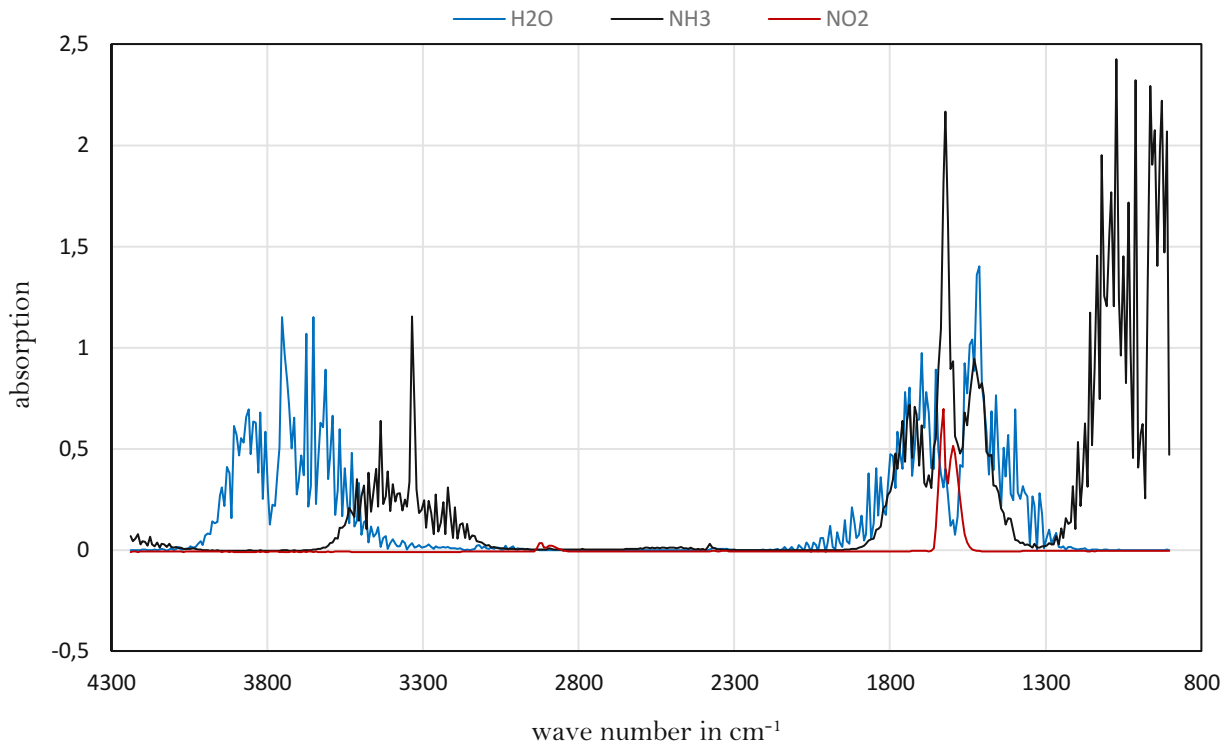


figure 42: Superimposed Spectra of $H_2O$, $NH_3$ and $NO_2$ – In this graph the different adsorption spectra of $H_2O$, $NH_3$ and $NO_2$ are shown.

Additionally, to $NO_2$, NO was detected. As it can be seen at the moist measurements in Figure 12, Figure 18,Figure 24,Figure 26,Figure 28 andFigure 30, NO was produced at higher temperatures. This happened as well against any expectations, because $NH_3$ usually reduces NO emissions to $N_2$ and $H_2O$ as it is described in Chapter

*Selective Catalytic* and None-Catalytic Reduction (3.6). Because of NO only appearing during moist experiments, a direct connection between the steam in the reformer and the production of NO exists. Any other source of oxygen, like a leak stream of air or oxides from the catalyst, can be excluded, with the argumentation that in this case this phenomenon would not just occur at moist measurements. In addition to that the pressure inside the reformer was always higher than the ambient pressure what is another reason why the steam must have been the only oxygen source. This assumption gets reassured by the measurement shown in Figure 24. Here a small interruption of the pump's water supply can be seen at 800 °C. During that time the NO also stopped being produced and the $NH_3$ concentration increased due to the missing dilution from the steam.

It can also be excluded that there are any cross-sensitivities. In this case NO would be detected at other moments as well. The temperature did not seem to be the decisive factor. The beginning of NO production was detected at different temperatures starting from 570 °C (Figure 18) up to 800 °C (Figure 28). All measurement had in common that the NO production started at an ammonia concentration of about (0,8 ± 0,2) vol-%. That means from the moment the ammonia concentration was low enough, NO was built. The reached NO concentration also seemed to reach a constant value around 25 ppm. Only Figure 30 shows a decline of the concentration at higher temperatures.

That NO was built out of $N_2$ and $H_2O$ is an interesting conclusion, since in industrial facilities NO build out of its elementary constituents does not happen under a temperature of 1200 °C [19]. This temperature was never reached during the experiments. It is likely that the catalyst is supporting the production of NO.

## 6.7. Catalysts Before and After Test Runs

The general composition of the catalysts was hard to get, and the manufacturer only gave a rough description, which is presented in Table 4 of Chapter 4.3. It was observed that the Ni-based catalysts (CAT 1 and CAT 4) turned darker after the measurements, whereas the Ru-based catalysts (CAT 2 and CAT 3) lost their colour or became brighter.

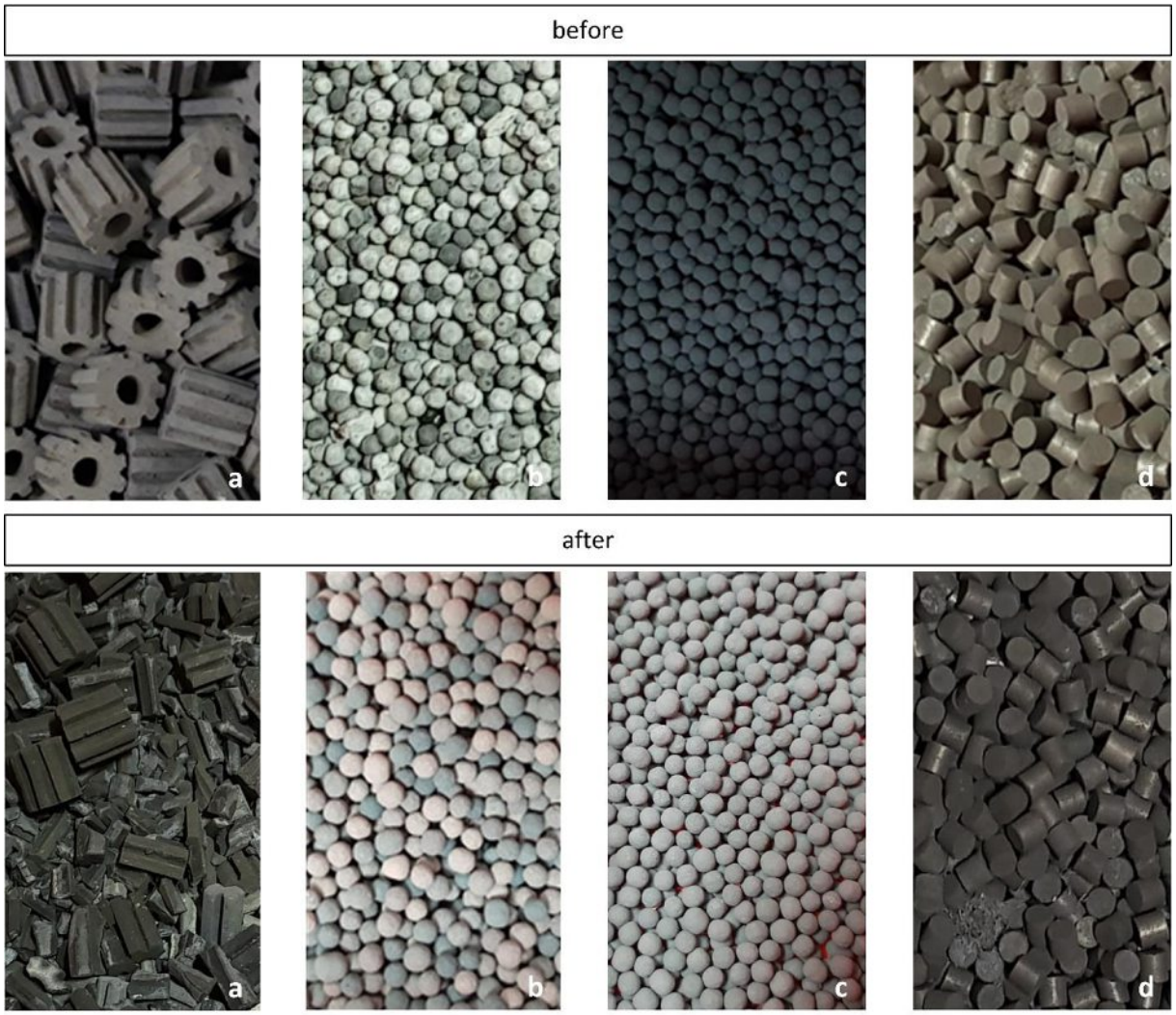


figure 43: Catalysts Before and After – In this image a real size picture of the catalysts, CAT 1 (a), CAT 2 (b), CAT 3 (c) and CAT 4 (d) is shown before and after the test were carried out. Catalyst (a) needed to get crushed before it was possible to fill it into the reformer.

The catalyst CAT 1 needed to get crushed before filling it into the reformer, due to its large particle size. An informative finding was, that just the Ni-covered surface areas of the catalyst turned dark, while the surface areas of the fractures did not change their colour. That tells us that the change of the colour does not come from soot or any other impurity inside the facility.

It must be a direct result of a chemical reaction with the active sites of the catalyst. A. G. Freidlander [28] made the finding that grey NiO catalysts turned black after they were reduced to their activated Ni form.

As it is shown in Table 8 and Table 9 a reduction of the catalyst weight was measured. The highest reduction was detected for CAT 1. This can be explained by the fact, that all small particles, that were produced during the crashing, were carried away by the gas stream during the measurements.

It could also be that a part of the weight loss can be dedicated to the reduction/activation of the catalyst. Literature sources are describing that around 25 % weight loss occurs during the activation of the catalyst for the Haber-Bosch process [17].

## 6.8. Error Estimation

To estimate what effect the error propagation has on the final results, the accuracy values of the different measuring devices were used. The accuracies for the devices that were considered are listed in Table 12 and where taken directly from the technical specification of the manufacturers.

Table 12: List of Inaccuracies – The accuracy values were taken from the manufacturers of the corresponding devices. A general list of the used equipment is shown in Table 3.

| Measuring Parameters | |
|---|---|
| Gilibrator: | |
| Accuracy: | ±1% of reading accuracy ($\Delta K_{Gili}$) |
| MFC: | |
| Accuracy: | ±1 % of output value ($\Delta U_{MFC}$) |
| FTIR: | |
| Zero-point drift: | ±2 % of measuring range per zero-point calibration interval ($I_{ZPD}$) |
| Linearity deviation: | ±2 % of measuring range ($I_{Lin}$) |
| Temperature drifts: | ±2 % of measuring range per 10 K temperature change ($I_T$) |
| Pressure influence: | ±1 % change of measuring value for 1 % sample pressure change ($I_p$) |
| Pump: | |
| Accuracy: | ±1% reading accuracy ($\Delta \dot{m}_p$) |

### Gilibrator

The gilibrator was used to calibrate the MFC. A set of measurements at different MFC set points was carried out to create a calibration graph. This graph was linear and had an offset (d) of zero. The gilibrator's error was calculated based on the following relation.

$$\dot{m}_{Gili}(x)\left[\frac{Nl}{h}\right] = K_{Gili}\left[\frac{Nl}{hV}\right] \cdot x\,[V] + d\left[\frac{Nl}{h}\right] \tag{6.4}$$

$$\Delta K_{Gili} = 1\% \cdot K_{Gili} = 0{,}01 \cdot 4{,}10\left[\frac{Nl}{hV}\right] = 0{,}04\left[\frac{Nl}{hV}\right] \tag{6.5}$$

Equation 6.4 is representing the linear calibration graph that is describing how the volume flow was linked to the voltage of the MFC set points (x). After deriving this function just, the calibration constant ($K_{Gili}$) of the gilibrator, had an impact on the gilibrators error ($\Delta K_{Gili}$).

### MFC

The basic equation for the mass flow ($\dot{m}_{MFC}$) of the MFC was dependent on the voltage measured by the MFC ($U_{MFC}$) and the calibration constant from the gilibrator.

$$\dot{m}_{MFC}(U_{MFC})\left[\frac{Nl}{h}\right] = U_{MFC}[V] \cdot K_{Gili}\left[\frac{Nl}{hV}\right] \tag{6.6}$$

After differentiating this equation with respect to $U_{MFC}$ and $K_{Gili}$ the error for the MFC($\Delta\dot{m}_{MFC}$) was determined to be linearly and proportionally increasing with the volume stream sent through the MFC.

$$\Delta\dot{m}_{MFC}\left[\frac{Nl}{h}\right] = U_{MFC}[V] \cdot \Delta K_{Gili}\left[\frac{Nl}{hV}\right] + \Delta U_{MFC}[V] \cdot K_{Gili}\left[\frac{Nl}{hV}\right] \tag{6.7}$$

$$\Delta\dot{m}_{MFC}\left[\frac{Nl}{h}\right] = U_{MFC}[V] \cdot 0{,}04\left[\frac{Nl}{hV}\right] + 0{,}01[V] \cdot 4{,}1\left[\frac{Nl}{hV}\right] \tag{6.8}$$

FTIR

Since the measurement of the FTIR was carried out separately from the other measurements, its error calculation was independent from any previous calculation. The error of the FTIR ($\Delta\vec{X}_{FTIR}$) was accumulated out of the zero-point drift ($I_{ZPD}$), linear deviations ($I_{Lin}$), temperature drift ($I_T$) and the influence of the pressure ($I_p$).

$$\Delta\vec{X}_{FTIR}[\%] = \underbrace{\vec{I}_{ZPD}[\%]}_{2\%} + \underbrace{\vec{I}_{Lin}[\%]}_{2\%} + \underbrace{I_T\left[\frac{\%}{K}\right]\cdot\Delta T[K]}_{0} + \underbrace{I_p\left[\frac{\%}{\Delta p/p}\right]\cdot\frac{\Delta p}{p}}_{0} = 4\,[\%] \tag{6.9}$$

The Temperature and the pressure stayed constant in the FTIR, due to a long enough heating tube and a separate gas supply unit. Therefore, just the error of the zero-point drift and the linear deviation were accumulated, what led to a total error of 4 % of the measured value.

Moist Measurements

As it can be seen in equation 6.3 the error of the corrected dry ammonia concentration $\Delta X_{NH3,dry}\,(X_{NH3}, n_{H2O}, n_{NH3,in})$ is dependent on three variables, which are further linked to accumulated errors of their own. The measured ammonia concentration of the moist measurement ($X_{NH3}$) contains the error of the FTIR ($\Delta\vec{X}_{FTIR}$), the constant water feed ($n_{H2O}$) contains the pump's inaccuracy ($\Delta\dot{m}_p$) and the ammonia feed stream ($n_{NH3,in}$) contains the error of the MFC ($\Delta\dot{m}_{MFC}$). Therefore, the error of the moist measurements, that where calculated on dry basis like it is shown in Chapter 6.4, is put together according the following equation.

$$X_{NH3,dry} = \frac{X_{NH3}}{1-\frac{n_{H2O}\cdot(1+X_{NH3})}{2\cdot n_{NH3,in}+n_{H2O}}} = \frac{x}{1-\frac{y\cdot(1+x)}{2\cdot z+y}} \tag{6.10}$$

It was then derived three times with respect to each variable based on the simplified structure in which $\Delta x, \Delta y$ *and* $\Delta z$ are representing the errors of the pre-steps.

$$\Delta X_{NH3,dry}\,(X_{NH3}) = \frac{df}{dx}\cdot\Delta x + \frac{df}{dy}\cdot\Delta y + \frac{df}{dz}\cdot\Delta z \tag{6.11}$$

The different derivations were calculated separately

$$\frac{df}{dx} = \frac{dX_{NH3,dry}}{dX_{NH3}} = \frac{2n_{NH3,in}(n_{H2O} + 2n_{NH3,in})}{(X_{NH3} \cdot n_{H2O} - 2n_{NH3,in})^2} \tag{6.12}$$

$$\frac{df}{dy} = \frac{dX_{NH3,dry}}{dn_{H2O}} = \frac{2X_{NH3}(X_{NH3} + 1)2n_{NH3,in}}{(X_{NH3} \cdot n_{H2O} - 2n_{NH3,in})^2} \tag{6.13}$$

$$\frac{df}{dz} = \frac{dX_{NH3,dry}}{dn_{NH3,in}} = \frac{2X_{NH3}(X_{NH3} + 1)n_{H2O}}{(X_{NH3} \cdot n_{H2O} - 2n_{NH3,in})^2} \tag{6.14}$$

and were then put together in combination with the already calculated errors of the pre-steps, which are shown above, to the error of the corrected moist measurements.

$$\Delta X_{NH3,dry}\,(X_{NH3}) = \frac{dX_{NH3,dry}}{dX_{NH3}} \cdot \Delta\vec{X}_{FTIR} + \frac{dX_{NH3,dry}}{dn_{H2O}} \cdot \Delta\dot{m}_p + \frac{dX_{NH3,dry}}{dn_{NH3,in}} \cdot \Delta\dot{m}_{MFC} \tag{6.15}$$

Based on the value from Table 12 the pump's inaccuracy is $\Delta\dot{m}_p = 0{,}01$. Within the calibrated measuring range the highest possible inaccuracy for moist measurements was determined to be ±0,05 or (10,00 ± 0,05) vol-% $NH_3$.

# 7 Conclusion and Outlook

Due to the high activation energy of the dissociation of ammonia a catalyst is needed to support the reaction. With the catalysts that were tested in this master thesis the average temperature, where a 99,9 % dissociation of $NH_3$ was reached, was 730 °C. This value is far higher than the theoretical estimation based on the Gibbs Energy calculation. It was also seen that at higher flow rates higher temperatures where needed. Two statements can be directly derived from this finding. The first is, that the higher the temperature (>730 °C), the better the dissociation of ammonia works, especially for higher flow rates. And second, the rate-limiting step for the reaction is a microcanonical one (Chapter 3.4.1). For the splitting of ammonia into nitrogen and hydrogen the limiting step is the desorption of the N-atom from the catalyst surface. That also means a lower space velocity or a higher residence time inside the reactor is beneficial for the reaction. The best results were obtained with residence times around 5 seconds.

It was also seen that Ni is a better catalyst than Ru for the dissociation of ammonia, what can be explained by the lower binding energy between nitrogen atoms and the surface of a Ni catalyst in comparison to a Ru catalyst (Chapter 6.5).

The effect water had on the reaction was not completely clear. Even though water should have no influence rather than a higher energy consumption and dilution, it seemed that it slightly reduced the activity of the Ru catalyst while it increased the catalytical activity of Ni. These findings where too unclear to take them for granted, and therefore they should be seen as tendencies instead of facts.

Really interesting was the appearance of NO in the off gas of the reformer, since $NH_3$ is normally used to reduce $NO_x$ emissions. NO started to arise after a $NH_3$ concentration of (0,8 ± 0,2) vol-% was reached and was independent from the reformer temperature. The temperature range where NO started to be produced was between 550 and 800 °C and always reached an equilibrium around 25 ppmv.

Table 13: Characteristics of the $NH_3$ Dissociation – In this table a summary of the findings of this thesis is given.

| characteristics of $NH_3$ dissociation |
|---|
| - high activation energy – catalyst is necessary<br>- the higher the temperature the better for the reaction<br>- lower SVs worked better for the reaction than high ones<br>- Ni catalyst was better than Ru catalyst<br>- $H_2O$ had no or just a slightly effect on the reaction (beside a higher energy consumption)<br>- NO was built under a $NH_3$ concentration of (0,8± 0,2) vol-% was reached independently from the temperature |

To improve the activity of the catalyst and therefore lower the temperature where 99,9 % of the $NH_3$ dissociation is done, a special catalyst would need to be produced, that is currently not commercially available. K. Kordesch [29] managed to reach an 99,9 % dissociation of ammonia at 550 °C with a similar catalyst consisting of NiO on $Al_2O_3$ spheres coated with Ru salts. A.G. Freidlander [28] reached 99,9 % conversion at 500 °C with his (NiO + Ru)-$Al_2O_3$ catalyst and additionally showed that Ru supported the activation of NiO to Ni. T.V. Choudhary [30] reached a 99 % $NH_3$ decomposition at 650 °C with a 10% $Ru/SiO_2$ catalyst and 97 % decomposition with a 65% $Ni/SiO_2/Al_2O_3$ catalysator.

In general, it can be said that a variety of researchers came to the same result that Ni in combination with Ru is the most effective catalyst for the reforming of ammonia. The best improvement of the catalysts that were used in this thesis would be an increase of the surface area in combination with an increase of the heat transport within the catalyst. This could be obtained by using fibrous material instead of $Al_2O_3$ spheres, like it was done by M. Wang [23].

To reliably confirm the findings of this thesis it would be necessary to increase the whole set of measurements. Due to a limited time frame it was not possible to repeate measurements with imperfect results. Nevertheless, a general tendency of the behaviour was visible and is stated in this master thesis.

# 8 Directories

## 8.1. List of Figures

## 8.2. List of Tables

## 8.3. List of References

[1] U. Bossel, The birth of the fuel cell: 1835-1845, Oberrohrdorf, Germany: Europ. Fuel Cell Forum, 2000.

[2] P. Welter, "Olympia in Tokio: 1964 der Shinkansen, 2020 der Wasserstoff," *Frankfurter Allgemeine,* pp. 1-2, 27. August 2016.

[3] J. Töpler and J. Lehmann, Wasserstoff und Brennstoffzelle, Esslingen, Germany: Springer Vieweg, 2017.

[4] A. Klerke, C. H. Christensen, J. K. Nørskovb and T. Vegge, Ammonia for hydrogen storage: challenges and opportunities, Denmark: The Royal Society of Chemistry, 2008.

[5] K. Kordesch, V. Hacker, G. Faleschini, G. Koscher and M. Cifrain, "Ammonia as Hydrogen Source for an Alkaline Fuel Cell-Battery Hybrid System," Technical University Graz, Graz, Austria, 2003.

[6] R. Lan, J. T. Irvine and S. Tao, "Ammonia and related chemicals as potential indirect hydrogen storage materials," Elsiver, Glasgow, UK, 2011.

[7] C. Zamfirescu and I. Dincer, "Using ammonia as a sustainable fuel," *Journal of Power Sources 185,* pp. 459-465, 17 July 2008.

[8] G. Cinti, U. Desideri, D. Penchini and G. Discepoli, "Experimental Analysis of SOFC Fuelled by Ammonia," *FUEL CELLS,* p. 221–230, 17 March 2014.

[9] N. Dekker and B. Rietveld, "Highly Efficient Conversion of Ammonia in Electricity by Solid Oxide Fuel Cells," Energy research Centre of the Netherlands, Lucerne, Switserland, 2004.

[10] "SAFETY DATA SHEET in accordance with REACH regulation 1907/2006/EC," Air Liquide, Düsseldorf, Germany, 2016.

[11] D. Steinborn, Grundlagen der metallorganischen Komplexkatalyse, 2nd Edition, Wiesbaden, Germany: Vieweg+Teubner, 2007.

[12] T. L. Brown, H. E. LeMay and B. E. Bursten, Chemie - Die Zentrale Wissenschaft, München, Germany: Pearson Studium, 2007.

[13] Ullmann's Encyclopedia of Industrial Chemistry: Electronic Release. CD, Weinheim, Germany: Wiley-VCH, 2003.

[14] G. Ertl, Reaktionen an Oberflächen: vom Atomaren zum Komplexen (Nobel-Vortrag), Weinheim, Germany: Angewandte Chemie, 2008.

[15] G. Ertl, "Surface Science and Catalysis—Studies on the Mechanism of Ammonia Synthesis: The P. H. Emmett Award Address," *Catalysis Reviews: Science and Engineering, 21:2,* pp. 201-223, 1980.

[16] J. Hagen, Industrial catalysis: a practical approach, Weinheim, Germany: Wiley-VCH, 2006.

[17] H. F. Rase, Handbook of commercial catalysts: heterogeneous catalysts, Austin, USA: CRC Press, 2000.

[18] W. Tsai and W. H. Weinberg, "Steady-State Decomposition of Ammonia on the Ru(001) Surface," American Chemical Society, Pasadena, USA, 1987.

[19] C. Hochenauer, Wärmetechnik 2 - Feuerungssysteme Rauchgasreinigung Thermische Energieanlagen Heizflächenauslegung, Graz, Austria: TU Graz, 2016.

[20] S. Wiesche, Reduction, Numerical Heat Transfer and Thermal Engineering of AdBlue (SCR) Tanks for Combustion Engine Emission, Bonn, Germany: Elsiver, 2006.

[21] C. Enderle, G. Vent and M. Paule, "BLUETEC Diesel Technology - Clean, Efficient and Powerful," *MTZ Motortechnische Zeitschrift (2008) 69: 376,* pp. 376-384, May 2008.

[22] P. W. Atkins and J. D. Paula, Elements of Physical Chemistry, 5th ed., New York, USA: W. H. Feeman and Company New York, 2009.

[23] M. Wang, J. Li, L. Chen and Y. Lu, "Miniature $NH_3$ Cracker Based on Microfibrous Entrapped Ni-CeO2/Al2O3 Catalyst Monolith for Portable Fuel Cell Power Supplies," Elsevier, Shanghai 200062, China, 2008.

[24] VDI-Wärmeatlas, 11th edition, Düsseldorf, Germany: VDI-Gesellschaft Verfahrenstechnik und Chemieingenieurwesen, 2013.

[25] W. Schreiter, Chemische Thermodynamik: Grundlagen, Übungen, Lösungen, Berlin, Germany: Walter de Gruyter GmbH & Co., KG, 2014.

[26] H. Kuhlmann, Strömungsmechanik, 1. ed., Munich, Germany: Pearson Studium, 2007.

[27] A. F. S. Molouk, T. Okanishi, H. Muroyama and T. Matsui, "Electrochemical and Catalytic Behaviors of Ni–YSZ Anode for the Direct Utilization of Ammonia Fuel in Solid Oxide Fuel Cells," *Journal of The Electrochemical Society,* pp. 1268-1274, 18. August 2015.

[28] A. G. Freidlander, R. Courty and R. Montarnal, "Ammonia Decomposition in the Presence of Water Vapor I. Nickel, Ruthenium and Palladium Catalysts," *Journal of Catalysts,* pp. 312-321, 28 February 1977.

[29] K. Kordesch and V. H. G. Faleschini, "Ammonia for High Density Hydrogen Storage," Technical University Graz, Graz, Austria, 2014.

[30] T. Choudhary, C. Sivadinarayana and D. Goodman, "Catalytic ammonia decomposition: COx-free hydrogen production," *Catalysis Letters,* pp. 197-201, 8 Jannuary 2001.

[31] Y. C. W. Y. L. L. L. Zhang, "A Direct Ammonia Tubular Solid Oxide Fuel Cell," CHINESE JOURNAL OF CATALYSIS, Beijing, China, 2007.

[32] Ü. L. Chemische Thermodynamik: Grundlagen, W. Schreiter, 2nd edition: Walter de Gruyter GmbH & Co., KG, 2014.

[33] R. Lan and S. Tao, "Ammonia as a suitable fuel for fuel cells," Department of Chemical & Process Engineering, University of Strathclyde, Glasgow, UK, 2014.

[34] A. Afif, N. Radenahmad, Q. Cheok, S. Shams and J. H. Kim, "Ammonia-fed fuel cells: a comprehensive review," *Renewableand Sustainable Energy Reviews,* p. 822–835, 12 February 2016.

[35] A. Wojcik, H. Middleton, I. Damopoulos and J. V. Herle, "Ammonia as a fuel in solid oxide fuel cells," *Journal of Power Sources,* p. 342–348, 2003.

[36] Q. Ma, J. Ma, S. Zhou, R. Yan, J. Gao and G. Meng, "A high-performance ammonia-fueled SOFC based on a YSZ thin-film electrolyte," Elsevier, Hefei, China, 2006.

[37] J. Yang, A. F. S. Molouk, T. Okanishi, H. Muroyama and T. Matsui, "A Stability Study of Ni/Yttria-Stabilized Zirconia Anode for Direct Ammonia Solid Oxide Fuel Cells," American Chemical Society, Kyoto, Japan, 2015.

[38] A. Fuertea, R. X. Valenzuelaa, M. J. Escuderoa and L. Dazaa, "Ammonia as efficient fuel for SOFC," *Journal of Power Sources,* p. 170–174, 18 November 2008.

[39] A. F. S. Molouk, J. Yang, T. Okanishi and H. Muroyama, "Comparative study on ammonia oxidation over Ni-based cermet anodes for solid oxide fuel cells," *Journal of Power Sources,* pp. 72-79, 21 November 2015.

[40] A. Hagen, "Use of alternative fuels in solid oxide fuel cells," Technical University of Denmark, Roskilde, Denmark, 2007.

[41] Z. Limin, C. You, Y. Weishen and L. Liwu, "A Direct Ammonia Tubular Solid Oxide Fuel Cell," *Chinese Journal of Catalysis,* p. 749–751, September 2007.